Institute of Thermoelectricity, Academy of Sciences and Ministry of Education and Science of Ukraine

Journal of THERMOELECTRICITY

International Research

Founded in December, 1993

published 6 times a year

No. 6 *2017*

Editorial Board

International Editorial Board

Founders – National Academy of Sciences, Ukraine
Institute of Thermoelectricity of National Academy of Sciences and Ministry of Education and Science of Ukraine

Certificate of state registration № КВ 15496-4068 ПР

Approved for printing by the Academic Council of Institute of Thermoelectricity of the National Academy of Sciences and Ministry of Education and Science, Ukraine

Address of editorial office:
Ukraine, 58002, Chernivtsi, General Post Office, P.O. Box 86.
Phone: +(380-372) 90 31 65.
Fax: +(380-3722) 4 19 17.
E-mail: jt@inst.cv.ua
http://www.jt.inst.cv.ua

Signed for publication 25.01.18. Format 70×108/16. Offset paper №1. Offset printing.
Printer's sheet 11.5. Publisher's signature 9.2. Circulation 400 copies. Order 5.

Printed from the layout original made by "Journal of Thermoelectricity" editorial board
in the printing house of "Bukrek" publishers,
10, Radischev Str., Chernivtsi, 58000, Ukraine

CONTENTS

P.V. Gorskiy

P.V. Gorskiy, *Doctor Phys.-math. science*

Institute of Thermoelectricity of the NAS and MES of Ukraine,
1, Nauky str, Chernivtsi, 58029, Ukraine; *e-mail: anatych@gmail.com*

THE THERMOELECTRIC FIGURE OF MERIT OF POWDER-BASED THERMOELECTRIC MATERIALS OF THE *Zn-Cd-Sb* SYSTEM

The paper presents the results of calculating the thermoelectric figure of merit of powder-based thermoelectric materials of the Zn-Cd-Sb system. In the process of calculations, we consider phonon-phonon scattering due to normal and Umklapp processes, as well as phonon scattering on the boundaries of powder particles. Moreover, charge carrier scattering on the acoustic phonon deformation potential and on the boundaries of powder particles is taken into account. In so doing, the effective mass of charge carriers, the Gruneisen tensor, the longitudinal and transverse phonon velocities, as well as Umklapp parameter are considered to be isotropic and equal to the direction-averaged values of components of corresponding tensors. Also, the dependence of charge carrier mobility on the concentration of single-charge doping acceptor impurities is taken into account. As a result of calculations, it is shown that, without sacrificing the thermoelectric figure of merit, for the manufacture of legs of thermocouple thermoelements, instead of single crystals, if it is technologically expedient, one can use powder-based materials of the Zn-Cd-Sb systems with the average particle diameter (2÷100) μm. The results of calculations are not only qualitatively but also quantitatively consistent with the experimental data. Bibl. 9, Fig. 4.

Key words: *Zn-Cd-Sb* system, thermoelectric material, thermoelectric figure of merit, powder, charge carriers, phonons, scattering, normal processes, Umklapp processes, acoustic phonon deformation potential, concentration dependence of charge carrier mobility.

Introduction

Powder-based thermoelectric materials, in comparison with single-crystal materials, have the technological advantage that thermoelectric legs of such materials can be manufactured by hot pressing, extrusion or electric spark plasma sintering (SPS), giving them any shape dictated by design of a particular thermoelectric device. Moreover, the use of such materials instead of single crystals makes it possible to automate and even robotize the technological process of manufacturing products, as well as to assure their required mechanical strength, especially in the case of reduction in size.

Such materials can be made by grinding polycrystalline ingots to the desired size [1]. However, in this case a question arises about the influence of material structure on its thermoelectric figure of merit, hence, on the output characteristics of finished devices, for instance, thermoelectric generators. The theoretical study of such influence on the materials of the *Zn-Cd-Sb* system by the example of zinc antimonide is the purpose of the present paper.

Calculation of the thermoelectric figure of merit of powder-based materials of the *Zn-Cd-Sb* system and discussion of the results

This calculation will be based on the approaches developed in [2, 3] using the results of [4]. In order to calculate the thermoelectric figure of merit ZT of powder-based materials, we must know the relation

between the thermoelectric characteristics of these materials, namely the thermoEMF, electrical conductivity and thermal conductivity and the average radius of powder particle. To obtain such a relation when calculating the above characteristics, it is necessary to take into account not only the mechanisms of charge carrier scattering inherent in single crystal, but also additional scattering on the boundaries of powder particles. This scattering becomes essential, if the average radius of powder particles becomes comparable to the mean free paths of charge carriers and phonons inherent in a single crystal.

We will start from calculating the thermoEMF. According to previous theoretical papers and experimental data [5,6], it is correct to assume that charge carrier scattering in materials of the *Zn-Cd-Sb* system in the temperature region relevant for practical applications takes place with an energy-independent cross-section. So, for materials with a parabolic band spectrum the respective scattering index $r = -0.5$. It follows that the thermoEMF of material does not depend on the average radius of powder particles and, therefore, is equal to:

$$\alpha = \frac{k_B}{e}\left[\frac{2F_1(\eta)}{F_0(\eta)} - \eta\right], \tag{1}$$

where k_B – the Boltzmann constant, e – electron charge, η – the reduced chemical potential, $F_m(\eta)$ – the Fermi integral which is determined as follows:

$$F_m(\eta) = \int_0^\infty \frac{x^m dx}{\exp(x-\eta)+1}. \tag{2}$$

The reduced chemical potential is found from the equation:

$$\frac{8\pi N_v \sqrt{2}\left(m^* k_B T\right)^{3/2} F_{1/2}(\eta)}{h^3 n_0} - 1 = 0, \tag{3}$$

where N_v – the number of equivalent valleys, m^* – the effective mass of charge carriers which is considered to be isotropic in case of powder, T – absolute temperature, h – the Planck constant, n_0 – the bulk concentration of charge carriers which is considered to be equal to concentration of single-charge doping impurities.

The electrical conductivity is determined from the general formula:

$$\sigma = en_0 b. \tag{4}$$

In so doing, the mobility of charge carriers with regard to their scattering on the boundaries of powder particles is found from the relation:

$$b = \frac{elF_0(\eta)}{2\sqrt{m^* k_B T}F_{1/2}(\eta)} \int_0^1 \int_{-1}^1 \frac{(r/l)y^2\sqrt{y^2-2zy+1}}{(r/l)\sqrt{y^2-2zy+1}+1} dzdy, \tag{5}$$

where l – the mean free path of charge carriers dependent on temperature and impurity concentration, hence, on charge carriers, which is inherent in a single crystal, r – the average radius of powder particles which are considered to be spherical. Therefore, part of material thermal conductivity related to free charge carriers is determined as follows:

$$\kappa_{cc} = L\sigma T, \tag{6}$$

where L – the Lorentz number equal to:

$$L = \left(\frac{k_B}{e}\right)^2 \left[\frac{3F_2(\eta)}{F_0(\eta)} - \frac{4F_1^2(\eta)}{F_0^2(\eta)}\right]. \tag{7}$$

In conformity with the approach stated in [4], the mean free path of charge carriers in nanometers as a function of temperature and charge carrier concentration is determined by the following semi-empirical relation:

$$l = 9519T^{-1}\left(n_0/10^{16}\right)^{-0.08552}, \tag{8}$$

where n_0 – the bulk concentration of charge carriers in sm^{-3}.

Lattice thermal conductivity, with regard to charge carrier scattering on the boundaries of powder particles is determined as follows:

$$\kappa_l = \frac{3\pi\rho\hbar}{64\gamma^2\theta^3 k_B T_D^2}\int_0^1\int_0^1\int_{-1}^1 \frac{x^4\exp(x/\theta)}{\left(\exp(x/\theta)-1\right)^2}\left[\frac{v_l^4 k_l^*\sqrt{y^2-2zy+1}}{1+k_l^* Q_l(x)\sqrt{y^2-2zy+1}}+\frac{2v_t^4 k_t^*\sqrt{y^2-2zy+1}}{1+k_t^* Q_t(x)\sqrt{y^2-2zy+1}}\right] y^2\,dzdydx, \tag{9}$$

where $k_l^* = 16\gamma^2 k_B^5 T T_D^4 r/\left(3\pi\rho v_l^6\hbar^4\right)$, $k_t^* = 16\gamma^2 k_B^5 T T_D^4 r/\left(3\pi\rho v_t^6\hbar^4\right)$, T_D – the Debye temperature, γ – the direction-averaged Gruneisen parameter, ρ – crystal density, $\theta = T/T_D$, v_l and v_t – are the direction-averaged longitudinal and transverse acoustic wave propagation velocities. In this case, frequency polynomials $Q_l(x)$ and $Q_t(x)$ are determined as:

$$Q_l(x) = x^4 + \mu x, \tag{10}$$

$$Q_t(x) = x\left(3.125\theta^3 + \mu\right). \tag{11}$$

As a result, the thermoelectric figure of merit ZT of material is determined as:

$$ZT = \alpha^2\sigma T/\left(\kappa_{cc} + \kappa_l\right). \tag{12}$$

The results of calculations made in conformity with relations (1 – 11) for zinc antimonide powders with particle radius 0.1 – 50 μm are given in Figs.1 – 4.

In the process of calculations, the following direction-averaged parameter values of single-crystal zinc antimonide were used: $m^* = 0.343m_0$, $N_v = 2$, $T_D = 225\,\text{K}$, $\rho = 6380\,\text{kg/m}^3$, $v_l = 3890\,\text{m/s}$, $v_t = 2222\,\text{m/s}$, $\gamma = 1.08$, $\mu = 4.925$ [5 – 8, 9].

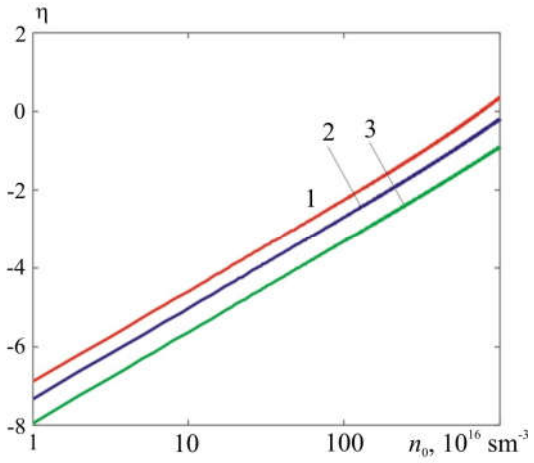

Fig.1. Concentration dependences of chemical potential of charge carrier gas at temperatures of:1 – 300; 2 – 400; 3 – 600 K

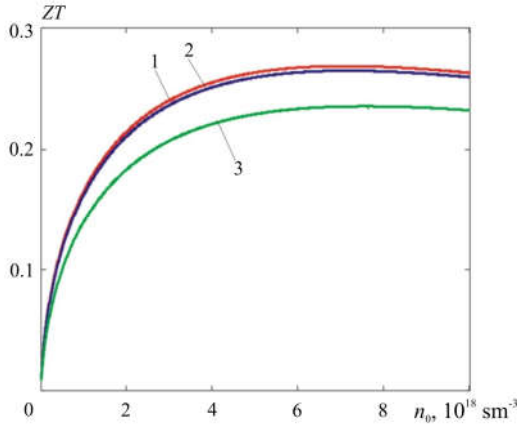

Fig. 2. Concentration dependences of the thermoelectric figure of merit of zinc antimonide at a temperature of 300 K for powder particles of radius: 1 – 50; 2 – 1; 3 – 0.1 μm

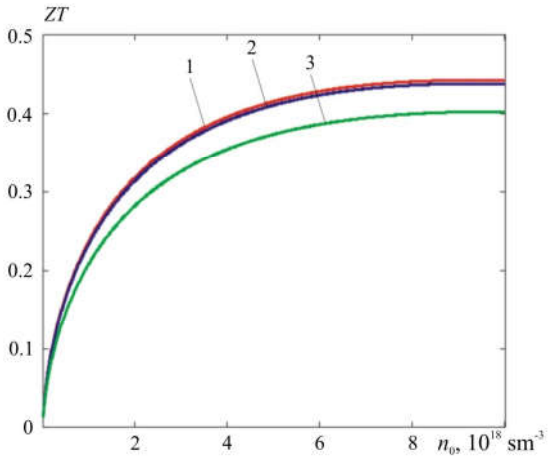

Fig.3. Concentration dependences of the thermoelectric figure of merit of zinc antimonide at a temperature of 400 K for powder particles of radius: 1 – 50; 2 – 1; 3 – 0.1 μm

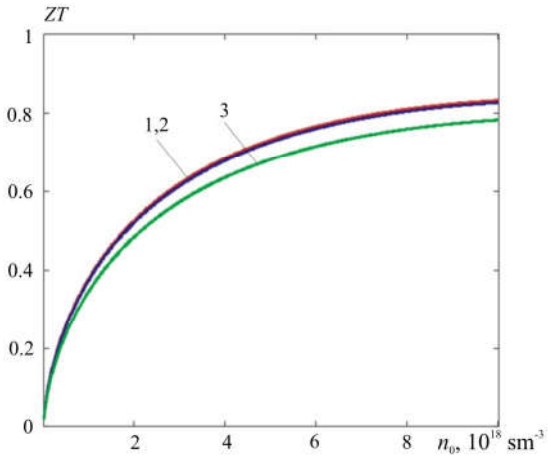

Fig.4. Concentration dependences of the thermoelectric figure of merit of zinc antimonide at a temperature of 600K for powder particles of radius: 1 – 50; 2 – 1; 3 – 0.1 μm

From the figures, firstly, it is evident that in the studied range of concentrations, the charge carrier gas is nondegenerate or weakly degenerate. Secondly, it is seen that a change in the radius of powder

particles in the range (1 ÷ 50) μm or diameter in the range (2 ÷ 100) μm practically does not change the thermoelectric figure of merit of material. And only transition to the submicron particles of radius 0.1 μm or diameter 0.2 μm reduces the thermoelectric figure of merit of material. This reduction is mainly due to the fact that Umklapp coefficient μ which determines the finite lattice thermal conductivity of materials of the *Zn-Cd-Sb* system is essentially greater than unity, and in these materials the lattice thermal conductivity is decisive.

Moreover, it is seen that at temperatures of 300 and 400 K in the investigated concentration range of charge carriers there are maxima of the thermoelectric figure of merit of materials, and at a temperature of 600 K the maximum values of the thermoelectric figure of merit of materials are achieved at the end of the interval.

As regards the specific numerical values of the maximum thermoelectric figure of merit of powder-based materials of the *Zn-Cd-Sb* system, in the considered case of zinc antimonide at powder particle radius, for instance, 50 μm, these values at temperatures of 300, 400 and 600 K are 0.268, 0.443 and 0.832, respectively, and are reached at charge carrier concentrations $(6.1 \div 8.2) \cdot 10^{18}$, $9 \cdot 10^{18}$ and 10^{19} sm^{-3}, respectively. This result is not only qualitatively but also quantitatively consistent with the experimental data [1].

Conclusion

1. Transition from single crystals of the *Zn-Cd-Sb* system to corresponding powder-based materials with particle diameter (2 ÷ 100) μm scarcely changes the thermoelectric figure of merit of materials.
2. Reduction of the thermoelectric figure of merit of materials of the *Zn-Cd-Sb* system in going from single crystals to powders with particle diameter less than 2 μm is mainly due to the fact that Umklapp coefficient which is responsible for phonon-phonon scattering at high temperatures and, hence, forms the finite value of lattice thermal conductivity, in the above materials is essentially higher than unity.
3. Maximum values of the thermoelectric figure of merit ZT of powder materials based on zinc antimonide with powder particle diameter 100 μm in the range of charge carrier concentrations $(10^{16} \div 10^{19}\ sm^{-3})$ at temperatures of 300, 400 and 600K are 0.268, 0.443 and 0.832, respectively, which is in agreement with the experimental data.

References

1. Fedorov M.I., Prokofieva L.V., Ravich Yu.I., Konstantinov P.P., Pshenai-Severin D.A., Shabaldin A.A. (2014). Termoelektricheskaia effektivnost intermetallida ZnSb [Thermoelectric figure of merit of ZnSb intermetallide]. *Fizika i Tekhnika Poluprovodnikov – Semiconductors*, 48(4), 448-453 [in Russian].
2. Gorskyi P.V., Mikhalchenko V.P. (2013). Reduction of thermoelectric material lattice thermal conductivity using shape-forming element. *J.Thermoelectricity*, 1, 19 - 27.
3. Gorskyi P.V., Mikhalchenko V.P. (2013). On the electric conductivity of contacting particles of thermoelectric material. *J.Thermoelectricity,* 2, 13-19.
4. Gorskyi P.V. (2017). Optimization of materials based on zinc antimonide for thermocouple thermoelements. *J.Thermoelectricity,* 4 (accepted for publ).
5. Lazarev V.B., Shevchenko V.Ya., Grinberg Ya.Kh., Sobolev V.V. (1978). *Poluprovodnikovyie soiedineniia $A^{II}B^{V}$ [Semiconductor compounds $A^{II}B^{V}$]*. Moscow: Nauka [in Russian].

6. Mlnarikova L., Triska A., Storac L. (1970). The transport phenomena of pure and doped *p*-type ZnSb. *Czech. J. Phys*., B20, 63-72.
7. Bokii G.B. , Voronina I.P., Dvoriankina G.G. (1973). *Kristallochimicheskiie, fiziko-khimicheskiie i fizicheskiie svoistva poluprovodnikovykh veshchestv [Chrystal-chemical, physico-chemical and physical properties of semiconductor substances]*. Moscow: Izdatelstvo standartov [in Russian].
8. Mikhalchenko V.P. (1976). Rentgen-difraktometricheskiie i akusticheskiie issledovaniia nekotorykh angarmonicheskikh effektov v kristallakh [X-ray diffraction and acoustic studies of some anharmonic effects in crystals*]. Doctors' thesis (Phys-Math).* Chernivtsi [in Russian].
9. Gorskyi P.V. (2016). Lattice thermal conductivity of thermoelectric materials based on *Zn-Cd-Sb*. *J. Thermoelectricity*, 5, 13-19.

Submitted 03.10.2017

Горський П.В. *докт. фіз.-мат. наук*

Інститут термоелектрики НАН і МОН України, вул. Науки, 1,
Чернівці, 58029, Україна*, e-mail: anatych@gmail.com*

ЕФЕКТИВНІСТЬ ТЕРМОЕЛЕКТРИЧНИХ МАТЕРІАЛІВ СИСТЕМИ *Zn-Cd-Sb* НА ОСНОВІ ПОРОШКІВ

У статті наведено результати розрахунку ефективності термоелектричних матеріалів системи Zn-Cd-Sb на основі порошків. У процесі розрахунків враховано розсіювання фононів одного на одному, обумовлене як нормальними процесами, так і процесами перекидання, а також розсіювання фононів на межах частинок порошку. Окрім того, враховано розсіювання носіїв заряду на деформаційному потенціалі акустичних фононів та на межах частинок порошку. При цьому ефективна маса носіїв заряду, тензор Грюнайзена, швидкості поздовжніх та поперечних фононів а також параметр перекидання вважаються ізотропними і рівними усередненим за напрямками значенням компонент відповідних тензорів. Також враховано залежність рухливості носіїв заряду від концентрації однозарядних легуючих акцепторних домішок. В результаті розрахунків показано, що без втрати термоелектричної ефективності для виготовлення гілок термопарних термоелементів замість монокристалів можна, якщо це технологічно доцільно, використовувати матеріали системи Zn-Cd-Sb на основі порошків з середнім діаметром частинок (2 ÷ 100) мкм. Результати розрахунків не лише якісно, а й кількісно узгоджуються з експериментальними даними. Бібл. 9, Рис. 4.

Ключові слова: система *Zn-Cd-Sb,* термоелектричний матеріал, термоелектрична ефективність, порошок, носії заряду, фонони, розсіювання, нормальні процеси, процеси перекидання, деформаційний потенціал акустичних фононів, концентраційна залежність рухливості носіїв заряду.

Горский П.В., *докт. физ.-мат. наук*

Институт термоэлектричества, ул. Науки, 1, Черновцы, 58029, Украина
e-mail: anatych@gmail.com

ЭФФЕКТИВНОСТЬ ТЕРМОЭЛЕКТРИЧЕСКИХ МАТЕРИАЛОВ СИСТЕМЫ *Zn-Cd-Sb* НА ОСНОВЕ ПОРОШКОВ

В статье приведены результаты расчетов эффективности термоэлектрических материалов системы Zn-Cd-Sb на основе порошков. В процессе расчетов учтено рассеяние фононов друг на друге, обусловленное как нормальными процессами, так и процессами переброса, а также рассеяние фононов на границах частиц порошка. Кроме того, учтено рассеяние носителей заряда на деформационном потенциале акустических фононов и на границах частиц порошка. При этом эффективная масса носителей заряда, тензор Грюнайзена, скорости продольных и поперечных фононов, а также параметр переброса предполагаются изотропными и равными усредненным по направлениям значениям компонент соответствующих тензоров. Также учтена зависимость подвижности носителей заряда от концентрации однозарядных легирующих акцепторных примесей. В результате расчетов показано, что без потерь термоэлектрической эффективности для изготовления ветвей термопарных термоэлементов вместо монокристаллов можно, если это технологически целесообразно, использовать материалы системы Zn-Cd-Sb на основе порошков со средним диаметром частиц (2 ÷ 100) мкм. Результаты расчетов не только качественно, но и количественно согласуются с экспериментальными данными. Библ. 9, Рис. 4.

Ключевые слова: система *Zn-Cd-Sb,* термоэлектрический материал, термоэлектрическая эффективность, порошок, носители заряда, фононы, рассеяние, нормальные процессы, процессы переброса, деформационный потенциал акустических фононов, концентрационная зависимость подвижности носителей заряда.

References

1. Fedorov M.I., Prokofieva L.V., Ravich Yu.I., Konstantinov P.P., Pshenai-Severin D.A., Shabaldin A.A. (2014). Termoelektricheskaia effektivnost intermetallida ZnSb [Thermoelectric figure of merit of ZnSb intermetallide]. *Fizika i Tekhnika Poluprovodnikov – Semiconductors*, 48(4), 448-453 [in Russian].
2. Gorskyi P.V., Mikhalchenko V.P. (2013). Reduction of thermoelectric material lattice thermal conductivity using shape-forming element. *J.Thermoelectricity*, 1, 19 - 27.
3. Gorskyi P.V., Mikhalchenko V.P. (2013). On the electric conductivity of contacting particles of thermoelectric material. *J.Thermoelectricity,* 2, 13-19.
4. Gorskyi P.V. (2017). Optimization of materials based on zinc antimonide for thermocouple thermoelements. *J.Thermoelectricity,* 4 (accepted for publ).
5. Lazarev V.B., Shevchenko V.Ya., Grinberg Ya.Kh., Sobolev V.V. (1978). *Poluprovodnikovyie soiedineniia $A^{II}B^{V}$ [Semiconductor compounds $A^{II}B^{V}$]*. Moscow: Nauka [in Russian].
6. Mlnarikova L., Triska A., Storac L. (1970). The transport phenomena of pure and doped p-type ZnSb. *Czech. J. Phys*., B20, 63-72.
7. Bokii G.B. , Voronina I.P., Dvoriankina G.G. (1973). *Kristallochimicheskiie, fiziko-khimicheskiie i fizicheskiie svoistva poluprovodnikovykh veshchestv [Chrystal-chemical, physico-chemical and physical properties of semiconductor substances]*. Moscow: Izdatelstvo standartov [in Russian].
8. Mikhalchenko V.P. (1976). Rentgen-difraktometricheskiie i akusticheskiie issledovaniia nekotorykh angarmonicheskikh effektov v kristallakh [X-ray diffraction and acoustic studies of some anharmonic effects in crystals*]. Doctors' thesis (Phys-Math).* Chernivtsi [in Russian].
9. Gorskyi P.V. (2016). Lattice thermal conductivity of thermoelectric materials based on Zn-Cd-Sb. *J.Thermoelectricity*, 5, 13-19.

Submitted 03.10.2017

V.P. Shafraniuk

V.P. Shafraniuk, *Docent, cand. phys.-math sciences,*
T.V. Protsak, *Docent, cand. medical sciences*

Higher State Educational Institution of Ukraine
"Bukovinian State Medical University",2, Theatre Square,
Chernivtsi, 58000, Ukraine, *e-mail: Petro.gryg@yahoo.com*

T.V. Protsak

RESEARCH ON STRUCTURAL PERFECTION OF *CdSb* THERMOELECTRIC MATERIALS USING X-RAY DIFFRACTION METHODS

In this paper, the results of research on structural perfection of CdSb crystals with different concentration of Te impurities using complementary X-ray diffraction methods are presented and it is established at which concentration these crystals are sufficiently perfect. The proof of their high structural perfection is that they were used to obtain Pendellösung fringes, dynamic oscillations of X-ray beams. Such perfect crystals with a certain content of impurities can be successfully used to create thermoelectric devices. Bibl. 10, Fig. 4.

Key words: *Te* impurities, X-ray diffraction methods, Pendellösung fringes, dislocation, dynamic oscillations of intensity, rocking curves, wedge-like samples.

Introduction

Manufacturing of optothermoelectric devices, thermoelectric comparators, thermoelectric elements for indication of radiant fluxes, active photovoltaic devices, thermoelectric sensor elements, etc. [1 – 5], requires highly perfect profiled or plate *CdSb* single crystals of different geometric shapes.

One of the main reasons that limit the use of these materials is the complexity of obtaining large and structurally perfect *CbSb* single crystals with reproducible stable characteristics. Thus, in *CbSb* crystals doped with silver, indium, tellurium, molecules of *CbTe, InSb* are formed, and their individual phases are centres for nucleation in the bulk of the crystal of separate twin units, dislocation clusters, and foreign phase inclusions [6], that resulted in a drastic deterioration of the structure.

The purpose of this paper is to study the nature of structure defects in *CdSb* crystals, their structural perfection depending on technological growth conditions.

To investigate the crystalline structure, complementary methods were used, such as X-ray diffraction reflection topography (the Berg-Barrett method) and transmission topography (Lang's method) [7] to visualize the defects that occur during the growing process (twins, small-angle boundaries, dislocations, foreign phase inclusions, etc.), Pendellösung fringes [8], the method of double-crystal spectrometer [7] to determine the disorientation between the blocks. It should be noted that these are express and non-destructive methods, providing an opportunity to obtain the most complete information on the crystalline perfection of *CbSb*, which allows adjusting the technological growing processes.

Experimental results and their discussion

Technological processes for growing *CdSb* crystals were corrected by the results of their studies by X-ray methods. Structural studies of less perfect crystals were performed by the modified Berg-Barret method using symmetrical (200), (400) and asymmetrical reflections. This method employed LLF X-ray

tube BSM-1 with a focal length of 50 μm, which made it possible to obtain a high resolution of the order of 0.5 μm. *CdSb* crystals with the additive of 0.5 at % Te after zone levelling at a velocity of molten zone 2 cm/h from the oriented seed comprised blocks, twins and stresses inside the crystal which indicated blurred images on the topograms. With a reduction of zone velocity to 0.5 sm/h and a decrease in the amount of impurities to 0.05 at % *Te, CbSb* crystals were more perfect, comprised large blocks up to 1 sm, with disorientation of 30 angular seconds.

To create thermoelectric comparators, the method of simultaneously growing many shaped plates from one seed was used. More perfect *CbSb* crystals were obtained when the walls of the combined container were as smooth as possible, which was achieved by coating them with pyrolytic graphite. The partitions between the grown plates were made of quartz for plane-parallel plates and from graphite and stamped pyrex. To eliminate the oxides produced during the synthesis and growing in an inert atmosphere, it is possible to use the asymmetry of zone heaters, which create the inclination of the crystallization front at an angle to the direction of growth, ahead of the formation of a solid phase in the lower part of the ingot. Then the surface area of the melt crystallizes in the last place perpendicular to the bottom of the cross-section, and the condition of the surface of the melt does not result in the formation of a block structure.

Fig. 1 shows a topogram obtained by the Berg-Barret method from a non-block crystal – *CbSb* plate: 0.005 at. % *Te*.

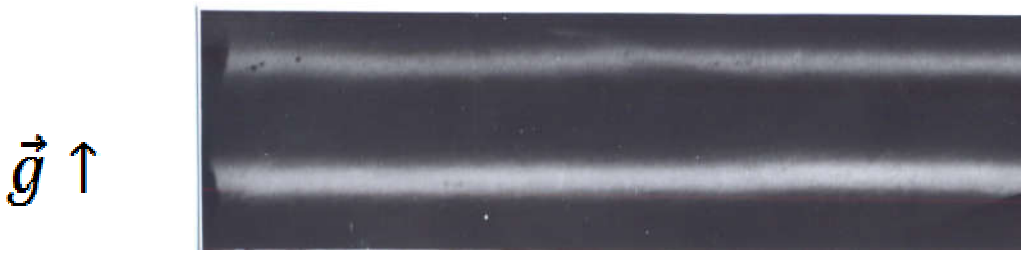

Fig. 1 Topogram of CbSb crystal: 0.005 at.% Te.
CuKα-radiation, reflection (004). x12.

Crystal that comprised no blocks, twins and other defects were investigated by the method of double-crystal spectrometer (n,-m) – *Si* (220). On these very crystals, using double-crystal spectrometer (*n, -m*) – *Si* (220), the values of half-width of rocking curves for reflections {200}, {400} were taken. Quantitative assessment of the degree of perfection of crystals under study was done by comparing the experimentally obtained values of the half-width of rocking curves θ_{exp} with the theoretically calculated value θ_{theor}, which is determined by the half-widths of lines of monochromator (*Si*) θ_m and *CdSb* sample (θ_{sample}) and the dispersion of device $D^2\Delta\lambda^2$:

$$\theta_{theor} = \left(\theta_m^2 + \theta_{sample}^2 + D^2\Delta\lambda^2\right)^{1/2} \quad (1)$$

The contribution of the half-width of rocking curve for a perfect crystal is determined by the formula:

$$\Theta_{cr} = \frac{2 \cdot C \cdot \chi_h}{\sin 2\theta},$$

where $C = 1$, for σ-polarization; $C = \cos 2\theta$, for π-polarization, χ_h is crystal Fourier component.

For reflections (200), (400) of a perfect *CdSb* crystal, the theoretical values of the half-width of rocking curve are ~ 14.5", 12.3", respectively. For real crystals, $\theta_{exp} > \theta_{theor}$, which is due to the presence of structure defects and micro imperfections. By broadening the rocking curves $\Delta\theta$, the density of dislocations *Nd* was determined, which serves as a quantitative estimate of crystals perfection:

$$N_d = \frac{\Delta\theta^2}{9.42 \cdot b^2} \quad (2),$$

where $\Delta\theta = (\theta^2_{exp} - \theta^2_{theor})^{1/2}$, b is the Burgers vector.

It follows from the calculations that the average density of dislocations in *CdSb* crystals is in the range from $3 \cdot 10^2$ to 10^3 sm^{-2}. The number of different structure defects depends on the conditions of growing and the content of doping impurities.

For a clearer idea of the dislocation structure of the most perfect *CdSb* crystals, Lang's method for thin specimens in which $\mu t < 1$, μ is the linear absorption coefficient, t is the crystal thickness, the Pendellösung fringes method, and also the dynamic oscillations of X-rays by tilted crystal method were used [8]. For *CbSb* crystals, the absorption coefficient μ is ~ 380 sm^{-1}, so the thickness of the samples in Lang's method should not exceed 50 μm. The studies of the dislocation structure of crystals were carried out on wedge-like and plane-parallel samples. Wedge-like and plane-parallel samples were prepared by mechanical grinding, with subsequent removal of the damaged layer by chemical-mechanical polishing and chemical etching. The input surfaces of the samples were perpendicular to crystallographic directions [100], [001]. The wedge-like samples had the angle of ~ 2°. The edge of the wedge for the samples with the input plane (100) coincided with the direction [010], for samples with the input plane (001), coincided with the direction [100].

Fig. 2*a,b* represents topograms of Pendellösung fringes from wedge-like samples of plate *CbSb* single crystals doped with Te in the amount of 0.005 at.%, grown at a rate of 0.5 sm/h.

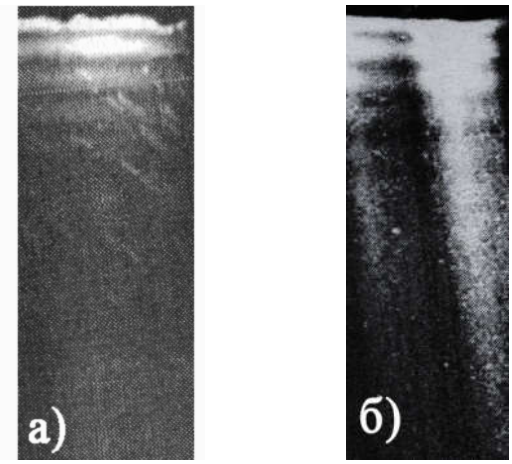

Fig.2. Pendellösung fringes from wedge-like samples of plate CdSb crystals.
a) – middle part of the plate, b)- plate edge. Mo Kα –radiation, reflection (004). x16

The presence of Pendellösung fringes and their fairly clear image shows that structural perfection of these crystals is high, the density of dislocations is rather small and they are close to non-dislocated crystals. On such crystals, as shown in [8,9], one can obtain the phenomenon of dynamic oscillations (Pendellösung) at X-ray diffraction, as well as observe the dynamic oscillations at X-ray diffraction by tilted thin crystal method. Thin samples of $\mu t < 1$ *CbSb* doped with *Te* in the amount of 0.005 % at.% were made using a special method when a 10 mm wide slit was polished on one side of a plane-parallel plate to a depth of 1/3 of the plate thickness. Turning the plate 90 ° from the opposite side, the same slit was polished to a depth of 1/3 of the plate thickness, owing to which the "window" in the centre of the plate was 1/3 of the plate thickness, and the cut (matrix) was 2/3 of the plate thickness. Processing was performed on M-5 abrasive powders and finishing – on ACM-2/1 diamond pastes with final removal of damaged layer and subsequent chemical etching to a depth of 30-50 μm. The input surfaces were perpendicular to

crystallographic directions [001], [100]. This method of manufacturing thin samples made it possible to avoid deformations when attaching them during the study.

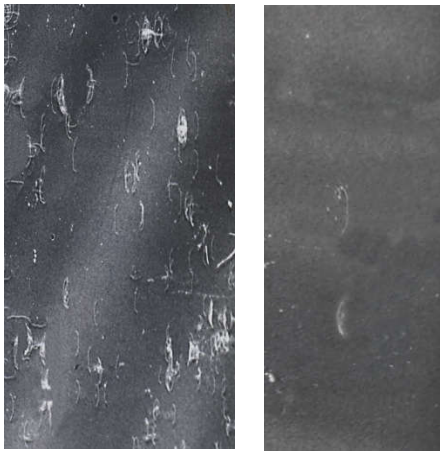

a) *b)*

Fig. 3. Topograms of thin plate samples of CdSb. Reflection (004), a- sample edge, b – sample centre. x12.

Fig.3a,b shows topograms from plane samples of *CdSb*: 0.005 at. % *Te* in $M_oK_{\alpha 1}$- radiation with the use of reflection (004). On topograms there are dislocations in the form of light lines the average density of which does not exceed 10^2 lines/sm^2. The contrast of dislocations is maximal, when diffraction vector *g* and the Burgers vector *b* are parallel, and disappears when they are mutually perpendicular. Taking of topograms from the same crystal site using different reflections made it possible to establish that the preferred direction of dislocations coincides with [010].

From the non-dislocation sites of *CdSb* crystal (Fig.3b) by tilted crystal method (the thickness of the crystal increases), dynamic oscillations were obtained at the diffraction of *MoK*α1 radiation (Fig. 4). It is known [4,5] that for an absorbing perfect crystal in the symmetrical Laue case the thickness dependence of the integral coefficient of reflection in the two-wave approximation can be represented as follows:

$$R_H^y = \frac{\pi}{2}\exp\{-\mu_0 t/(\cos\theta_0\cos\alpha)\}\left\{\int_0^{2A_\perp} J_0(X)dx + I_0(2A_\perp k) - 1 + bc\left[\int_0^{2A_\parallel} J_0(x)dx + I_0(2A_\parallel k) - 1\right]\right\} \quad (3)$$

where $C = 1$ (cosθ) for σ(π) polarization, $J_0(x)$ is zero-order Bessel function, $I_0(x)$ is modified zero-order Bessel function, $k = F_{Hi}/F_{Hr}$, $b = 1$ for non-polarized incident radiation, $A = e^2\lambda|F_H|e^{-M}ct/mc^2V\cos\theta\cos\alpha$, F_H is structural factor. Other notations are generally accepted. For a non-absorbing crystal, function R^y_H is periodic at high values of argument $2A$, the period of which is averaged with respect to polarizations and extensional distances:

$$\Lambda = 2\pi t(1+\cos 2\theta)^{-1} A_\perp^{-1} \quad (4)$$

The tilted crystal method is to increase the path of rays in the crystal $t = t_o\sec\alpha/\cos\theta$ by turning it around the normal to the reflecting planes while maintaining the diffraction condition. The main criterion for setting the crystal was the invariance of the Bragg reflection angle in the process of tilting the crystal. Micrometric screws were used to provide a smooth tilt of the crystal to within 20 arc minutes, which made it possible to obtain an experimental dependence of the intensity of the symmetric Laue reflections on the thickness of *CdSb* crystal (Fig. 4).

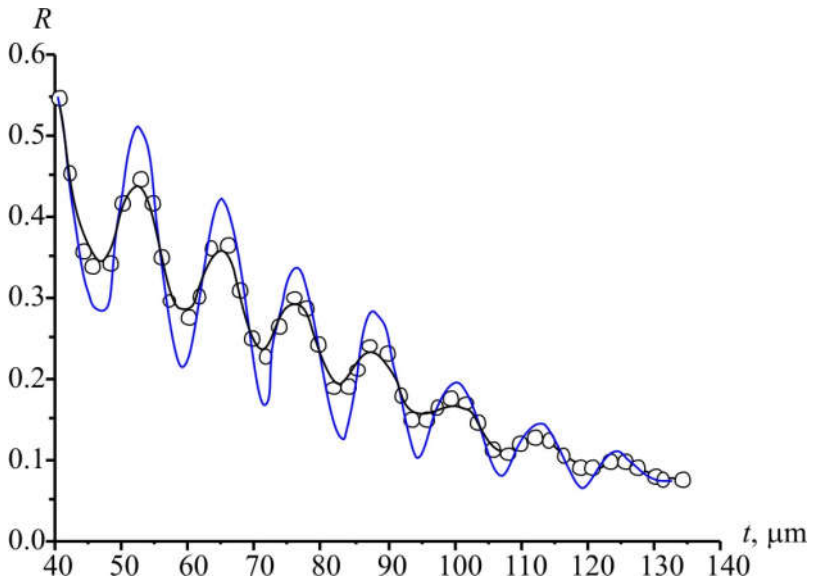

Fig. 4.Experimental and calculated dependences of intensities on the thickness of CdSb crystal. MoKα_1 - radiation, reflection (004).

From Fig.4 it is seen that with increasing crystal thickness there is extinction of oscillations which is caused by polarization effect. There is a clear shift of intensity maxima to thin crystal part, and minima – to the thick crystal part. Comparison of experimental data to those calculated by formula (3) shows a good coincidence of positions of maxima and minima.

It should be noted that the dependence $R^Y_H(t)$ is an aperiodic function, and the location of extremes is found from equation $dR^Y_H(t)/d(2A_\perp) = 0$. Coordinates of extremes of function $R^Y_H(2A_\perp)$ depend on the absorption and polarization of radiation incident on the crystal. Determination of the experimental position of the maxima and minima makes it possible to determine the values of structural amplitudes, using the relationship:

$$|F_H| = \frac{2A^n}{t^n}\frac{V\cos\theta}{2r_0\lambda\exp\{-M\}} \tag{5}$$

where t^n is measured crystal thickness which corresponds to the n–th extreme of function $R^Y_H(t)$. When calculating by formula (5) the value $|F_{004}|$ equals 512.6 ± 0.4. The measurement was performed at a temperature of 293 K with regard to temperature factor $\exp\{-M\}=0.981$. For other reflections, the values of structural amplitudes determined from the dynamic oscillations at X-ray diffraction by tilted *CdSb* crystal method are equal to: $F_{200} = 218.5 \pm 0.4$, $F_{020} = 246.8 \pm 0.2$, $F_{004} = 512.6 \pm 0.4$, $F_{040} = 353.7 \pm 0.5$. Structural amplitudes that we determined from the dynamic oscillations by tilted *CdSb* crystal method are in good agreement with those calculated theoretically [10].

CdSb single crystals: 0.003 ÷ 0.005 at.% Te were sufficiently perfect with the density of dislocations from 10 to 100 lines/cm^2, and can be successfully used to manufacture thermoelectric devices, infrared filters, the surfaces of which coincide mainly with (100). In this direction [100], crystal plates offer the highest mechanical strength. The proposed method for making thin samples provides an opportunity to obtain reliable information on the structural perfection of *CdSb* single crystals. The presence of Pendellösung fringes and dynamic oscillations at X-ray diffraction makes it possible to argue that *CdSb* single crystals are almost non-dislocated.

Conclusion

The complementary X-ray diffraction methods were used to determine the content of doped impurities $10^{-3} – 10^{-5}$ at.% that are uniformly distributed in *CdSb* single crystals and the density of dislocations in them is about 10^2 sm^{-2}, which can be helpful in the manufacture of thermoelectric and optical devices. The Pendellösung fringes and dynamic oscillations of X-ray diffraction were obtained on these crystals which testify to their high perfection.

References

1. Ashcheulov A.A., Gutsul I.V., Rarenko A.I., Voronka N.K. (1997). Anisotropic thermoelectric batteries based on cadmium antimonide. *J.Thermoelectricity*, 3, 65-68.
2. Ashcheulov A.A., Gutsul I.V., Rarenko A.I. (1993). Anisotropnyi termoelement vnutrennego opticheskogo otrazheniia [Anisotropic thermoelement of internal optical reflection]. *Ukrainian J. of Physics*, 38(6), 923 [in Russian].
3. Ashcheulov A.A., Gutsul I.V., Rarenko A.I. (1998). Issledovaniie eletrodvizhushchei sily i koeffitsienta poleznogo deistviia anisotropnykh optikotermoelementov [Research on the electromotive force and efficiency of anisotropic optothermoelements]. *Ukrainian J. of Physics*, 77(3), 538-541 [in Russian].
4. Ashcheulov A.A., Gutsul I.V., Rarenko A.I. (1998). Koordinatno-chuvstvitelnyi anizotropnyi datchik lazernogo izlucheniia [Coordinate-sensitive anisotropic sensor of laser radiation]. *Tekhnologiia i Konstruirovaniie v Elektronnoi Apparature*, 3, 42 [In Russian].
5. Ashcheulov A.A., Gutsul I.V., Rarenko A.I. (1999). Metod “prozrachnoi stenki” dlia kontrolia luchistykh potokov razlichnoi moshchnosti [The “transparent wall” method for control of radiant fluxes of various power]. *Tekhnologiia i Konstruirovaniie v Elektronnoi Apparature,* 2-3, 33-36 [In Russian].
6. Kosenkov E.M., Rarenko A.I., Shafraniuk V.P., Zaiets I.I. (2004). Research on structural perfection of CdSb crystals for thermoelectric converters depending on the technology of their growth and doping. *J.Thermoelectricity*, 3, 52-59.
7. Shafraniuk V., Dremliuzhenko S., Solodin S., Fodchuk P. (2017). Technological conditions’ effect on structural perfection of $Cd_{1-x}Mn_xTe$ crystals. *Functional Materials,* 24(4), 649-653.
8. Shafraniuk V. (2014). Maiatnykovi polosy v krystalakh i realna struktura *CdTe* [Pendellösung fringes in crystals and real structure in CdTe.] Materialy mizhnarodnoi naukovo-praktychnoi konferentsii “Informatsiini tekhnologii, ekonomika i pravo: stan ta perspektyvy rozvytku” – *Proc. of international scientific and practical conference “Information technologies, economics and justice: state-of-the art and development prospects”* (Chernivtsi, 2014). [in Ukrainian].
9. Kato N. (1961). A theoretical study of Pendellösungfringes. Part II. *Acta Cryst*., 14 (5), 526-532.
10. Cromer D. T. (1965). Anomalous dispersion corrections computed from self-consistent field relativistic Dirac-Slater wave functions. *Acta Cryst*., 18(1), 17-23.

Submitted 29.12.2017

Шафранюк В.П. *доц.канд. фіз.-мат. наук*,
Процак Т.В. *доц. канд. медичних наук*

Вищий державний навчальний заклад України, «Буковинський державний медичний університет», Театральна площа, 2,
м. Чернівці,58000, Україна
e-mail: Petro.gryg@yahoo.com

ДОСЛІДЖЕННЯ СТРУКТУРНОЇ ДОСКОНАЛОСТІ ТЕРМОЕЛЕКТРИЧНИХ МАТЕРІАЛІВ *CdSb X*-Ray ДИФРАКЦІЙНИМИ МЕТОДАМИ

У роботі представлені результати дослідження структурної досконалості кристалів CdSb з різною концентрацією домішок Te з використанням взаємодоповнюючих X-Ray дифракційних методів, і встановлено, при якій концентрації ці кристали є досить досконалими. Доказом їх високої структурної досконалості є те, що з допомогою них були одержані маятникові смуги, динамічні осциляції інтенсивності X-Ray променів. Такі досконалі кристали з певним вмістом домішок, можуть бути успішно використані для створення термоелектричних приладів. Бібл. 10, Рис. 4.

Ключові слова: домішки *Te*, *X*-Ray дифракційні методи, маятникові смуги, дислокація, динамічні осциляції інтенсивності, криві гойдання, клиноподібні зразки.

Шафранюк В.П. *доц., канд. физ.-мат. наук*,
Процак Т.В. *доц., канд. медицинских наук*

Высшее государственное учебное заведение Украины, «Буковинский государственный медицинский университет», Театральная площадь, 2, г. Черновцы,58000, Украина
e-mail: Petro.gryg@yahoo.com

ИССЛЕДОВАНИЕ СТРУКТУРНОГО СОВЕРШЕНСТВА ТЕРМОЭЛЕКТРИЧЕСКИХ МАТЕРИАЛОВ *CdSb* РЕНТГЕНОДИФРАКЦИОННЫМИ МЕТОДАМИ

В работе представлены результаты исследования структурного совершенства кристаллов CdSb с различной концентрацией примесей Te с использованием взаимодополняющих рентгенодифракционных методов, и установлено, при какой концентрации эти кристаллы являются достаточно совершенными. Доказательством их высокого структурного совершенства служит то, что с помощью их были получены маятниковые полосы и динамические осцилляции интенсивности рентгеновского излучения. Такие совершенные кристаллы с определенным содержанием примесей, могут быть успешно использованы для создания термоэлектрических приборов. Библ. 10, Рис. 4.

Ключевые слова: примеси *Te*, рентгенодифракционные методы, маятниковые полосы, дислокация, динамические осцилляции интенсивности, кривые качания, клинообразные образцы.

References

1. Ashcheulov A.A., Gutsul I.V., Rarenko A.I., Voronka N.K. (1997). Anisotropic thermoelectric batteries based on cadmium antimonide. *J.Thermoelectricity*, 3, 65-68.
2. Ashcheulov A.A., Gutsul I.V., Rarenko A.I. (1993). Anisotropnyi termoelement vnutrennego opticheskogo otrazheniia [Anisotropic thermoelement of internal optical reflection]. *Ukrainian J. of Physics*, 38(6), 923 [in Russian].
3. Ashcheulov A.A., Gutsul I.V., Rarenko A.I. (1998). Issledovaniie eletrodvizhushchei sily i koeffitsienta poleznogo deistviia anisotropnykh optikotermoelementov [Research on the electromotive force and efficiency of anisotropic optothermoelements]. *Ukrainian J. of Physics*, 77(3), 538-541 [in Russian].
4. Ashcheulov A.A., Gutsul I.V., Rarenko A.I. (1998). Koordinatno-chuvstvitelnyi anizotropnyi datchik lazernogo izlucheniia [Coordinate-sensitive anisotropic sensor of laser radiation]. *Tekhnologiia i Konstruirovaniie v Elektronnoi Apparature*, 3, 42 [In Russian].
5. Ashcheulov A.A., Gutsul I.V., Rarenko A.I. (1999). Metod “prozrachnoi stenki” dlia kontrolia luchistykh potokov razlichnoi moshchnosti [The “transparent wall” method for control of radiant fluxes of various power]. *Tekhnologiia i Konstruirovaniie v Elektronnoi Apparature,* 2-3, 33-36 [In Russian].
6. Kosenkov E.M., Rarenko A.I., Shafraniuk V.P., Zaiets I.I. (2004). Research on structural perfection of CdSb crystals for thermoelectric converters depending on the technology of their growth and doping. *J.Thermoelectricity*, 3, 52-59.
7. Shafraniuk V., Dremliuzhenko S., Solodin S., Fodchuk P. (2017). Technological conditions’ effect on structural perfection of $Cd_{1-x}Mn_xTe$ crystals. *Functional Materials,* 24(4), 649-653.
8. Shafraniuk V. (2014). Maiatnykovi polosy v krystalakh i realna struktura CdTe [Pendellösung fringes in crystals and real structure in CdTe.] Materialy mizhnarodnoi naukovo-praktychnoi konferentsii “Informatsiini tekhnologii, ekonomika i pravo: stan ta perspektyvy rozvytku” – *Proc. of international scientific and practical conference “Information technologies, economics and justice: state-of-the art and development prospects”* (Chernivtsi, 2014). [in Ukrainian].
9. Kato N. (1961). A theoretical study of Pendellösungfringes. Part II. *Acta Cryst*., 14 (5), 526-532.
10. Cromer D. T. (1965). Anomalous dispersion corrections computed from self-consistent field relativistic Dirac-Slater wave functions. *Acta Cryst*., 18(1), 17-23.

Submitted 29.12.2017

V.A. Romaka *Doctor tech sciences*[1,2], **L.P. Romaka** *Candidate chem sciences*[3],
P.-F.Rogl *Doctor physics*[4], **V.V. Romaka** *Doctor tech sciences* [2,4],
Yu.V.Stadnyk *Candidate chem sciences* , **A.M.Horyn** *Candidate chem sciences* ,
I.M.Romaniv[3], **I.R.Opirskyy** *Candidate tech. science* [2]

[1]Ya. Pidstryhach Institute for Applied Problems of Mechanics and Mathematics
National Academy of Sciences of Ukraine, 3-b, Naukova Str., Lviv,
79060, Ukraine; *e-mail: vromaka@polynet.lviv.ua*;
[2]National University "Lvivska Politechnika", 12, S. Bandera Str., Lviv,
79013, Ukraine; *e-mail: vromakal@gmail.com*;
[3]Ivan Franko National University of Lviv, 6, Kyryla and Mefodiya Str.,
Lviv, 79005, Ukraine; *e-mail: stadnyk_yuriy@franko.lviv.ua*;
[4]Universität Wien, 42, Währinger Str., Wien, A-1090, Österreich;
e-mail: peter.franz.rogl@univie.ac.at.

ELECTRONIC STRUCTURE OF $ZrNi_{1-x}Rh_xSn$ THERMOELECTRIC MATERIAL

The features of the electronic and crystalline structures of $ZrNi_{1-x}Rh_xSn$ thermoelectric material which are based on the simultaneous generation of structural defects of acceptor and donor nature are studied. The mechanism of generating structural defects of the donor nature and the corresponding donor zone εD2 is shown, as a result of the occupation by the Ni atoms of tetrahedral vacant sites (vacancies). Substitution of Ni by Rh in the 4c position of $ZrNi_{1-x}Rh_xSn$ generates structural defects of acceptor nature and generates in the bandgap the impurity acceptor zone εA1, which together with the existing donor zone εD2 makes the semiconductor heavily doped and strongly compensated. The dependence of the bandgap εg of n-ZrNiSn and $ZrNi_{1-x}Rh_xSn$ is determined as a function of Ni concentration at tetrahedral vacant sites, and also in the case of vacancies in the 4a position of Zr atoms and acceptor zone εA2. Bibl. , Fig. .
Key words: electronic structure, resistivity, Seebeck coefficient.

Introduction

In the study of semiconductor thermoelectric material $ZrNi_{1-x}Rh_xSn$ [1] an interesting feature of the behavior of the Fermi level ε_F was found depending on the temperature and concentration of *Rh* impurity atoms, which *n-ZrNiSn* base semiconductor was doped with at optimization of kinetic characteristics for obtaining the maximum efficiency of thermal energy into electrical energy conversion [2]. This made it possible for the authors to suggest that, either in $ZrNi_{1-x}Rh_xSn$ simultaneously with the acceptors ε_A, donors ε_D^2 of unknown origin are generated with ionization energy greater than that of the acceptors, or these donors ε_D^2 already exist in the base semiconductor *n-ZrNiSn*. In so doing, the mechanism of generating donors ε_D^2 differs from the mechanism of "a priori doping" [3], according to which the crystalline structure of the compound *ZrNiSn* (structural type *MgAgAs*, space group $F\bar{4}3m$ [4]) is disordered as a result of a partial, up to 1 % (z = 0.01) filling with atoms of *Ni* ($3d^8 4s^2$) of the 4*a* position of *Zr* atoms (4d25*s*2), which generates donors ε_D^1 (*Ni* has more *d*-electrons).

In [1] it was established that in $ZrNi_{1-x}Rh_xSn$ at a temperature of $T = 80$ K and the lowest concentration of *Rh* ($x = 0.005$) the sign of the Seebeck coefficient $\alpha(x)$ is positive, since substitution of *Ni* atoms by *Rh*($4d^8 5s^1$) generates in crystal structural defects of acceptor nature (*Rh* has less *s*-electrons), and the Fermi level ε_F is arranged close to valence band ε_V. In a semiconductor, such a change in the sign of

$\alpha(x)$ occurs when, for example, the concentration of acceptors exceeds the concentration of donors, provided that the values of their ionization energies are close, or when donor ionization energy is greater than that of acceptor, and the temperature is sufficient for the acceptor ionization and too low for electron throw into conduction band (donor ionization) [5]. In its turn, the behavior of the Fermi level ε_F of $ZrNi_{1-x}Rh_xSn$ at a temperature $T = 80$ K is a classical reaction of *n*-type semiconductor doped with acceptors, which makes it heavily doped and strongly compensated [5]. We note that the behavior of the Fermi level ε_F and of the Seebeck coefficient $\alpha(x)$ of $ZrNi_{1-x}Rh_xSn$ were similar even at the higher concentrations of *Rh*, in particular for $x = 0.01$ та $x = 0.03$.

However, in $ZrNi_{1-x}Rh_xSn$, $x = 0.005$, $x = 0.01$ та $x = 0.03$ with a rise in temperature, $T_{inv} \geq 254$ K, $T_{inv} \geq 295$ K and $T_{inv} \geq 362$ K, respectively, the sign of the Seebeck coefficient became negative (as in *n-ZrNiSn*[3]). It means that at these concentrations of *Rh* the Fermi level ε_F of thermoelectric material $ZrNi_{1-x}Rh_xSn$ with a rise in temperature drifts from the valence band ε_V (low temperatures) to conduction band ε_C (high temperatures), intersecting hereby the midgap ε_g (full compensation of semiconductor) at temperatures $T_{inv} \approx 254$ K, $T_{inv} \approx 295$ K and $T_{inv} \approx 362$ K. And this is despite the fact that the concentration of acceptors is much in excess of the concentration of donors ε_D^1 of "a priori doping" [3] of *n-ZrNiSn*. This behavior of the Fermi level ε_F of $ZrNi_{1-x}Rh_xSn$ shows that in the crystal simultaneously with the acceptors ε_A there are donors ε_D^2 of unknown origin with greater ionization energy than that of acceptors, and the change in temperature leads to a change in the compensation ratio (the ratio of ionized acceptors and donors) of the semiconductor thermoelectric material.

The authors [1] outlined the most probable variants of the spatial arrangement of atoms in $ZrNi_{1-x}Rh_xSn$, which generates acceptors and donors in the crystal.

Thermodynamic calculations have established that it is energetically favourable to substitute *Ni* atoms in the *4c* crystallographic position by *Rh* atoms, which generates structural defects of acceptor nature, with accumulation of part of *Ni* atoms at tetrahedral vacant sites, which creates structural defects of donor nature. However, this information was not enough for a final understanding of the mechanism of generation of donors ε_D^2, since the results of thermodynamic calculations directly relate to the structural studies of $ZrNi_{1-x}Rh_xSn$ and do not allow them to be bound to electrokinetic studies [1].

The proposed work solves this problem. Based on the calculations of the distribution of the electronic density of states (DOS) for all possible variants of the spatial arrangement of atoms in the nodes of the elementary cell and in the interstitial sites of $ZrNi_{1-x}Rh_xSn$, a mechanism was found for the generation of structural defects of acceptor and donor nature which generate the corresponding energetic levels (zones) ε_A and ε_D^2 in the bandgap and are also consistent with the results of kinetic studies [1].

Investigation procedures

Calculations of the electronic structure $ZrNi_{1-x}Rh_xSn$ were performed by the Korringa-Kohn-Rostoker method (KKR) in coherent potential approximation (CPA) and local density approximation (LDA) [6]. The value of constant unit cell in *k*-space of size 10×10×10 and parametrization type of Moruzzi-Janak-Williams exchange-correlation potential were used [7]. The width of energy window was 22 eV, and the accuracy of calculating the position of the Fermi level ε_F was ±8 meV for 1000 energy values.

Research on the electronic structure of $ZrNi_{1-x}Rh_xSn$

To predict the behavior of the Fermi level ε_F, the bandgap ε_g and the kinetic characteristics of $ZrNi_{1-x}Rh_xSn$, the electronic density of states (DOS) was calculated for several variants of spatial arrangement of atoms in the unit cell nodes (or their absence – vacancies) and in the interstitial sites.

a) In the "ideal" (ordered) model of *n-ZrNiSn* structure (Fig.1*a*) atoms occupy positions according to structural type of *MgAgAs*[4]. Doping of *n-ZrNiSn* with acceptor impurity *Rh* (substitution of *Ni* atoms in the 4*c* position) generates structural defects of acceptor nature and creates impurity acceptor zone ε_A[1]. This doping forces the Fermi level ε_F to drift from conduction band ε_C to valence band ε_V, to intersect it at concentration $x \approx 0.05$ (Fig. 2): there will be dielectric-metal conductivity transition (Anderson transition [5, 8]).

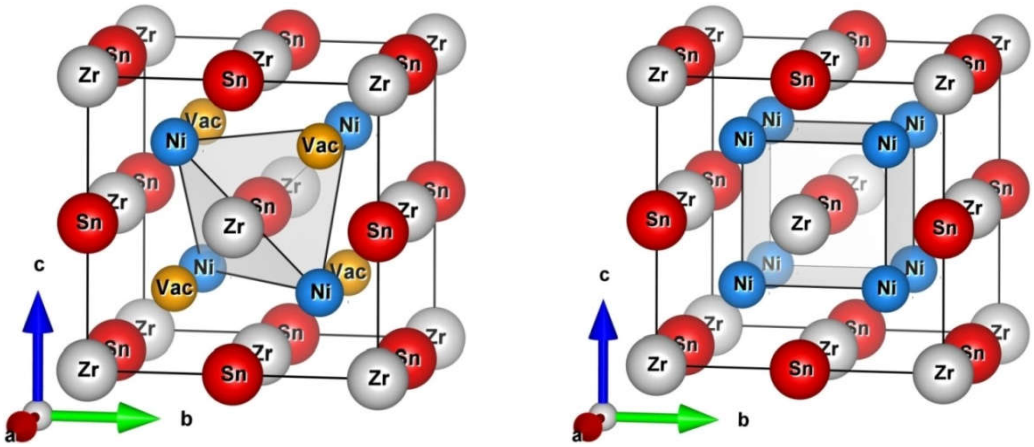

a) b)

Fig. 1. Transformation of crystalline structure of ZrNiSn compound (a) into $ZrNi_2Sn$ (b) at accumulation of excess Ni atoms at tetrahedral vacant sites of the structure (occupation of Vac by Ni atoms).

Calculations show that at the lowest concentrations of *Rh* atoms the electronic density of states at the Fermi level $g(\varepsilon_F)$ of $ZrNi_{1-x}Rh_xSn$ will first decrease, passing through the minimum at intersection by ε_F of the midgap $\varepsilon_g(x \approx 0.025)$, and then will monotonously increase. Moreover, at intersection by the Fermi level ε_F of the midgap ε_g and further drift towards valence band ε_V, the type of conductivity of $ZrNi_{1-x}Rh_xSn$ will change because of change in compensation ratio (the holes will become majority carriers) and the bandgap ε_g will decrease.

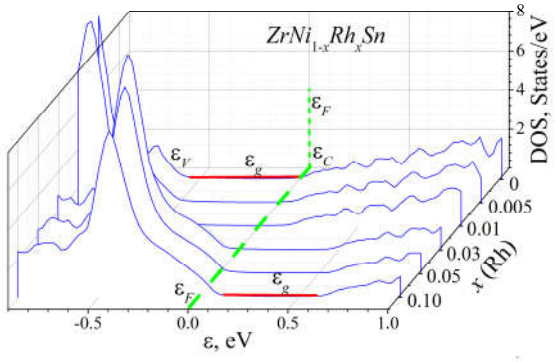

Fig. 2. Calculation of the distribution of the electronic density of states DOS for a "perfect" (ordered) model of $ZrNi_{1-x}Rh_xSn$ structure.

The model of $ZrNi_{1-x}Rh_xSn$ electronic structure (Fig. 2), calculated on the basis of ordered crystalline structure (Fig. 1*a*), cannot be taken as a basis for analyzing the results of electrokinetic research [1], because in principle does not involve the appearance of donors the presence of which is proven by the results of the experiment.

b). In [9,10], the authors first highlighted and studied the features of *ZrNiSn* crystalline structure which essentially redistributes the electronic density of states DOS (Fig. 3).

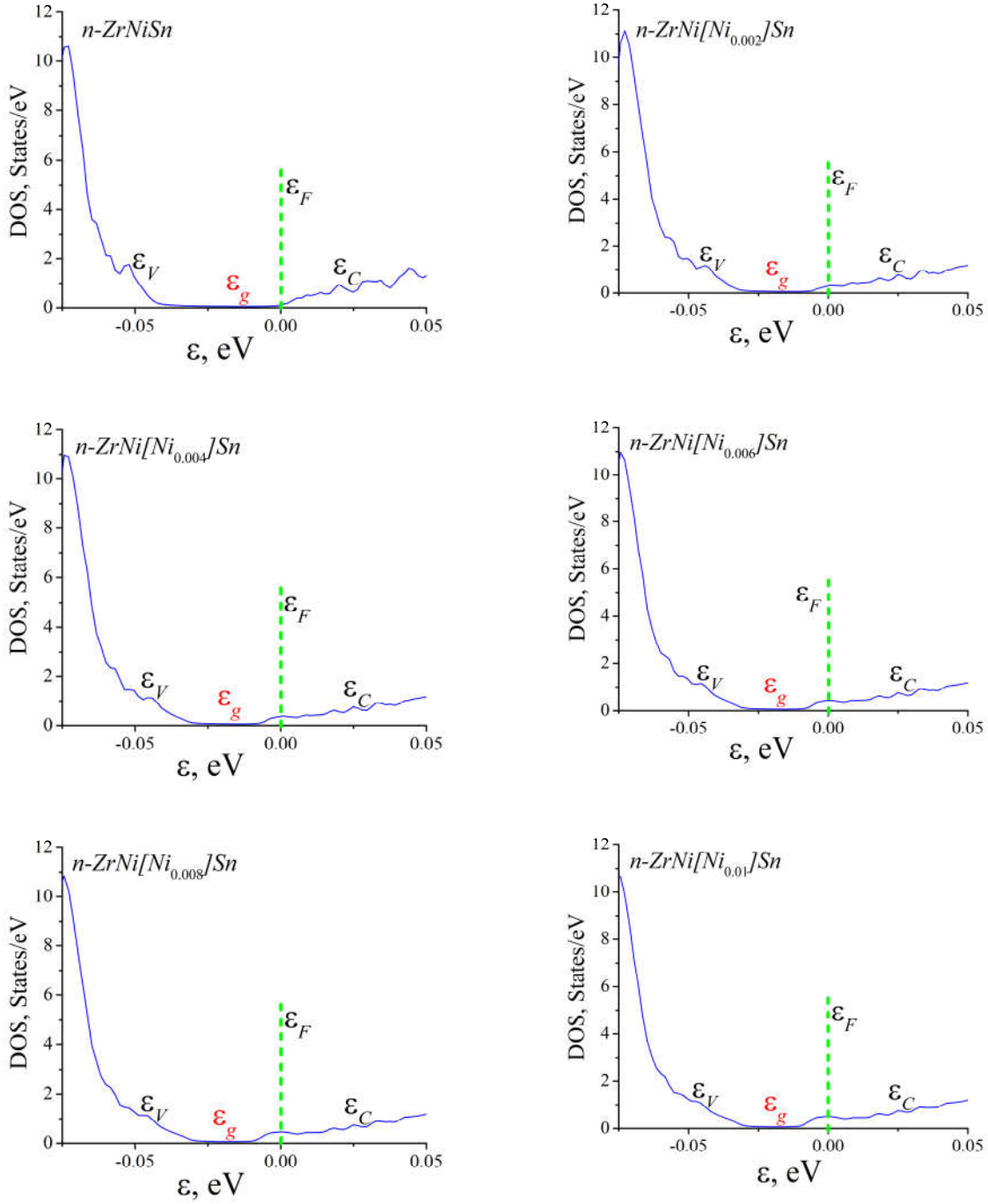

Fig. 3. Calculation of the distribution of the electronic density of states DOS of $ZrNi[Ni_y]Sn$.

According to the results of experimental studies [1] it was established that in the electrical conductivity of $ZrNi_{1-x}Rh_xSn$, $x \geq 0.01$ electrons are involved which in the model of "a priori doping" [3] at such *Rh* concentrations must be absent due to structure ordering. This forces one to consider in more detail the mechanism of generation of structural defects of donor nature. The specific feature of *ZrNiSn* crystalline structure is the presence of tetrahedral vacant sites (Fig. 1*a*) which occupy ~ 24 % of unit cell volume. The authors [9,10] revealed the effect of accumulation of excess atoms of Ni_{1+y} (later $[Ni_y]$) at the vacant sites of *ZrNiSn* structure without structure variations to concentrations of $y \leq 0.30$, and compound formula is transferred into $ZrNi[Ni_y]Sn$.

On the other hand, the analysis of the phase equilibrium diagram of the *Zr-Ni-Sn* system showed that alongside with the compound *ZrNiSn* here is a *related* compound $ZrNi_2Sn$ (structural type $MnCu_2Al$, spatial group $Fm\bar{3}m$ [4]). The term *"related"* means the following. Assuming that the tetrahedral vacant sites in the *ZrNiSn* structure (Fig. 1*a*) are occupied by *Ni* atoms and considering the vacant site as a vacancy (Vac) of the 4*d* crystallographic position in the $ZrNi_2Sn$ structure (Fig. 1b), the occupation by [Ni_y] atoms of the 4*d* position (filling the vacancy) will change crystal symmetry, and at certain concentrations of *Ni* the compound $ZrNi_2Sn$ is formed. In this context, it is important to note that due to different symmetry of *ZrNiSn* and $ZrNi_2Sn$ compounds there is no continuous solid solution between them [4]. This means that up to concentrations of $y \le 0.30$ [Ni_y] atoms generate structural defects of donor nature in *ZrNiSn*, and at higher concentrations ($y > 0.30$) already in the structure of the compound $ZrNi_2Sn$, additional *N* atoms will fill the 4*d* crystallographic position. It also turned out that the bandgap ε_g of $ZrNi[Ni_y]Sn$ depends on the concentration of [Ni_y] at the vacant sites.

Fig. 3 shows the results of refined calculation of *DOS* for $ZrNi[Ni_y]Sn$. The point is that in [9,10] at the calculations of DOS the width of the energy window was 16 eV, which is insufficient to get the exhaustive information on the distribution of the electronic density of states. For this reason, we performed calculations of DOS of $ZrNi[Ni_y]Sn$ for the width of the energy window 22 eV, the results of which are shown in Fig. 3. We can see that in the *n-ZrNiSn*, the Fermi level ε_F is located near the conduction band ε_C, while at the lowest *Ni* concentrations in the 4*d* position near the ε_C zone, the donor region ε_D^2 is formed on which ε_F is arranged. Such doping is accompanied by reduction of compensation ratio and bandgap $\varepsilon_g$of thermoelectric material (Fig. 4).

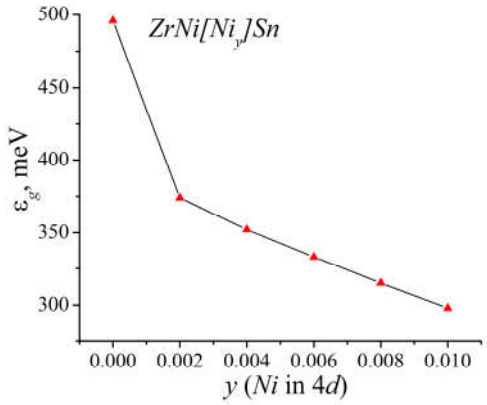

Fig. 4. Change in the values of bandgap ε_g of $ZrNi[Ni_y]Sn$.

With increase in concentration of [Ni_y], the Fermi level ε_F will intersect the bottom of conduction band ε_C: there will be dielectric-metal conductivity transition (Anderson transition) [5,8]. It should be noted that in the experimental studies [1], the heavy doping of *n-ZrNiSn* by Rh impurity also led to a decrease (~ 2.5 times) of the bandgap width ε_g of $ZrNi_{1-x}Rh_xSn$.

It is important to specify that in the experimental studies the compensation ratio is determined as the ratio between ionized acceptors and donors, and ionization process proper (throw of carriers to continuous energy zones) depends on the temperature (carrier energy). In case of calculations it is *a priori* assumed that acceptors are ionized, so compensation ratio is determined as the concentration ratio of acceptors and donors. In addition, under the term "bandgap" ε_g we mean the energy gap between the vertices of continuous energy zones and not between the mobility thresholds [8] of these zones or the "tails" of the zones [5]. Thus, occupation by *Ni* atoms of tetrahedral vacant sites ([Ni_y]) in the structure of compound *ZrNiSn* is an efficient mechanism for generating structural defects of donor nature, reducing simultaneously the value of bandgap ε_g and compensation ratio.

c) The third model studies the influence on the location of the Fermi level ε_F and the value of ε_g of the substitution of *Ni* atoms by *Rh* in the 4*c* crystallographic position at the presence at tetrahedral sites of various concentrations of *Ni* atoms: $ZrNi_{1-x}Rh_x[Ni_{0.002}]Sn$ (Fig. 5) $ZrNi_{1-x}Rh_x[Ni_{0.004}]Sn$ (Fig. 6).

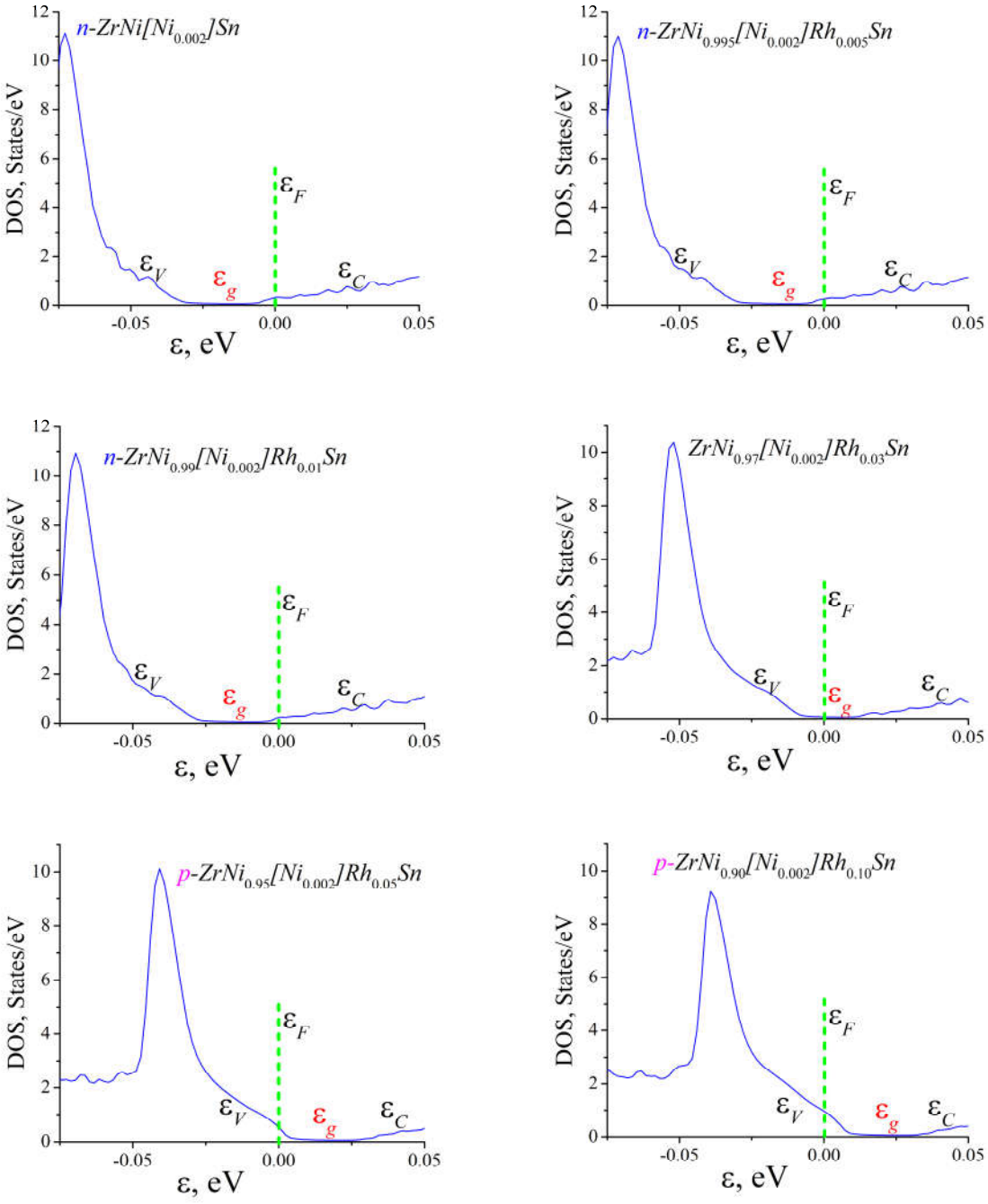

Fig. 5.Calculation of the distribution of the electronic density of states DOS of $ZrNi_{1-x}Rh_x[Ni_{0.002}]Sn$.

As can be seen in Fig. 5, in $ZrNi[Ni_{0.002}]Sn$ the Fermi level ε_F is located in donor band ε_D[2] close to the bottom of conduction band ε_C. Introduction into $ZrNi[Ni_{0.002}]Sn$ of the lowest in the experiment concentration of impurity *Rh* ($x = 0.005$) generates structural defects of acceptor nature and impurity acceptor zone ε_A[1], which does not lead to apparent motion of the Fermi level ε_F from conductivity band deep into bandgap ε_g. During the experimental investigations, at ionization of acceptors and donors, the electrical conductivity of $ZrNi_{0.995}Rh_{0.005}[Ni_{0.002}]Sn$ will be determined by electrons which will cause

negative values of the Seebeck coefficient $\alpha(x)$. The Fermi level ε_F behaves in a similar way at higher concentrations of impurity *Rh* in $ZrNi_{0.99}Rh_{0.01}[Ni_{0.002}]Sn$.

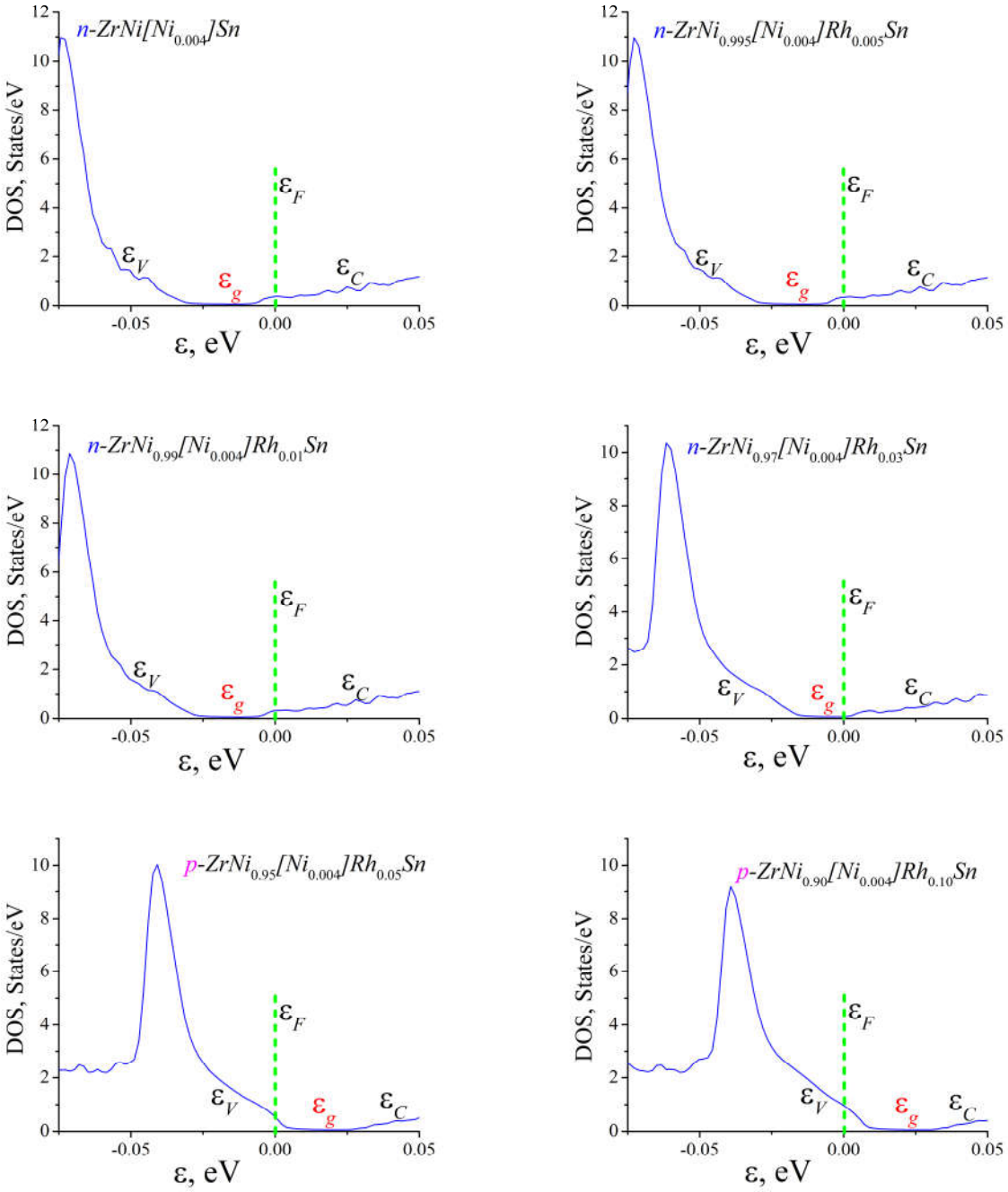

Fig. 6.Calculation of the distribution of the electronic density of states DOS of $ZrNi_{1-x}Rh_x[Ni_{0.004}]Sn$.

In the case of $ZrNi_{0.97}Rh_{0.03}[Ni_{0.002}]Sn$ the Fermi level ε_F is located close to the midgap ε_g, and the sign of the Seebeck coefficient $\alpha(x)$ is extremely sensitive to the smallest changes in semiconductor compensation ratio. And only at concentration ratio *Ni*/*Rh* of thermoelectric material $ZrNi_{0.95}Rh_{0.05}[Ni_{0.002}]Sn$ the Fermi level ε_F will come to the ceiling of the valence band ε_V, which will lead to inversion of the electrical conductivity type, and holes will become the majority carriers. With increase in the concentration of *Rh* impurity ($x = 0.10$), the Fermi level ε_F will intersect the valence band ε_V, and conductivity of $ZrNi_{0.90}Rh_{0.10}[Ni_{0.002}]Sn$ will be metallic in nature (Anderson transition will take place

[5, 8]). Note that the obtained results of calculating the behavior of the Fermi level ε_F, the bandgap ε_g, the Seebeck coefficient $\alpha(x)$ of $ZrNi_{1-x}Rh_x[Ni_{0.002}]Sn$ coincide with the results of experimental studies [1].

For comparison, we give the results of calculating DOS for greater concentration of *Ni* atoms ($y = 0.004$) at tetrahedral vacant sites (Fig. 6). Thus, due to considerable concentration of generated structural defects of donor nature and the absence of *Rh* impurity atoms, the Fermi level ε_F of $ZrNi[Ni_{0.004}]Sn$ is arranged in the resulting donor band ε_D^2 which merged with the bottom of conduction band ε_C, having formed a "tail" of the band [5] (or mobility threshold [8]). With increase in *Rh* concentration to the values $x = 0.005 – 0.03$, there will be neutralization of donors and compensation ratio of $ZrNi_{1-x}Rh_x[Ni_{0.004}]Sn$ will increase, which will force the Fermi level ε_F to leave the impurity donor band ε_D^2 and drift toward the midgap ε_g. The inversion of conductivity type of $ZrNi_{1-x}Rh_x[Ni_{0.004}]Sn$ will occur at *Rh* concentrations $x \geq 0.05$, when holes will become the majority carriers. Note that the behavior of the Fermi level ε_F in the model of $ZrNi_{1-x}Rh_x[Ni_{0.004}]Sn$ differs from the results of the experiment [1].

d) Let us consider another variant of spatial arrangement of atoms in *ZrNiSn* and $ZrNi_{1-x}Rh_xSn$, that demonstrates mechanisms of generation of structural defects of acceptor and donor nature, as well as allows efficient control of the position of the Fermi level ε_F and the bandgap ε_g of thermoelectric material . Recall that the mechanism of "a priori doping" of *n-ZrNiSn* [3] involves the presence of vacancies in the 4*a* crystallographic position of *Zr* atoms that are occupied by *Ni* atoms, generating in this case the donor band ε_D^1. We were interested in the way how DOS, the position of the Fermi level ε_F and the bandgap ε_g in *n-ZrNiSn* and $ZrNi_{1-x}Rh_xSn$ will change in the case when vacancies (λ) in the 4*a* position of *Zr* atoms are not occupied by *Ni* atoms, but part of *Ni* atoms will fill tetrahedral vacant sites of ($[Ni_y]$) structure?

Fig. 7 shows the results of calculating DOS for $Zr_{1-\lambda}Ni[Ni_y]Sn$ (*a*) and $Zr_{1-\lambda}Ni_{1-x}Rh_x[Ni_y]Sn$(b) in the presence of vacancies (λ) in the 4*a* position of *Zr* atoms, and Ni_y atoms in the 4*d* position ($[Ni_y]$). In both cases the concentration of vacancies in the 4*a* and *Ni* atoms in the 4*d* is the same: $\lambda = 0.0016$, $y = 0.0018$.

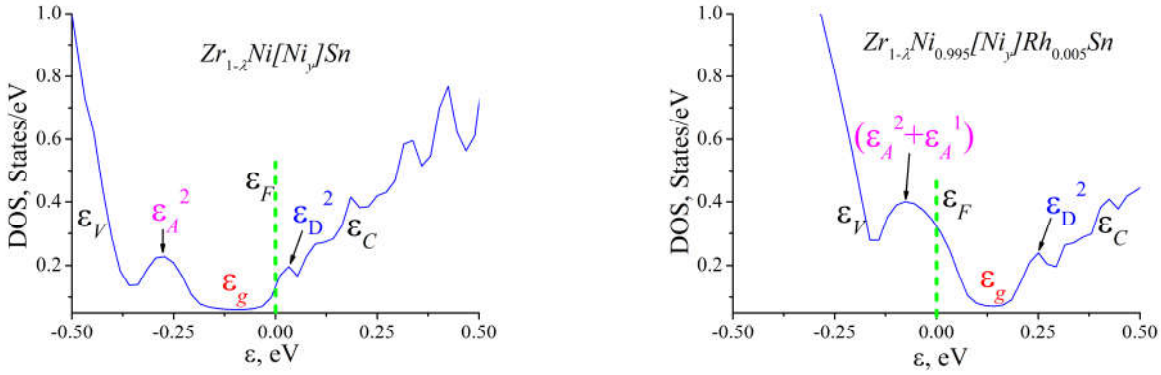

a) *b)*

Fig. 7.Calculation of the distribution of the electronic density of states DOS of $Zr_{1-\lambda}Ni[Ni_y]Sn$ (a) and $Zr_{1-\lambda}Ni_{1-x}Rh_x[Ni_y]Sn$ (b) at concentrations: λ=0.0016 and y=0.0018.

In the case of $Zr_{1-\lambda}Ni[Ni_y]Sn$, vacancies generate energy acceptor levels in the bandgap, and acceptor zone ε_A^2 was formed close to valence band ε_V (Fig. 7*a*). At the same time, *Ni* atoms in the 4*d* position generate donor levels, and donor zone ε_D^2 appears close to conduction band ε_C. As long as the concentration of donors ($y = 0.0018$) is greater than the concentration of acceptors ($\lambda = 0.0016$), the Fermi level ε_F is fixed in the donor zone ε_D^2.

The presence of vacancies in the 4*a*(λ) position of *Zr* atoms, just as *Ni* atoms at tetrahedral vacant sites of the structure leads to decrease in the values of bandgap ε_g of *n-ZrNiSn* (as in the experiment [1])

and is the mechanism of generating the defects of acceptor and donor nature. Fig. 8 shows a dependence of bandgap ε_g of $Zr_{1-\lambda}Ni[Ni_{0.002}]Sn$ on the concentration of vacancies (λ). It is seen that the values of ε_g decrease from the values of $\varepsilon_g(y = 0.002) = 244$ meV to $\varepsilon_g(y = 0.003) = 220$ meV and $\varepsilon_g(y = 0.01) = 146$ meV.

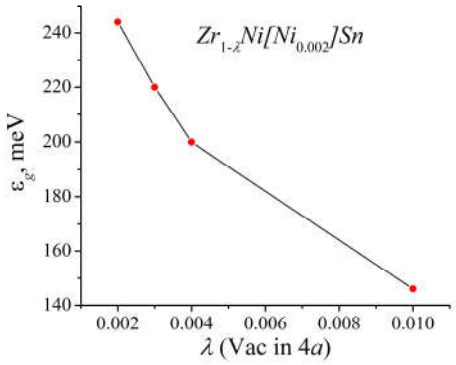

Fig. 8.Change in the values of bandgap ε_g in $Zr_{1-\lambda}Ni[Ni_{0.002}]Sn$.

Increasing the concentration of donors in *n-ZrNiSn* by increasing the concentration of *Ni* at tetrahedral vacant sites to $y = 0.003$, we can retard decreasing the values of bandgap ε_g of $Zr_{1-\lambda}Ni[Ni_{0.003}]Sn$, for instance, from the values of $\varepsilon_g(y = 0.002) = 249$ meV to $\varepsilon_g(y = 0.003) = 226$ meV. Note that in the calculation of DOS (represented in Fig. 7*a*) in $Zr_{1-\lambda}Ni[Ni_y]Sn$ semiconductor, $\lambda = 0.0016$ and $y = 0.0018$, the bandgap $\varepsilon_g = 252$ meV.

In the case of thermoelectric material $Zr_{1-\lambda}Ni_{0.995}Rh_{0.005}[Ni_{0.0018}]Sn$, $\lambda = 0.0016$, the Fermi level ε_F left the donor zone $\varepsilon_D{}^2$ (Fig. 7*b*) and was arranged at the edge of acceptor zone formed by two zones $\varepsilon_A{}^1$ and $\varepsilon_A{}^2$. It is seen that in $Zr_{1-\lambda}Ni_{0.995}Rh_{0.005}[Ni_{0.0018}]Sn$ the donor zone is the same as in the case of $Zr_{1-\lambda}NiSn$, and the acceptor zone became more powerful due to a greater concentration of acceptors ($\varepsilon_A{}^1$ and $\varepsilon_A{}^2$). Such a transformation of the acceptor zone is understandable, since in the semiconductor thermoelectric material there exist two mechanisms for generation of acceptors:

– substitution of *Ni* atoms by *Rh*y in the 4*c* position (generation of acceptor zone $\varepsilon_A{}^1$);

– the presence of vacancies (λ) in the 4*a* position of Zr atoms (generation of acceptor zone $\varepsilon_A{}^2$) .

The represented approach to simulation of energy levels (bands) in the bandgap of semiconductor thermoelectric material $ZrNi_{1-x}Rh_xSn$ demonstrates extreme sensitivity of its fundamental parameters, in particular, position of the Fermi level ε_F, density of states at the Fermi level $g(\varepsilon_F)$, the bandgap ε_g, etc. to the smallest structural changes of material. On the other hand, the probability of existence of a considerable number of vacancies in a multi-component compound at the presence of small-size impurity atoms is small.

Conclusion

The above investigations show complex changes in the crystalline and electronic structures of the semiconductor thermoelectric material $ZrNi_{1-x}Rh_xSn$, the basis of which is determined by the simultaneous generation of structural defects of acceptor and donor nature. The mechanism of generation of structural defects of donor nature and the corresponding donor zone $\varepsilon_D{}^2$ in *n-ZrNiSn* is shown as a result of arrangement of *Ni* atoms at tetrahedral vacant sites (vacancies). The substitution in $ZrNi_{1-x}Rh_xSn$ in the 4*c* position of *Ni* atoms by *Rh* generates structural defects of acceptor nature and creates in the bandgap the impurity acceptor zone $\varepsilon_A{}^1$, which together with the existing donor zone $\varepsilon_D{}^2$ makes the semiconductor heavily doped and strongly compensated. The dependence of bandgap ε_g of *n-ZrNiSn* and $ZrNi_{1-x}Rh_xSn$ on the concentration of *Ni* at tetrahedral vacant sites ($[Ni_y]$), as well as in the case of vacancies in the 4*a*

position of *Zr* atoms was established, which is consistent with the results of the experiment [1]. The obtained results will allow *purposeful* optimization of thermoelectric material characteristics to obtain the maximum efficiency of thermal into electric energy conversion [2].

The work was performed in the framework of Ministry of Education of Ukraine grant (№ 0118U003609) and Austrian BMWFW Ernst Mach grant (ICM-2017-06580).

References

1. Ромака В.А., Ромака Л.П.,Рогль П.-Ф., Ромака В.В., Стадник Ю.В, Горинь А.М., Опірський І.Р. Особливості механізмів електропровідності термоелектричного матеріалу $ZrNi_{1-x}Rh_xSn$, Термоелектрика, № 5, 24-40 (2017).
2. Анатычук Л.И.Термоэлементы и термоэлектрическиеустройства. Справочник. Киев, Наукова думка, 1979, 768 с.
3. Romaka V.A., Fruchart D., Hlil E.K., Gladyshevskii R.E., Gignoux D., Romaka V.V., Kuzhel B.S. and Krayjvskii R.V. Features of an Intermetallic *n-ZrNiSn* Semiconductor Heavily Doped with Atoms of Rare-EarthMetals,Semiconductors, 44(№ 3), 293–302 (2010).
4. Ромака В.В., Ромака Л.П., Крайовський В.Я., Стадник Ю.В. Станіди рідкісноземельних та перехідних металів. Львів, Львівська політехніка, 2015, 224 с.
5. Шкловский Б.И., Эфрос А.Л. Электронные свойства легированных полупроводников. Москва, Наука, 1979, 416 с.
6. Schroter M., Ebert H., Akai H., Entel P., Hoffmann E., Reddy G.G. First-Principles Investigations of Atomic Disorder Effects on Magnetic and Structural Instabilities in Transition-Metal Alloys, Phys. Rev. B 52, 188–209 (1995).
7. Moruzzi V.L., Janak J.F., Williams A.R. Calculated Electronic Properties of Metals, NY, 1978, 348 P.
8. Мотт Н.,Дэвис Т. Электронныепроцессы в некристаллическихвеществах, Москва, Мир, 1982, 368 с.
9. Romaka V.A., Rogl P., Romaka V.V., StadnykYu.V., Hlil E.K.,KraiovskiiV.Ya., and Goryn' A.M. Effect of the Accumulation of Excess *Ni* Atoms in the CrystalStructure of the Intermetallic Semiconductor *n-ZrNiSn*, Semiconductors, 47(№ 7), 892–898 (2010).
10. Romaka V.V., Rogl P., Romaka L., Stadnyk Yu., Grytsiv A., Lakh O., Krayovsky V. Peculiarites of Structural disor derin *Zr*- and*Hf*- Containing Heusler and Half-heusler Stannides, Intermetallics, 35, 45-52 (2013).

Submitted 11.12.2017

Ромака В.А. *док. техн. наук.*[1,2], **Ромака Л.П.** *канд. хім. наук.*[3],
Рогль П.-Ф. *док. фізики*[4], **Ромака В.В.** *док. техн. наук.*[2,4],
Стадник Ю.В. *канд. хім. наук.*[3], **Горинь А.М.** *канд. хім. наук.*[3],
Романів І.М.[3], **Опірський І.Р.** *канд. техн. наук.*[2]

[1]Інститут прикладних проблем механіки і математики
імені Я.С. Підстригача НАН України,
вул. Наукова, 3-б, Львів, 79060, Україна,

e-mail: vromaka@polynet.lviv.ua;
[2]Національний університет "Львівська політехніка",
вул. С. Бандери, 12, Львів, 79013, Україна,
e-mail: vromakal@gmail.com;
[3]Львівський національний університет ім. І. Франка,
вул. Кирила і Мефодія, 6, Львів, 79005, Україна,
e-mail: stadnyk_yuriy@franko.lviv.ua;
[4]Віденський університет, вул. Верінгерштрасе, 42,
Відень, А-1090, Австрія,
e-mail: peter.franz.rogl@univie.ac.at.

ЕЛЕКТРОННА СТРУКТУРА ТЕРМОЕЛЕКТРИЧНОГО МАТЕРІАЛУ $ZrNi_{1-x}Rh_xSn$

Досліджено особливості електронної та кристалічної структур термоелектричного матеріалу $ZrNi_{1-x}Rh_xSn$, в основі яких одночасне генерування структурних дефектів акцепторної та донорної природи. Показано механізм генерування структурних дефектів донорної природи та відповідної донорної зони ε_D^2 в n-ZrNiSnяк результат зайняття атомами Niтетраедричних пустот структури (вакансій). Заміщення в $ZrNi_{1-x}Rh_xSn$ в позиції 4c атомів Ni на Rh генерує структурні дефекти акцепторної природи та породжує у забороненій зоні домішкову акцепторну зону ε_A^1, що разом з існуючою донорною зоною ε_D^2робить напівпровідник сильно легованим та сильно компенсованим. Встановлена залежність ширини забороненої зони ε_gn-ZrNiSnmaZrNi$_{1-x}$Rh$_x$Snвід концентрації атомів Niутетраедричних пустотах, а також у випадку появи вакансій у позиції 4аатомівZr при генеруванні акцепторної зони ε_A^2.
Ключові слова: електронна структура, електроопір, коефіцієнт термоЕРС.

Ромака В.А. *док. техн. наук.*[1,2], **Ромака Л.П.** *канд. хим. наук.*[3],
Рогль П.-Ф. *док. физики*[4], **Ромака В.В.** *док. техн. наук.*[2,4],
Стадник Ю.В. *канд. хим. наук.*[3], **Горинь А.М.** *канд. хим. наук.*[3],
Романив И. М.[3],**Опирский И.Р.** *канд. техн. наук.*[2]

[1]Институт прикладных проблем механики и математики
им. Я.С. Пидстригача НАН Украины, ул. Научная, 3-б,
Львов, 79060, Украина, *e-mail: vromaka@polynet.lviv.ua*;
[2]Национальный университет "Львовская политехника",
ул. С. Бандеры, 12, Львов, 79013, Украина,
e-mail: vromakal@gmail.com;
[3]Львовский национальный университет им. І. Франко,
ул. Кирилла и Мефодия, 6, Львов, 79005, Украина,
e-mail: stadnyk_yuriy@franko.lviv.ua;
[4]Венский университет, ул. Верингерштрассе, 42,
Вена, А-1090, Австрия,
e-mail: peter.franz.rogl@univie.ac.at.

ЭЛЕКТРОННАЯ СТРУКТУРА ТЕРМОЭЛЕКТРИЧЕСКОГО МАТЕРИАЛА $ZrNi_{1-x}Rh_xSn$

Исследована особенности электронной и кристаллической структур термоэлектрического материала $ZrNi_{1-x}Rh_xSn$, в основе которых одновременное генерирование структурных дефектов акцепторной и донорної природы. Показан механизм генерирования структурных дефектов донорної природы и соответствующей донорної зоны εD^2 в n-$ZrNi_{1-x}Rh_xSn$ к результат занятия атомами Ni тетраедричних пустот структуры (вакансий). Замещение в $ZrNi_{1-x}Rh_xSn$ в позиции 4 с атомов Ni на Rh генерує структурные дефекты акцепторной природы и порождает в запрещенной зоне домішкову акцепторную зону εA^1, что вместе с существующей донорною зоной εD^2 делает полупроводник сильно легированным и сильно компенсированным. Установленная зависимость ширины запрещенной зоны ε_g n-ZrNiSn та $ZrNi_{1-x}Rh_xSn$ від концентрации атомов Ni утетраедричних пустотах, а также в случае появления вакансий в позиции 4атомов Zr при генерировании акцепторной зоны εA^2.

Ключевые слова: электронная структура, электросопротивление, коэффициент термоЕРС.

References

1. Romaka V.A., Romaka L.P., Rogl P.-F., Romaka V.V., Stadnyk Yu.V., Horyn A.M., Opirskyy I.R. (2017). Features of electrical conductivity mechanisms of *$ZrNi_{1-x}Rh_xSn$* thermoelectric material. *J.Thermoelectricity*, 5, 24 – 40.
2. Anatychuk L.I. (1979). *Termoelementy i termoelektricheskiie ustroistva. Spravochnik [Thermoelements and thermoelectric devices. Handbook]*. Kyiv: Naukova Dumka [in Russian].
3. RomakaV.A., Fruchart D., Hlil E.K., Gladyshevskii R.E., Gignoux D., RomakaV.V., Kuzhel B.S. and Krayjvskii R.V. (2010). Features of an intermetallic *n-ZrNiSn s*emiconductor heavily doped with atoms of rare-earth metals. *Semiconductors*, 44 (3), 293 – 302.
4. Romaka V.V., Romaka L.P., Krayovskyy V.Ya., Stadnyk Yu.V. (2015). *Stanidy ridkisnozemelnykh ta perekhidnykh metaliv [Stannides of rare-earth and transient metals]*. Lviv: Lvivska Politechnika [In Ukrainian].
5. Shklovskyi B.I., Efros A.L. (1979). *Elektronnnyie svoistva legirovannykh poluprovodnikov [Electronic properties of doped semiconductors]*. Moscow: Nauka [in Russian].
6. Schroter M., Ebert H., Akai H., Entel P., Hoffmann E., Reddy G.G. (1995). First-principles investigations of atomic disorder effects on magnetic and structural instabilities in transition-metal alloys. *Phys. Rev. B* 52, 188 – 209.
7. Moruzzi V.L., Janak J.F., Williams A.R. (1978). Calculated electronic properties of metals. NY.
8. Mott H., Davis T. (1982). *Elektronnyiie processy v nekristallicheskikh veshchestvakh [Electronic processes in noncrystalline substances]*. Moscow: Mir [Russian transl].
9. Romaka V.A., Rogl P., Romaka V.V., Stadnyk Yu.V., Hlil E.K., Krayovskyy V.Ya., and Horyn A.M. (2010). Effect of the accumulation of excess *Ni a*toms in the crystal structure of the intermetallic semiconductor *n-ZrNiSn. Semiconductors*, 47(7), 892 – 898 .
10. Romaka V.V., Rogl P., Romaka L., Stadnyk Yu., Grytsiv A., Lakh O., Krayovsky V. (2013). Peculiarites of structural disorder in *Zr*- and *Hf*-containing Heusler and half-Heusler stannides. *Intermetallics*, 35, 45 – 52.

Submitted 11.12.2017

L. I. Anatychuk

L. I. Anatychuk[1,2] *acad. National Academy of Sciences of Ukraine*,
A. V. Prybyla[1,2] *Candidate Phys.-math. Sciences*

[1]Institute of Thermoelectricity of the NAS and MES of Ukraine, 1, Nauky str, Chernivtsi, 58029, Ukraine;
[2]Yu.Fedkovych Chernivtsi National University, 2, Kotsiubynskyi str., Chernivtsi, 58000, Ukraine
e-mail: anatych@gmail.com

A. V. Prybyla

ON THE COEFFICIENT OF PERFORMANCE OF THERMOELECTRIC LIQUID-LIQUID HEAT PUMPS WITH REGARD TO ENERGY LOSS FOR HEAT CARRIER TRANSFER

This paper presents the results of research on the coefficient of performance of thermoelectric liquid-liquid heat pump with regard to energy loss for heat carrier transfer, in particular, for its use as a high-performance heater for space –purpose water regeneration device. Bibl. 9, Fig. 2.
Key words: thermoelectric heat pump, efficiency, distillation unit, heat exchanger.

Introduction

General characterization of the problem. The use of thermoelectric heat pumps (THP) in air and liquid conditioning systems, special-purpose evaporators is due to their unique properties [1 – 5].

An example of efficient use of thermoelectric heat pumps is systems of water recovery from liquid biowaste aboard manned spacecrafts (urine, atmospheric condensate, sanitary and hygienic water) [4, 5].

The paper [6] presents the results of calculations of the limiting possibilities of thermoelectric liquid-liquid heat pumps with the use of modern computer design methods. In [7], studies were made of the influence on the efficiency of thermoelectric heat pump of the quality of heat exchange system which assures heat flux transfer to and from thermoelectric modules. However, these studies were performed without taking into account the influence of energy on heat carrier transfer in the heat exchange system of the thermoelectric heat pump, which is essential in the conditions of this problem.

The purpose of our work is to study the coefficient of performance of thermoelectric liquid-liquid heat pump with regard to the energy loss for heat carrier transfer, which will enable us to determine the optimal ratio between the energy spent on heat carrier pumping and total efficiency of thermoelectric heat pump.

Physical model of THP

A physical model of thermoelectric liquid-liquid heat pump is represented in Fig. 1. It comprises a system of heat exchangers 1 assuring passage of heat flux Q_h through the hot side of thermoelectric modules, thermoelectric modules 3, heat exchangers 2 assuring passage of heat flux Q_c through the cold side of thermoelectric modules and a system of hydraulically bound channels 4 providing for circulation of liquid in the thermoelectric heat pump.

The model takes into account temperature difference losses in heat exchangers, as well as energy losses on pumping of heat carrier through heat exchange system.

To assure optimal operation of thermoelectric modules, each of them has individual power supply.

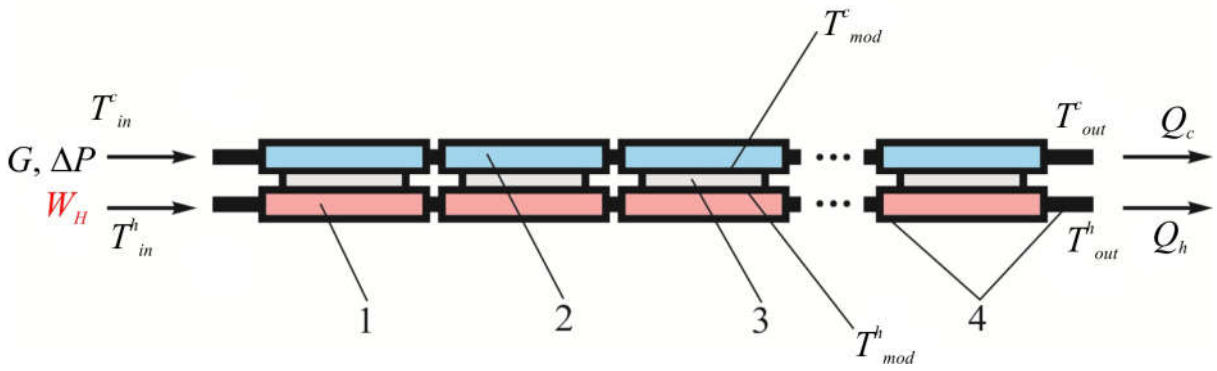

Fig. 1. Physical model of thermoelectric heat pump.

Mathematical and computer description of the model

To describe heat and electric current fluxes, we will use the laws of conservation of energy

$$div\vec{E} = 0 \tag{1}$$

and electric charge

$$div\vec{j} = 0, \tag{2}$$

where

$$\vec{E} = \vec{q} + U\vec{j}, \tag{3}$$

$$\vec{q} = \kappa\nabla T + \alpha T\vec{j}, \tag{4}$$

$$\vec{j} = -\sigma\nabla U - \sigma\alpha\nabla T. \tag{5}$$

Here, $\vec{E}$ is energy flux density, $\vec{q}$ is thermal flux density, $\vec{j}$ is electric current density, U is electric potential, T is temperature, α, σ, κ are the Seebeck coefficient, electric conductivity and thermal conductivity.

With regard to (3) – (5), one can obtain

$$\vec{E} = -(\kappa + \alpha^2\sigma T + \alpha U\sigma)\nabla T - (\alpha\sigma T + U\sigma)\nabla U. \tag{6}$$

Then the laws of conservation (1), (2) will acquire the form:

$$-\nabla\left[(\kappa + \alpha^2\sigma T + \alpha U\sigma)\nabla T\right] - \nabla\left[(\alpha\sigma T + U\sigma)\nabla U\right] = 0, \tag{7}$$

$$-\nabla(\sigma\alpha\nabla T) - \nabla(\sigma\nabla U) = 0. \tag{8}$$

These nonlinear differential equations of second order in partial derivatives (7) and (8) determine the distribution of temperature T and potential U in thermoelements.

An equation describing the process of heat transport in the walls of heat exchangers in the steady-state case is written as follows:

$$\nabla(-k_1 \cdot \nabla T_1) = Q_1. \tag{9}$$

where k_1 is thermal conductivity of heat exchanger walls, ∇T_1 is temperature gradient, Q_1 is heat flux.

The processes of heat-and-mass transfer of heat carriers in heat exchanger channels in the steady-state case are described by equations [8]

$$-\Delta p - f_D \frac{\rho}{2d_h} v|\vec{v}| + \vec{F} = 0, \tag{10}$$

$$\nabla(A\rho\vec{v}) = 0, \tag{11}$$

$$\rho AC_p\vec{v}\cdot\nabla T_2 = \nabla\cdot Ak_2\nabla T_2 + f_D\frac{\rho A}{d_h}|\vec{v}|^3 + Q_2 + Q_{wall}, \tag{12}$$

where p is pressure, ρ is heat carrier density, A is cross-section of the tube, $\vec{F}$ is the sum of all forces, C_p is heat carrier heat capacity, T_2 is temperature, $\vec{v}$ is velocity vector, k_2 is heat carrier thermal conductivity, f_D is the Darcy coefficient, $d = \frac{4A}{Z}$ is effective diameter, Z is perimeter of tube wall, Q_2 is heat which is released due to viscous friction [W/m] per unit length of heat exchanger, Q_{wall} is heat flux coming from the heat carrier to the tube walls [W/m]

$$Q_{wall} = h\cdot Z\cdot(T_1 - T_2), \tag{13}$$

where h is heat exchange coefficient which is found from equation

$$h = \frac{Nu\cdot k_2}{d}. \tag{14}$$

The Nusselt number is found with the use of the Gnielinski equation ($3000<Re<6\cdot10^6$, $0.5<Pr<2000$)

$$Nu = \frac{\left(\frac{f_d}{8}\right)(Re-1000)Pr}{1+12.7\left(\frac{f_d}{8}\right)^{\frac{1}{2}}\left(Pr^{\frac{2}{3}}-1\right)}, \tag{15}$$

where $Pr = \frac{C_p\mu}{k_2}$ is the Prandtl number, μ is dynamic viscosity, $Re = \frac{\rho vd}{\mu}$ is the Reynolds number.

The Darcy coefficient f_D is found with the use of the Churchill equation for the entire spectrum of the Reynolds number and all the values of e/d (e is roughness of wall surface)

$$f_D = 8\left[\left(\frac{8}{Re}\right)^{12} + (A+B)^{-1.5}\right]^{1/12}, \tag{16}$$

where $A = \left[-2.457\cdot\ln\left(\left(\frac{7}{Re}\right)^{0.9} + 0.27(e/d)\right)\right]^{16}$, $B = \left(\frac{37530}{Re}\right)^{16}$.

Solving Eqs. (7) – (12), we obtain the distributions of temperatures, electric potential (for thermoelements), velocities and pressure (for heat carrier).

The above differential equations with the respective boundary conditions were solved using Comsol Multiphysics package of applied programs.

Computer simulation results

Below are given the results of calculations of the parameters of thermoelectric pump with respect to physical model shown in Fig. 1. The influence of energy loss W_{loss} for heater carrier pumping through heat exchange system on the integral coefficient of performance ε^{int} of thermoelectric heat pump was investigated. The optimal number of thermoelectric modules N was determined to assure the required cooling capacity Q_0, as well as the optimal supply current I_{opt} of each module to assure the highest integral coefficient of performance ε^{int}.

The initial data for calculations:

cooling capacity – 600 W;

heat carrier temperature at inlet to hot heat transfer loop – 36 ºC;
heat carrier temperature at inlet to cold heat transfer loop – 31 ºC;
heat carrier flow rate in each loop – 22 ml/s.

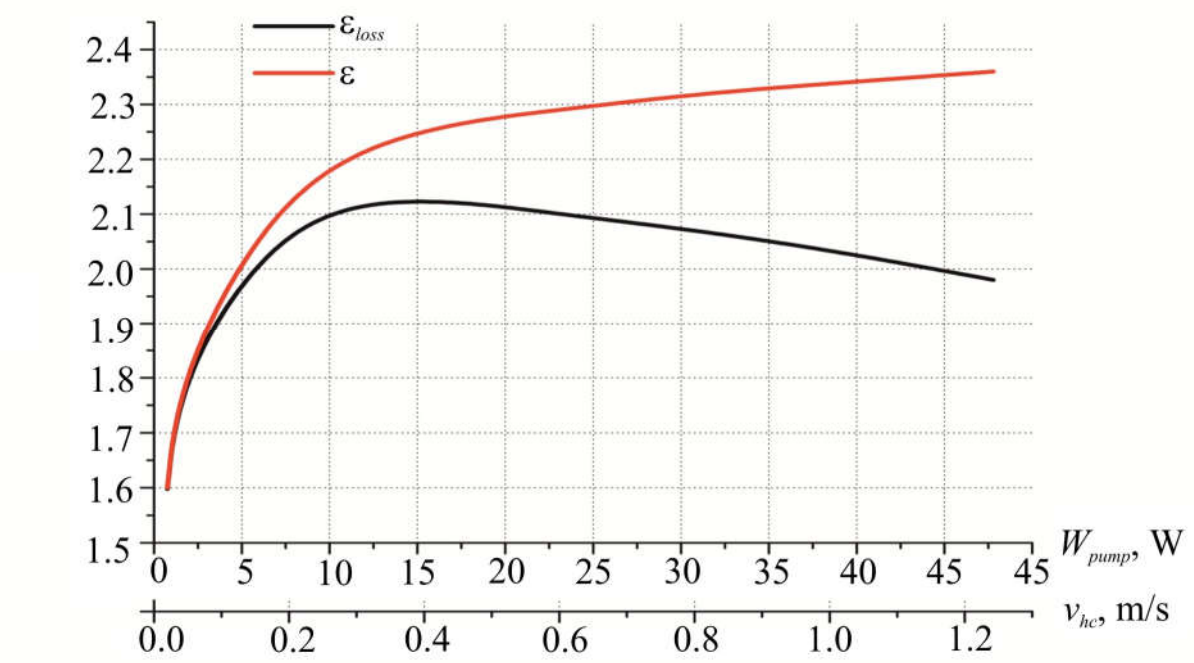

Fig. 2. Dependence of integral coefficient of performance of thermoelectric heat pump (with regard to energy loss for pumping ε_{loss} and without regard to it ε) on the energy necessary for pumping of heat carrier W_{pump} (heat carrier pumping velocity in the channels of heat exchanger v_{hc})

Thus, as a result of simulation it was established that with increase in power supply to liquid pump which assures heat carrier circulation in heat exchange system, the integral coefficient of performance increases (ε in Fig. 2), which is due to reduction of temperature difference loss in heat exchange system as a result of increase in heat carrier circulation velocity v_{hc}.

Taking into account in the expression for coefficient of performance of thermoelectric heat pump (17) the energy loss for heat carrier pumping (18) leads to the fact that coefficient of performance at first drastically increases, reaches the maximum $\varepsilon \approx 2.12$ in the area of $W_{pump} = 15$ W (which corresponds to heat carrier pumping velocity $v_{hc} = 0.4$ m/s), and then gradually decreases, because energy loss on heat carrier pumping starts to reach the level of energy loss for operation of thermoelectric modules.

$$\varepsilon = \frac{Q_0}{W_{тм}}, \tag{17}$$

$$\varepsilon_{втр} = \frac{Q_0}{W_{тм} + W_{нас}}, \tag{18}$$

where Q_0 is cooling capacity of THP, W_{tm} is power supply to thermoelectric modules, W_{pump} is power supply to liquid pumps of heat exchange system.

Comparison of the results obtained to the results of experimental studies of thermoelectric heat pump [9] testifies that the value of THP coefficient of performance $\varepsilon = 1.85$ achieved to date corresponds to heat carrier pumping velocity $v_{hc} \approx 0.1$ m/s (which is equivalent to the level of energy loss for heat carrier pumping $W_{pump} \approx 4$ W). This brings us to the conclusion about the possibility of further improvement of THP efficiency by optimization of power supply to its heat exchange system.

Conclusion

1. It was established that with increase in power supply to liquid pump, the integral coefficient of performance of thermoelectric heat pump (without regard to energy loss for heat carrier pumping) increases to theoretically possible maximum $\varepsilon \sim 2.5$, which is caused by reduced temperature difference loss in heat exchange system due to growing velocity of heat carrier circulation v_{hc}.
2. Taking into account the energy loss for heat carrier pumping leads to the fact that coefficient of performance of THP at first drastically increases, reaches the maximum $\varepsilon \approx 2.12$ in the area of $W_{pump} = 15$ W (which corresponds to heat carrier pumping velocity $v_{hc} = 0.4$ m/s), and then gradually decreases.
3. Comparison of the results obtained to the results of experimental studies of THP testifies that the value of THP coefficient of performance $\varepsilon = 1.85$ achieved to date corresponds to heat carrier pumping velocity $v_{hc} \approx 0.1$ m/s (which is equivalent to the level of energy loss for heat carrier pumping $W_{pump} \approx 4$ W).

References

1. Rozver Yu.Yu. (2003). Thermoelectric air-conditioner for vehicles. *J. Thermoelectricity*, 2, 52 – 56.
2. Anatychuk L.I., Vikhor L.N., Rozver Yu.Yu. (2004). Investigation on performance of thermoelectric cooler of liquid or gas flows. *J. Thermoelectricity*, 1, 73 – 80.
3. Anatychuk L.I., Sudzuki N., Rozver Yu.Yu. (2005). Thermoelectric indoor air-conditioner. *J. Thermoelectricity*, 3, 53 – 56.
4. Rifert V.G., Usenko V.I., Barabash P.A., et al. (2011). Development and test of water regeneration system from liquid biowaste on board of manned spacecrafts with the use of thermoelectric heat pump. *J. Thermoelectricity*, 2, 63 – 74.
5. Anatychuk L.I., Barabash P.A., Rifert V.G., Rozver Yu.Yu., Usenko V.I., Cherkez R.G. (2013). Thermoelectric heat pump as a means of improving efficiency of water purification systems on space missions. *J. Thermoelectricity*, 6, 78 – 83.
6. Anatychuk L.I., Prybyla A.V. (2017). Limiting possibilities of thermoelectric liquid-liquid heat pump. *J. Thermoelectricity,* 4, 33 – 39.
7. Anatychuk L.I., Prybyla A.V. (2017). The influence of quality of heat exchangers on the properties of thermoelectric liquid-liquid heat pumps. *J. Thermoelectricity*, 5, 27 – 33.
8. Lurie Michael V. (2008). *Modeling of oil product and gas pipeline transportation*. Weinheim: WILEY-VCH Verlag Gmbh & Co. Kgaa.
9. Anatychuk L.I., Rozver Yu.Yu., Prybyla A.V. (2017). Experimental study of thermoelectric liquid-liquid heat pump. *J. Thermoelectricity*, 3, 33-39.

Submitted 10.01.2018

Анатичук Л.І. *ак. НАН України*,[1,2]
Прибила А.В. *кандидат фіз.-мат. наук*[1,2]

Інститут термоелектрики НАН і МОН України, вул. Науки, 1,
Чернівці, 58029, Україна, *e-mail: anatych@gmail.com*
Чернівецький національний університетім. Юрія Федьковича,
вул. Коцюбинського 2, Чернівці, 58000, Україна,
e-mail: anatych@gmail.com

ПРО ХОЛОДИЛЬНИЙ КОЕФІЦІЄНТ ТЕРМОЕЛЕКТРИЧНИХ ТЕПЛОВИХ НАСОСІВ РІДИНА-РІДИНА З ВРАХУВАННЯМ ЕНЕРГІЇ НА ПЕРЕМІЩЕННЯ ТЕПЛОНОСІЯ

У роботі наводяться результати досліджень холодильного коефіцієнта термоелектричного теплового насоса рідина-рідина з врахуванням енергії на переміщення теплоносія, зокрема для його використання у якості високоефективного нагрівника для приладу очистки води космічного призначення.. Бібл. 9, Рис. 2.
Ключові слова: термоелектричний тепловий насос, ефективність, дистилятор, теплообмінник.

Анатычук Л.И.[1,2] *ак. НАН Украины*,
Прибыла А.В.[1,2] *канд.физ.-мат. наук*

Институт термоэлектричества, ул. Науки, 1, Черновцы, 58029, Украина
e-mail: anatych@gmail.com
Черновицкий национальный университет им. Юрия Федьковича,
ул. Коцюбинського 2, Черновцы, 58000, Украина
e-mail: anatych@gmail.com

О ХОЛОДИЛЬНОМ КОЭФФИЦИЕНТЕ ТЕРМОЭЛЕКТРИЧЕСКИХ ТЕПЛОВЫХ НАСОСОВ ЖИДКОСТЬ-ЖИДКОСТЬ С УЧЕТОМ ЭНЕРГИИ НА ПЕРЕМЕЩЕНИЕ ТЕПЛОНОСИТЕЛЯ

В *работе приводятся результаты исследований холодильного коэффициента термоэлектрического теплового насоса жидкость-жидкость с учетом затрат энергии на перемещение теплоносителя, в частности для его использования в качестве высокоэффективного нагревателя для прибора очистки воды космического назначения. Библ. 9, Рис. 2.*
Ключевые слова: термоэлектрический тепловой насос, эффективность, дистиллятор, теплообменник.

References

1. Rozver Yu.Yu. (2003). Thermoelectric air-conditioner for vehicles. *J. Thermoelectricity*, 2, 52 – 56.
2. Anatychuk L.I., Vikhor L.N., Rozver Yu.Yu. (2004). Investigation on performance of thermoelectric cooler of liquid or gas flows. *J. Thermoelectricity*, 1, 73 – 80.
3. Anatychuk L.I., Sudzuki N., Rozver Yu.Yu. (2005). Thermoelectric indoor air-conditioner. *J. Thermoelectricity*, 3, 53 – 56.
4. Rifert V.G., Usenko V.I., Barabash P.A., et al. (2011). Development and test of water regeneration system from liquid biowaste on board of manned spacecrafts with the use of thermoelectric heat pump. *J. Thermoelectricity*, 2, 63 – 74.
5. Anatychuk L.I., Barabash P.A., Rifert V.G., Rozver Yu.Yu., Usenko V.I., Cherkez R.G. (2013). Thermoelectric heat pump as a means of improving efficiency of water purification systems on space missions. *J. Thermoelectricity*, 6, 78 – 83.
6. Anatychuk L.I., Prybyla A.V. (2017). Limiting possibilities of thermoelectric liquid-liquid heat pump. *J. Thermoelectricity,* 4, 33 – 39.

7. Anatychuk L.I., Prybyla A.V. (2017). The influence of quality of heat exchangers on the properties of thermoelectric liquid-liquid heat pumps. *J. Thermoelectricity*, 5, 27 – 33.
8. Lurie Michael V. (2008). *Modeling of oil product and gas pipeline transportation*. Weinheim: WILEY-VCH Verlag Gmbh & Co. Kgaa.
9. Anatychuk L.I., Rozver Yu.Yu., Prybyla A.V. (2017). Experimental study of thermoelectric liquid-liquid heat pump. *J. Thermoelectricity*, 3, 33-39.

Submitted 10.01.2018

O.S. Kshevetsky

O.S. Kshevetsky, *PhD in Physics and Mathematics, assistant professor*

Chernivtsi Institute of Trade and Economics of Kyiv National University of Trade and Economics, 7, Tsentralna Square, Chernivtsi, 58002, Ukraine
e-mail: kshevos@gmail.com

ESTIMATION OF THE EFFICIENCY OF PARTIAL CASE OF HEAT AND MASS TRANSFER PROCESSES BETWEEN HEAT PUMPS AND MOVING SUBSTANCE, PART 1

Mathematical expressions have been obtained for estimation of the efficiency of partial case of heat and mass transfer between moving substance and heat pumps with their heat exchangers, whereby moving substance (or at least part of this moving substance) is brought into thermal contact with the heat absorbing and heat releasing heat exchangers of at least two real heat pumps. Bibl. 16, Fig. 3.
Key words: heat pump, thermoelectric heat pump, moving substance, heat and mass transfer, efficiency, energy efficiency.

Introduction

The values of coefficient of performance and heating coefficient of typical heat pumps (hereinafter in the text instead of the phrase "heat pump" or instead of the phrase "heat pumps" we will use the abbreviation HP) are known to increase with a decrease in the temperature difference between their heat absorbing and heat releasing heat exchangers (HEs) at a fixed temperature of one of the HP HEs [1, 2]. In this connection, in particular, in terms of energy efficiency, it is relevant to find such applications of HPs, including thermoelectric HPs, whereby these HPs could work at possibly smaller, relatively low temperature differences between their heat absorbing and heat releasing HEs.

Let us consider the processes with participation of moving substance, where this moving substance must be heated and/or cooled. In such processes, HPs can be employed for heating and/or cooling of moving substance, as well as for reducing energy consumption necessary for heating and/or cooling of this substance [3 – 16].

Different methods of heat and mass transfer between moving substance and one or several HPs with corresponding HEs which do not involve bringing moving substance (or at least part of this moving substance) into thermal contact with the heat absorbing and heat releasing HEs of at least two HPs are described, for instance, in [3 – 13].

In [12], moving substance is brought into thermal contact with two metal heat exchangers (HP HEs) that have thermal contact with four thermoelectric modules. In so doing, there is thermal contact between thermoelectric modules through their common metal heat exchangers mentioned above. So, in this case four thermoelectric modules which have only one common heat absorbing and only one common heat releasing HE can be functionally considered as one HP based on the four thermoelectric modules that are thermally connected in parallel.

Just as in [12], several thermoelectric modules are used in [13]. However, in contrast to [12], in [13] each thermoelectric module has its individual HEs which are thermally insulated from each other. This

allows us to talk about several HPs. However, in this case different HEs of each separate HP are used for heat exchange with different moving substances.

If we consider the processes in which moving substance (or at least part of this moving substance) is brought into thermal contact with the heat absorbing and heat releasing HEs of at least two HPs, in some of these processes [14 – 16] a situation can be implemented when these HPs will work at relatively low temperature differences between their heat absorbing and heat releasing HEs. In [14 – 15], mathematical expressions are given for the approximate estimation of moving substance temperature distribution when these processes employ ideal HPs which operate on the Carnot cycle. At the same time, it is well known that the efficiency of real HPs can differ from the efficiency of HPs which operate on the Carnot cycle [2].

The purpose of this work is to create mathematical prerequisites for the approximate quantitative estimation of the efficiency (primarily, energy efficiency) of partial case of heat and mass transfer between moving substance and HPs with their HEs, whereby moving substance (or at least part of this moving substance) is brought into thermal contact with the heat absorbing and heat releasing HEs of at least two HPs [14 – 16]. This partial case (described in [14 – 16]) will be considered, because in this case it is possible to implement a situation when HPs will work at relatively low temperature differences between their heat absorbing and heat releasing HEs. Hereinafter, in order to indicate this partial case of the method of heat and mass transfer between moving substance and HPs with their HEs, we will use the phrase *"investigated method of heat and mass transfer"*. The fact that in the *investigated method of heat and mass transfer* the situation is possible when HPs will work at relatively low temperature differences between their heat absorbing and heat releasing HEs, can create prerequisites for a possible increase of the energy efficiency of heat and mass transfer processes which involve heating and cooling of moving substance [14 – 16]. To accomplish this goal, the task of this work is to obtain mathematical expressions that could be used to estimate the efficiency of the *investigated heat and mass transfer method*, using, in particular, the actual HPs, for example, thermoelectric HPs or compression HPs.

General description and peculiarities of the investigated method of heat and mass transfer

The general diagram of the *investigated method of heat and mass transfer* is presented in Fig. 1. In the diagram, HPs are designated by triangles. Each separate HP has the 1st HE and the 2nd HE. One of these HEs is heat absorbing, and the other – heat releasing. Which of these HEs is heat absorbing, and which - heat releasing is not specified here. Heat exchangers in this and further diagrams are not designated separately. Moving substance according to the diagram shown in Fig. 1 moves from the entrance to the exit in such a way that thermal contact and the respective heat transfer processes of this moving substance with all HEs of all HPs occur alternately. The flow of moving substance between points 1.0 and 1.n will be considered to be the input flow of moving substance in this and further schematics. And the flow of moving substance between points 2.n and 2.0 will be considered to be the output flow of moving substance in this and further diagrams.

For further evaluative calculations we will use a simplified model with the following assumptions.

1. Heat exchange between HPs takes place only due to movement of moving substance.

2. Heat exchange of HP and moving substance with the environment is absent (except for possible heat exchange of moving substance with the environment with the use of additional volume).

3. Temperature changes within each separate HP HE are absent.

4. Heat exchange of moving substance with HP HEs (surfaces, heat sinks) is such that moving substance after its thermal contact with certain HE of respective HP acquires the temperature of this HE.

5. All moving substance is alternately brought into thermal contact with each separate HE of all HPs.

6. For all positions of moving substance in the process of its movement the following ratio is valid:

$$\Delta T^{PP} = d \cdot Q^{PP}, \tag{1}$$

where Q^{PP} is heat flow from or to moving substance on certain section of its motion, whose value is always not negative; ΔT^{PP} is the difference in moving substance temperatures on this section of its movement, which will be determined (here and afterwards) by subtracting from the temperature of moving substance that has a higher value the temperature of moving substance that has a lower value; d is proportionality factor. This can take place if, for instance, the heat capacity of moving substance is constant in the entire process of heat and mass transfer, and in the absence of various processes (for instance, phase transitions, changes in pressure), accompanied by heat release or absorption.

7. The amount of moving substance during its movement is not changed.

8. All HPs work under such conditions that the temperature of the heat absorbing HE of each separate HP is lower than the temperature of the heat releasing HE of the same HP.

Also in certain cases we will use the following assumption.

9. All changes in moving substance temperature as a result of its thermal control with each separate HP HE in the input flow of this moving substance are equal.

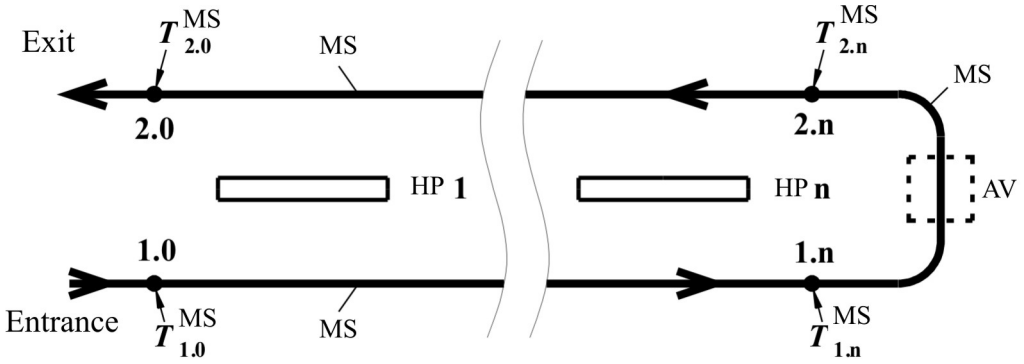

Fig. 1. Diagram of the investigated method of heat and mass transfer: direction of moving substance movement is indicated by arrows; HP 1, ...,HP n – HP of total amount n; AV – additional volume (for instance, drying chamber of drying installation, room or compartment of transport means),in which moving substance can take part in heat and mass transfer processes with other substance or the environment; 1.0, 1.n, 2.n, 2.0 – points that correspond to successive positions of moving substance in the process of its movement (1.0 – immediately before thermal contact of moving substance with the 1st HE of HP 1, 1.n – immediately after thermal contact of moving substance with the 1st HE of HP n, 2.n – immediately before thermal contact of moving substance with the 2nd HE of HP n, 2.0 – immediately after thermal contact of moving substance with the 2nd HE of HP 1); $T_{1.0}^{PP}$, $T_{1.n}^{PP}$, $T_{2.n}^{PP}$, $T_{2.0}^{PP}$ – temperature of moving substance at respective points.

The use of this assumption 9 will be indicated specially.

Using the respective assumptions (described above), in particular, relation (1), for coefficient of performance ε_i and heating coefficient μ_i of arbitrary *i*-th HP one can write the following relations:

$$\varepsilon_i = \frac{Q_{cool,i}^{TH}}{W_i^{TH}} = \frac{Q_{cool,i}^{TH}}{Q_{hot,i}^{TH} - Q_{cool,i}^{TH}} = \frac{\Delta T_{cool,i}^{PP}}{\Delta T_{hot,i}^{PP} - \Delta T_{cool,i}^{PP}}; \tag{2}$$

$$\mu_i = \frac{Q_{hot,i}^{TH}}{W_i^{TH}} = \frac{Q_{hot,i}^{TH}}{Q_{hot,i}^{TH} - Q_{cool,i}^{TH}} = \frac{\Delta T_{hot,i}^{PP}}{\Delta T_{hot,i}^{PP} - \Delta T_{cool,i}^{PP}}, \tag{3}$$

where $Q_{cool,i}^{TH}$ is thermal flow which the *i* -th HP absorbs (due to its corresponding heat absorbing HE) from moving substance; $Q_{hot,i}^{TH}$ is thermal flow which the *i*-th HP gives away (due to its corresponding heat releasing HE) to moving substance; W_i^{TH} is power which the *i*-th HP consumes and owing to which it works (for instance, this can be electric power consumed by the *i*-th HP from the external separate supply source); $\Delta T_{cool,i}^{PP}$, $\Delta T_{hot,i}^{PP}$ are differences in temperature of moving substance which are formed due to thermal contact of moving substance with the heat absorbing and heat releasing HEs of the *i*-th HP on the respective sections of its motion.

Coefficient of performance and heating coefficient of real HPs may be lower than the coefficient of performance and heating coefficient, respectively, of ideal HPs that operate on the Carnot cycle [2]. To take this into consideration, we will assume that for the *i*-th HP its coefficient of performance ε_i and its heating coefficient μ_i are determined by the relations:

$$\varepsilon_i = A_i \cdot \varepsilon_{K,i} = A_i \cdot \frac{Q_{cool,i}^{TH^K}}{W_i^{TH^K}} = A_i \cdot \frac{T_{cool,i}^{TH_i^K}}{T_{hot,i}^{TH_i^K} - T_{cool,i}^{TH_i^K}},\ A_i \le 1; \tag{4}$$

$$\mu_i = B_i \cdot \mu_{K,i} = B_i \cdot \frac{Q_{hot,i}^{TH^K}}{W_i^{TH^K}} = B_i \cdot \frac{T_{hot,i}^{TH_i^K}}{T_{hot,i}^{TH_i^K} - T_{cool,i}^{TH_i^K}},\ B_i \le 1, \tag{5}$$

under conditions that:

$$W_i^{TH^K} = W_i^{TH}; \tag{6}$$

$$T_{cool,i}^{TH^K} = T_{cool,i}^{TH}; \tag{7}$$

$$T_{hot,i}^{TH^K} = T_{hot,i}^{TH}, \tag{8}$$

where A_i is a dimensionless factor that takes into account the specific features of structure and use of the *i*-th HP that cause the difference of coefficient of performance of this HP from the coefficient of performance of an ideal HP which under the same conditions operates on the Carnot cycle; B_i is a dimensionless factor that takes into account the specific features and use of the *i*-th HP that cause the difference of the heating coefficient of this HP from the heating coefficient of an ideal HP which under the same conditions operates on the Carnot cycle; $\varepsilon_{K,i}$ is coefficient of performance of an ideal HP that operates on the Carnot cycle under the same conditions as the *i*-th HP; $\mu_{K,i}$ is heating coefficient of an ideal HP that operates on the Carnot cycle under the same conditions as the *i*-th HP; $Q_{cool,i}^{TH^K}$ is thermal flow that is absorbed by an ideal HP which operates on the Carnot cycle under the same conditions as the *i*-th HP; $Q_{hot,i}^{TH^K}$ is thermal flow given by an ideal HP that operates on the Carnot cycle under the same conditions as the *i*-th HP; $W_i^{TH^K}$ is power consumed by an ideal HP and owing to which it operates on the Carnot cycle under the same conditions as the *i*-th HP; $T_{cool,i}^{TH^K}$ is temperature of the heat absorbing HE of an ideal HP that operates on the Carnot cycle under the same conditions as the *i*-th HP; $T_{cool,i}^{TH}$ is the temperature of the heat absorbing HE of the *i*-th HP; $T_{hot,i}^{TH^K}$ is the temperature of the heat releasing HE of an ideal HP that operates on the Carnot cycle under the same conditions as the *i*-th HP; $T_{hot,i}^{TH}$ is the temperature of the heat releasing HE of the *i*-th HP.

From Eqs. (4), (7) and (8), as well as from Eqs. (5), (7) and (8), respectively, follows:

$$\varepsilon_i = A_i \cdot \frac{T_{cool,i}^{TH}}{T_{hot,i}^{TH} - T_{cool,i}^{TH}},\ A_i \le 1; \tag{9}$$

$$\mu_i = B_i \cdot \frac{T_{hot,i}^{TH}}{T_{hot,i}^{TH} - T_{cool,i}^{TH}},\ B_i \le 1. \tag{10}$$

It is well known that ε_i and μ_i, as well as $\varepsilon_{K,i}$ and $\mu_{K,i}$ are related by relations:

$$\mu_i = \varepsilon_i + 1; \tag{11}$$

$$\mu_{K,i} = \varepsilon_{K,i} + 1. \tag{12}$$

If we use relations (11), (12), as well as relations (9), (10), we can find the ratio between A_i and B_i:

$$A_i = (B_i - 1)\frac{T_{hot,i}^{TH}}{T_{cool,i}^{TH}} + 1; \tag{13}$$

$$B_i = (A_i - 1)\frac{T_{cool,i}^{TH}}{T_{hot,i}^{TH}} + 1. \tag{14}$$

On the basis of Eqs. (2) and (9), and also on the basis of Eqs. (3) and (10), the following relations can be written, respectively, which can be used to determine the temperature mode of the i-th HP:

$$\frac{\Delta T_{cool,i}^{PP}}{\Delta T_{hot,i}^{PP} - \Delta T_{cool,i}^{PP}} = A_i \frac{T_{cool,i}^{TH}}{T_{hot,i}^{TH} - T_{cool,i}^{TH}}; \tag{15}$$

$$\frac{\Delta T_{hot,i}^{PP}}{\Delta T_{hot,i}^{PP} - \Delta T_{cool,i}^{PP}} = B_i \frac{T_{hot,i}^{TH}}{T_{hot,i}^{TH} - T_{cool,i}^{TH}}. \tag{16}$$

Next we consider two partial cases of the *investigated method of heat and mass transfer*.

The case of moving substance cooling in its input flow by all HPs

A diagram of the *investigated method of heat and mass transfer* when moving substance in its input flow is cooled by all separate HPs is shown in Fig.2.

For this case of the *investigated method of heat and mass transfer* taking into account that moving substance according to the diagram shown in Fig. 2 in its input flow is cooled by all separate HPs, and in its output flow is heated by all separate HPs we can write (using the notation employed in Fig.2):

$$T_{cool,i}^{TH} = T_{1.i}^{TH},\ i = 1 \div n; \tag{17}$$

$$T_{cool,(i-1)}^{PP} = T_{1.(i-1)}^{PP},\ T_{cool,i}^{PP} = T_{1.i}^{PP},\ i = 1 \div n; \tag{18}$$

$$T_{hot,i}^{TH} = T_{2.i}^{TH},\ i = 1 \div n; \tag{19}$$

$$T_{hot,(i-1)}^{PP} = T_{2.(i-1)}^{PP},\ T_{hot,i}^{PP} = T_{2.i}^{PP},\ i = 1 \div n; \tag{20}$$

$$\Delta T_{cool,i}^{PP} = T_{cool,(i-1)}^{PP} - T_{cool,i}^{PP}; \tag{21}$$

$$\Delta T_{hot,i}^{PP} = T_{hot,(i-1)}^{PP} - T_{hot,i}^{PP}, \tag{22}$$

where $T_{cool,(i-1)}^{PP}$ is temperature of moving substance in the process of its movement immediately before its thermal contact with the heat absorbing HE of the *i*-th HP; $T_{cool,i}^{PP}$ is temperature of moving substance in

the process of its movement immediately after its contact with the heat absorbing HE of the *i*-th HP; $T^{PP}_{hot,(i-1)}$ is temperature of moving substance in the process of its movement immediately after its thermal contact with the heat releasing HE of the *i*-th HP; $T^{PP}_{hot,i}$ is temperature of moving substance in the process of its movement immediately before its thermal contact with the heat releasing HE of the *i*-th HP.

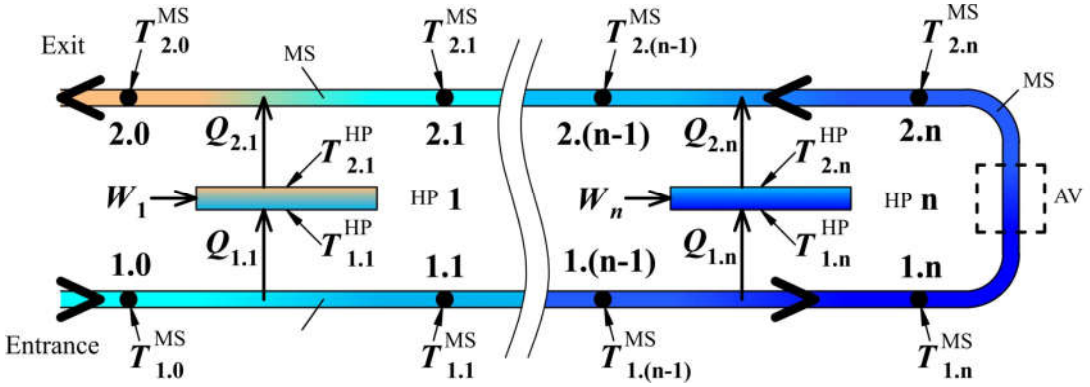

Fig. 2. Diagram of the investigated method of heat and mass transfer for the case of moving substance cooling in its input flow by separate HPs: 1.0, …, 1.n, 2.n, …, 2.0 – points corresponding to successive positions of moving substance in the process of its movement (1.0 – immediately before thermal contact of moving substance with the 1st (heat absorbing) HE of HP 1, 1.1 – immediately after thermal contact of moving substance with the 1st HE of HP 1, …, 1.(n-1) – immediately before thermal contact of moving substance with the 1st (heat absorbing) HE of HP n, 1.n – immediately after thermal contact of moving substance with the 1st HE of HP n, 2.n – immediately before thermal contact of moving substance with the 2nd (heat releasing) HE of HP n, 2.(n-1) – immediately after thermal contact of moving substance with the 2nd HE of HP n, …, 2.1 – immediately before thermal contact of moving substance with the 2nd (heat releasing) HE of HP 1, 2.0 – immediately after thermal contact of moving substance with the 2nd HE of HP 1); $T^{PP}_{1.0}$, …, $T^{PP}_{1.n}$, $T^{PP}_{2.n}$, …, $T^{PP}_{2.0}$ *– temperatures of moving substance at respective points;* W_1, …, W_n *– supply powers (for instance, electric) of respective HPs;* $Q_{1.1}$, …, $Q_{1.n}$ *– thermal flows from moving substance to the 1st (heat absorbing) HEs of respective HPs;* $Q_{2.n}$, …, $Q_{2.1}$ *–thermal flows from the 2nd (heat releasing) HEs to moving substance;* $T^{TH}_{1.1}$, …, $T^{TH}_{1.n}$ *– temperatures of the 1st (heat absorbing) HEs of respective HPs;* $T^{TH}_{2.1}$, …, $T^{TH}_{2.n}$ *– temperatures of the 2nd (heat releasing) HEs of respective HPs; other designations in this figure are similar to corresponding notation in Fig.1.*

According to Fig.2 for this case of the *investigated method of heat and mass transfer* we denote:

$$\Delta T^{PP}_{cool} = \sum_{i=1}^{n} \Delta T^{PP}_{cool,i} = T^{PP}_{1.0} - T^{PP}_{1.n} = \Delta T^{PP}_{1}, \tag{23}$$

$$\Delta T^{PP}_{hot} = \sum_{i=1}^{n} \Delta T^{PP}_{hot,i} = T^{PP}_{2.0} - T^{PP}_{2.n} = \Delta T^{PP}_{2}; \tag{24}$$

where ΔT^{PP}_{cool} - the difference in moving substance temperature which is formed due to cooling of moving substance in its input flow by all separate HPs; ΔT^{PP}_{1} – according to the diagram shown in Fig.2 the difference in moving substance temperature which is formed due to thermal contact of moving substance in its input flow with HEs of all separate HPs; ΔT^{PP}_{hot} – the difference in moving substance temperature which is formed due to heating of moving substance in its output flow by all separate HPs; ΔT^{PP}_{2} – according to the diagram shown in Fig. 2 the difference in moving substance temperature which is formed due to thermal contact of moving substance in its output flow with HEs of all separate HPs.

If we use the respective assumptions, in particular, assumption 4, then for the case when moving substance in the input flow is cooled by all separate HPs according to the diagram shown in Fig. 2 it can be written:

$$T^{PP}_{hot,(i-1)} = T^{TH}_{hot,i}; \tag{25}$$

$$T^{PP}_{cool,i} = T^{TH}_{cool,i}. \tag{26}$$

Eqs. (13) and (14) which establish the ratios between A_i and B_i for this case of the *investigated method of heat and mass transfer* according to Fig. 2 and with the use of Eqs. (25), (26), (22) and (26), (25), (22), respectively, will take on the form:

$$A_i = (B_i - 1)\frac{T^{PP}_{hot,i} + \Delta T^{PP}_{hot,i}}{T^{PP}_{cool,i}} + 1; \tag{27}$$

$$B_i = (A_i - 1)\frac{T^{PP}_{cool,i}}{T^{PP}_{hot,i} + \Delta T^{PP}_{hot,i}} + 1. \tag{28}$$

Let us transform the right sides of Eqs. (15) and (16) with the use of Eqs. (26), (25), (22) and (25), (26), (22), respectively:

$$A_i \frac{T^{TH}_{cool,i}}{T^{TH}_{hot,i} - T^{TH}_{cool,i}} = A_i \frac{T^{PP}_{cool,i}}{T^{PP}_{hot,i} + \Delta T^{PP}_{hot,i} - T^{PP}_{cool,i}}; \tag{29}$$

$$B_i \frac{T^{TH}_{hot,i}}{T^{TH}_{hot,i} - T^{TH}_{cool,i}} = B_i \frac{T^{PP}_{hot,i} + \Delta T^{PP}_{hot,i}}{T^{PP}_{hot,i} + \Delta T^{PP}_{hot,i} - T^{PP}_{cool,i}}. \tag{30}$$

In order to obtain an expression for the definition of $\Delta T^{PP}_{hot,i}$ which will include factor A_i using Eq.(29) we rewrite Eq.(15) and obtain the following relation:

$$\frac{\Delta T^{PP}_{cool,i}}{\Delta T^{PP}_{hot,i} - \Delta T^{PP}_{cool,i}} = A_i \frac{T^{PP}_{cool,i}}{T^{PP}_{hot,i} + \Delta T^{PP}_{hot,i} - T^{PP}_{cool,i}}. \tag{31}$$

As a result of mathematical transformations of Eq. (31), we obtain the following ratio for the definition of temperature operating mode of the *i*-th HP (the expression that relates the temperatures of moving substance before and after its thermal contact with HE of the *i*-th HP):

$$\Delta T^{PP}_{hot,i} = \frac{T^{PP}_{hot,i} - (1 - A_i)T^{PP}_{cool,i}}{\frac{A_i T^{PP}_{cool,i}}{\Delta T^{PP}_{cool,i}} - 1}. \tag{32}$$

In the case of using HPs the coefficient of performance of which is assigned by Eq.(9), according to the diagram shown in Fig. 2 the total temperature difference of moving substance in its output flow based on Eqs. (24) and (32):

$$\Delta T^{PP}_{hot} = \sum_{i=1}^{n} \frac{T^{PP}_{hot,i} - (1 - A_i)T^{PP}_{cool,i}}{\frac{A_i T^{PP}_{cool,i}}{\Delta T^{PP}_{cool,i}} - 1}. \tag{33}$$

For the case when the *i*-th HP operates on the Carnot cycle (in so doing, $A_i = 1$) expression (32) will be simplified:

$$\Delta T_{hot,i}^{PP} = \frac{T_{hot,i}^{PP}}{\frac{T_{cool,i}^{PP}}{\Delta T_{cool,i}^{PP}} - 1}. \tag{34}$$

And then in this case the total temperature difference of moving substance in its output flow based on Eqs. (24) and (34):

$$\Delta T_{hot}^{PP} = \sum_{i=1}^{n} \frac{T_{hot,i}^{PP}}{\frac{T_{cool,i}^{PP}}{\Delta T_{cool,i}^{PP}} - 1}. \tag{35}$$

In order to obtain an expression for the definition of $\Delta T_{hot,i}^{PP}$ which will include factor B_i, using Eq. (30) we will rewrite Eq.(16) and obtain the following relation:

$$\frac{\Delta T_{hot,i}^{PP}}{\Delta T_{hot,i}^{PP} - \Delta T_{cool,i}^{PP}} = B_i \frac{T_{hot,i}^{PP} + \Delta T_{hot,i}^{PP}}{T_{hot,i}^{PP} + \Delta T_{hot,i}^{PP} - T_{cool,i}^{PP}}. \tag{36}$$

As a result of mathematical transformations of Eq.(36) for the definition of $\Delta T_{hot,i}^{PP}$ we will obtain a quadratic equation:

$$(1-B_i)\left(\Delta T_{hot,i}^{PP}\right)^2 + \left((1-B_i)T_{hot,i}^{PP} + B_i\Delta T_{cool,i}^{PP} - T_{cool,i}^{PP}\right)\Delta T_{hot,i}^{PP} + B_i T_{hot,i}^{PP}\Delta T_{cool,i}^{PP} = 0. \tag{37}$$

The same equation can be also obtained, if the expression for A_i (27) is substituted into Eq.(32).

The root of this quadratic equation that has a physical meaning:

$$\Delta T_{hot,i}^{PP} = \frac{T_{cool,i}^{PP} - (1-B_i)T_{hot,i}^{PP} - B_i\Delta T_{cool,i}^{PP} - \sqrt{D_{cool,i}}}{2(1-B_i)}, \tag{38}$$

where $D_{cool,i} = \left((1-B_i)T_{hot,i}^{PP} + B_i\Delta T_{cool,i}^{PP} - T_{cool,i}^{PP}\right)^2 - 4(1-B_i)B_i T_{hot,i}^{PP}\Delta T_{cool,i}^{PP}$.

In the case of using HP, the heating coefficient of which is assigned by Eq.(10), according to the schematic of Fig. 2 the total temperature difference of moving substance in its output flow based on Eq. (38):

$$\Delta T_{hot}^{PP} = \sum_{i=1}^{n} \frac{T_{cool,i}^{PP} - (1-B_i)T_{hot,i}^{PP} - B_i\Delta T_{cool,i}^{PP} - \sqrt{D_{cool,i}}}{2(1-B_i)}. \tag{39}$$

If the *i*-th HP from the diagram shown in Fig. 2 operates on the Carnot cycle (in this case $B_i = 1$), then the quadratic equation will be simplified as follows:

$$\left(\Delta T_{cool,i}^{PP} - T_{cool,i}^{PP}\right)\Delta T_{hot,i}^{PP} + T_{hot,i}^{PP}\Delta T_{cool,i}^{PP} = 0. \tag{40}$$

From Eq. (40) for the definition of $\Delta T_{hot,i}^{PP}$ one can obtain Eq.(34).

Let us consider the case which corresponds to assumption 9 (when all changes in moving substance temperature as a result of its thermal contact with each separate HP HE in the input flow of this moving substance are equal) and the diagram shown in Fig. 2 comprises *n* HPs. Then, for this case according to Fig. 2 and using Eq.(23):

$$\Delta T_{cool}^{PP} = n \cdot \Delta T_{cool,i}^{PP}. \tag{41}$$

For the case when the diagram shown in Fig. 2 comprises *n* HPs whose coefficients of performance are assigned by *Eq*. (9) and assumption 9 is valid, the total temperature difference of moving substance in its output flow with the use of *Eqs*.(33), (41):

$$\Delta T_{hot}^{PP} = \sum_{i=1}^{n} \frac{T_{hot,i}^{PP} - (1 - A_i) T_{cool,i}^{PP}}{\frac{A_i T_{cool,i}^{PP}}{\frac{1}{n}\Delta T_{cool}^{PP}} - 1}. \tag{42}$$

And for the case of using HPs whose heating coefficients are assigned by Eq.(10), according to the diagram shown in Fig. 2 with the use of assumption 9 the total temperature difference of moving substance in its output flow using Eqs. (39), (41):

$$\Delta T_{hot}^{PP} = \sum_{i=1}^{n} \frac{T_{cool,i}^{PP} - (1 - B_i) T_{hot,i}^{PP} - \frac{1}{n} B_i \Delta T_{cool}^{PP} - \sqrt{D_{9,cool,i}}}{2(1 - B_i)}, \tag{43}$$

where $D_{9,cool,i} = \left((1 - B_i) T_{hot,i}^{PP} + \frac{1}{n} B_i \Delta T_{cool}^{PP} - T_{cool,i}^{PP} \right)^2 - \frac{4}{n} (1 - B_i) B_i T_{hot,i}^{PP} \Delta T_{cool}^{PP}$.

For the case when the diagram shown in Fig. 2 comprises n HPs each of which operates on the Carnot cycle in such a way that assumption 9 is valid, using Eqs. (34) and (41) we obtain the following ratio for the definition of temperature operating mode of the i-th HP:

$$\Delta T_{hot,i}^{PP} = \frac{T_{hot,i}^{PP}}{\frac{T_{cool,i}^{PP}}{\frac{1}{n}\Delta T_{cool}^{PP}} - 1}. \tag{44}$$

It can be shown that for this case of the *investigated method of heat and mass transfer*, when all HPs in the diagram shown in Fig. 2 operate by the Carnot cycle and when all temperature changes of moving substance as a result of its thermal control with each separate HP HE in the input flow of this moving substance are equal (assumption 9), then all temperature changes of moving substance as a result of its thermal control with each separate HP HE in the output flow of this moving substance will be also equal:

$$\Delta T_{hot,(i-1)}^{PP} = \Delta T_{hot,i}^{PP}. \tag{45}$$

Then for this case on the basis of Eqs. (24), (45) and (44) we obtain the following expression for the definition of total temperature difference of moving substance in its output flow:

$$\Delta T_{hot}^{PP} = n \cdot \Delta T_{hot,i}^{PP} = \frac{T_{hot,i}^{PP}}{\frac{T_{cool,i}^{PP}}{\Delta T_{cool}^{PP}} - \frac{1}{n}}. \tag{46}$$

If we use direct designations from the diagram shown in Fig. 2, as well as Eqs.(24), (23), (20) and (18), then Eq.(46) will have the form:

$$\Delta T_2^{PP} = \frac{T_{2.i}^{PP}}{\frac{T_{1.i}^{PP}}{\Delta T_1^{PP}} - \frac{1}{n}}. \tag{47}$$

The case of moving substance heating in its input flow by all HPs

A diagram of the *investigated method of heat and mass transfer* when moving substance in its input flow is heated by all separate HPs is presented in Fig.3.

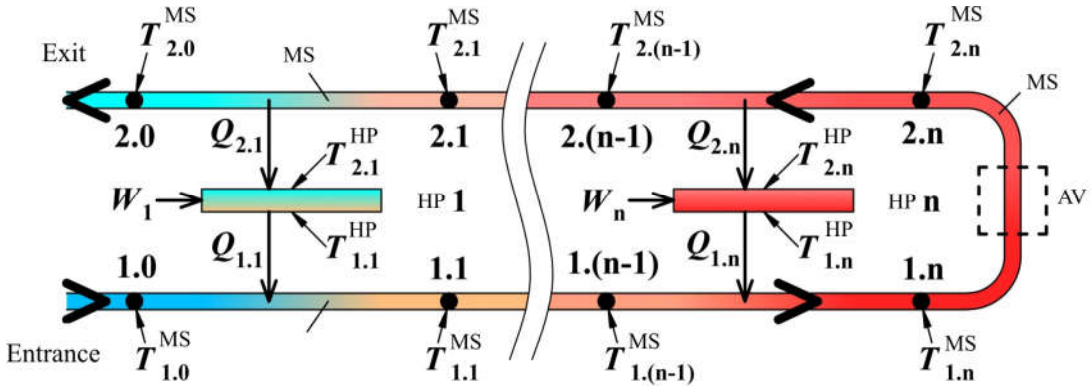

Fig. 3. Diagram of the investigated method of heat and mass transfer for the case of moving substance heating in its input flow by all separate HPs: 1.0, …, 1.n, 2.n, …, 2.0 – points that correspond to successive positions of moving substance in the process of its movement (1.0 – immediately before thermal contact of moving substance with the 1st (heat releasing) HE of HP 1, 1.1 – immediately after thermal contact of moving substance with the 1st HE of HP 1, …, 1.(n-1) – immediately before thermal contact of moving substance with the 1st (heat releasing) HE of HP n, 1.n – immediately after thermal contact of moving substance with the 1st HE of HP n, 2.n –immediately before thermal contact of moving substance with the 2nd (heat absorbing) HE of HP n, 2.(n-1) –immediately after thermal contact of moving substance with the 2nd HE of HP n, …, 2.1 – immediately before thermal contact of moving substance with the 2nd (heat absorbing) HE of HP 1, 2.0 – immediately after thermal contact of moving substance with the 2nd HE of HP 1); $T_{1.0}^{PP}$, …, $T_{1.n}^{PP}$, $T_{2.n}^{PP}$, …, $T_{2.0}^{PP}$ *– temperatures of moving substance at respective points;* $Q_{1.1}$, …, $Q_{1.n}$ *– heat flows from the 1st (heat releasing) HEs of respective HPs to moving substance;* $Q_{2.n}$, …, $Q_{2.1}$ *– heat flows from moving substance to the 2nd (heat absorbing) HEs of respective HPs;* $T_{1.1}^{TH}$, …, $T_{1.n}^{TH}$ *–temperatures of the 1st (heat releasing) HEs of respective HPs;* $T_{2.1}^{TH}$, …, $T_{2.n}^{TH}$ *– temperatures of the 2nd (heat absorbing) HEs of respective HPs; other designations in this figure are similar to corresponding notation in the previous figures.*

For this case of the *investigated method of heat and mass transfer* taking into account that moving substance according to the diagram shown in Fig. 3 in its input flow is heated by all separate HPs, we can write:

$$T_{hot,i}^{TH} = T_{1.i}^{TH},\ i = 1 \div n; \tag{48}$$

$$T_{hot,(i-1)}^{PP} = T_{1.(i-1)}^{PP},\ T_{hot,i}^{PP} = T_{1.i}^{PP},\ i = 1 \div n; \tag{49}$$

$$T_{cool,i}^{TH} = T_{2.i}^{TH},\ i = 1 \div n; \tag{50}$$

$$T_{cool,(i-1)}^{PP} = T_{2.(i-1)}^{PP},\ T_{cool,i}^{PP} = T_{2.i}^{PP},\ i = 1 \div n; \tag{51}$$

$$\Delta T_{hot,i}^{PP} = T_{hot,i}^{PP} - T_{hot,(i-1)}^{PP}; \tag{52}$$

$$\Delta T_{cool,i}^{PP} = T_{cool,i}^{PP} - T_{cool,(i-1)}^{PP}, \tag{53}$$

where $T_{hot,(i-1)}^{PP}$ is temperature of moving substance in the process of its movement immediately before its thermal contact with the heat releasing HE of the *i*-th HP; $T_{hot,i}^{PP}$ is temperature of moving substance in the process of its movement immediately after its thermal contact with the heat releasing HE of the *i*-th HP; $T_{cool,(i-1)}^{PP}$ is temperature of moving substance in the process of its movement immediately after its thermal contact with the heat absorbing HE of the *i*-th HP; $T_{cool,i}^{PP}$ is temperature of moving substance in the process of its movement immediately before its thermal contact with the heat absorbing HE of the *i*-th HP.

For this case of the *investigated method of heat and mass transfer* according to Fig. 3 we denote:

$$\Delta T_{hot}^{PP} = \sum_{i=1}^{n} \Delta T_{hot,i}^{PP} = T_{1.n}^{PP} - T_{1.0}^{PP} = \Delta T_1^{PP}; \tag{54}$$

Similar to the way we obtained mathematical expressions for the definition of temperature operating mode of the *investigated method of heat and mass transfer* in the previous case when moving substance in its input flow is cooled by all separate HPs, according to Fig. 2 one can also obtain the following mathematical expressions for this case of the *investigated method of heat and mass transfer*, when moving substance in its input flow is heated by all separate HPs according to Fig. 3.

$$\Delta T_{cool}^{PP} = \sum_{i=1}^{n} \Delta T_{cool,i}^{PP} = T_{2.n}^{PP} - T_{2.0}^{PP} = \Delta T_2^{PP}, \tag{55}$$

where ΔT_{hot}^{PP} is temperature difference of moving substance which is formed due to heating of moving substance in its input flow by all separate HPs; ΔT_1^{PP} – according to the diagram shown in Fig. 3 the temperature difference of moving substance which is formed due to thermal contact of moving substance in its input flow with HEs of all separate HPs; ΔT_{cool}^{PP} is the temperature difference of moving substance which is formed due to cooling of moving substance in its output flow by all separate HPs; ΔT_2^{PP} – according to the diagram shown in Fig. 3 the temperature difference of moving substance which is formed due to thermal contact of moving substance in its output flow with HEs of all separate HPs.

If we use the respective assumptions, such as assumption 4, then for the case when moving substance in the input flow is heated by all separate HPs, according to the diagram shown in Fig. 3 we can write:

$$T_{hot,i}^{PP} = T_{hot,i}^{TH}; \tag{56}$$

$$T_{cool,(i-1)}^{PP} = T_{cool,i}^{TH}. \tag{57}$$

Eqs. (13) and (14) which establish the ratios between A_i and B_i for this case of *investigated method of heat and mass transfer* according to Fig. 3 and with the use of Eqs. (56), (57), (53) та (57), (56), (53), respectively, will take on the form:

$$A_i = (B_i - 1)\frac{T_{hot,i}^{PP}}{T_{cool,i}^{PP} - \Delta T_{cool,i}^{PP}} + 1; \tag{58}$$

$$B_i = (A_i - 1)\frac{T_{cool,i}^{PP} - \Delta T_{cool,i}^{PP}}{T_{hot,i}^{PP}} + 1. \tag{59}$$

Similar to the way we obtained mathematical expressions for the definition of temperature operating mode of the *investigated heat and mass transfer method* in the previous case, when moving substance in its input flow is cooled by all separate HPs, according to Fig. 2 one can also obtain the following mathematical expressions for this case of *investigated method of heat and mass transfer*, when moving substance in its input flow is heated by all separate HPs in conformity with Fig. 3.

For the case of using HPs whose heating coefficients are assigned by Eq.(10), according to the schematic of Fig. 3 the ratio for the definition of temperature operating mode of the *i*-th HP is as follows:

$$\Delta T_{cool,i}^{PP} = \frac{T_{cool,i}^{PP} + (B_i - 1)T_{hot,i}^{PP}}{\frac{B_i T_{hot,i}^{PP}}{\Delta T_{hot,i}^{PP}} + 1}. \tag{60}$$

For the same case, the total temperature difference of moving substance in its output flow:

$$\Delta T_{cool}^{PP} = \sum_{i=1}^{n} \frac{T_{cool,i}^{PP} + (B_i - 1) T_{hot,i}^{PP}}{\frac{B_i T_{hot,i}^{PP}}{\Delta T_{hot,i}^{PP}} + 1}. \tag{61}$$

In the case of using HPs whose coefficient of performance is assigned by Eq. (9), according to the diagram shown in Fig. 3 the ratio for the definition of temperature operating mode of the *i*-th HP is as follows:

$$\Delta T_{cool,i}^{PP} = \frac{(1 - A_i) T_{cool,i}^{PP} - T_{hot,i}^{PP} - A_i \Delta T_{hot,i}^{PP} + \sqrt{D_{hot,i}}}{2(1 - A_i)}, \tag{62}$$

where $D_{hot,i} = \left(T_{hot,i}^{PP} - (1 - A_i) T_{cool,i}^{PP} + A_i \Delta T_{hot,i}^{PP}\right)^2 + 4(1 - A_i) A_i \Delta T_{hot,i}^{PP} T_{cool,i}^{PP}$.

For the same case, the total temperature difference of moving substance in its output flow:

$$\Delta T_{cool}^{PP} = \sum_{i=1}^{n} \frac{(1 - A_i) T_{cool,i}^{PP} - T_{hot,i}^{PP} - A_i \Delta T_{hot,i}^{PP} + \sqrt{D_{hot,i}}}{2(1 - A_i)}. \tag{63}$$

For the case when the *i*-th HP operates on the Carnot cycle, the ratio for the definition of temperature operating mode of the *i*-th HP is as follows:

$$\Delta T_{cool,i}^{PP} = \frac{T_{cool,i}^{PP}}{\frac{T_{hot,i}^{PP}}{\Delta T_{hot,i}^{PP}} + 1}. \tag{64}$$

Also for the case when the *i*-th HP operates on the Carnot cycle, the total temperature difference of moving substance in its output flow:

$$\Delta T_{cool}^{PP} = \sum_{i=1}^{n} \frac{T_{cool,i}^{PP}}{\frac{T_{hot,i}^{PP}}{\Delta T_{hot,i}^{PP}} + 1}. \tag{65}$$

For the case which corresponds to assumption 9 and the diagram shown in Fig. 3 comprises *n* HPs, the ratio between the total temperature difference of moving substance in its input flow and the temperature difference of moving substance which is formed as a result of thermal contact of moving substance with the heat releasing HE of arbitrary *i*-th HP, is as follows:

$$\Delta T_{hot}^{PP} = n \cdot \Delta T_{hot,i}^{PP}. \tag{66}$$

For the case when the diagram shown in Fig. 3 comprises *n* HPs, whose heating coefficients are assigned by Eq. (10) and assumption 9 is valid, the total temperature difference of moving substance in its output flow:

$$\Delta T_{cool}^{PP} = \sum_{i=1}^{n} \frac{T_{cool,i}^{PP} + (B_i - 1) T_{hot,i}^{PP}}{\frac{B_i T_{hot,i}^{PP}}{\frac{1}{n} \Delta T_{hot}^{PP}} + 1}. \tag{67}$$

And for the case when the diagram shown in Fig. 3 comprises *n* HPs, whose coefficients of performance are assigned by Eq. (9) and assumption 9 is valid, the total temperature difference of moving substance in its output flow:

$$\Delta T_{cool}^{PP} = \sum_{i=1}^{n} \frac{(1 - A_i) T_{cool,i}^{PP} - T_{hot,i}^{PP} - \frac{1}{n} A_i \Delta T_{hot}^{PP} + \sqrt{D_{9,hot,i}}}{2(1 - A_i)}, \tag{68}$$

where $D_{9,hot,i} = \left(T_{hot,i}^{PP} - (1 - A_i) T_{cool,i}^{PP} + \frac{1}{n} A_i \Delta T_{hot}^{PP} \right)^2 + \frac{4}{n} (1 - A_i) A_i \Delta T_{hot}^{PP} T_{cool,i}^{PP}$.

For the case when the diagram shown in Fig. 3 comprises n HPs, each of which operates on the Carnot cycle in such a way that assumption 9 is valid, the ratio for the definition of temperature operating mode of the i-th HP is given below:

$$\Delta T_{cool,i}^{PP} = \frac{T_{cool,i}^{PP}}{\frac{T_{hot,i}^{PP}}{\frac{1}{n}\Delta T_{hot}^{PP}} + 1}. \tag{69}$$

In the case when all HPs in the diagram shown in Fig. 3 operate on the Carnot cycle, and when all changes of moving substance temperature resulting from its thermal contact with each HP HE in the input flow of this moving substance are equal (assumption 9), then all changes of moving substance temperature resulting from its thermal contact with each separate HP HE in the output flow of this moving substance are also equal:

$$\Delta T_{cool,(i-1)}^{PP} = \Delta T_{cool,i}^{PP}. \tag{70}$$

For the same case, total temperature difference of moving substance in its output flow:

$$\Delta T_{cool}^{PP} = n \cdot \Delta T_{cool,i}^{PP} = \frac{T_{cool,i}^{PP}}{\frac{T_{hot,i}^{PP}}{\Delta T_{hot}^{PP}} + \frac{1}{n}}. \tag{71}$$

With the use of direct designations of the diagram shown in Fig. 3, Eq.(71) is of the form:

$$\Delta T_2^{PP} = \frac{T_{2.i}^{PP}}{\frac{T_{1.i}^{PP}}{\Delta T_1^{PP}} + \frac{1}{n}}. \tag{72}$$

Conclusion

Mathematical expressions have been obtained for estimation of the efficiency of using the *investigated method of heat and mass transfer* for creation and maintenance of temperature difference between different parts of moving substance.

From the preliminary analysis of these mathematical expressions we can conclude about the opportunity in principle to use at least two HPs instead of one HP in the diagrams shown in Fig. 2 and Fig. 3 for increasing the energy efficiency of corresponding energy consuming heat and mass transfer processes.

At the same time, further theoretical and / or experimental studies may be required to make decisions regarding practical applications of the heat and mass transfer method described herein.

References

1. Anatychuk L.I., Prybyla A.V. (2016). Comparative analysis of thermoelectric and compression heat pumps for individual air-conditioners. *J. Thermoelectricity,* 2, 33–42.
2. Bonin J. (2015). *Heat pump planning handbook*. London and New York: Routledge.
3. Anatychuk L.I., Prybyla A.V., Rozver Yu.Yu. (2017). Experimental study of thermoelectric liquid-liquid heat pump. *J. Thermoelectricity,* 3, 47–53.

4. Anatychuk L.I., Prybyla A.V. (2017). Limiting possibilities of thermoelectric liquid-liquid heat pump. *J.Thermoelectricity,* 4, 49–54.
5. Anatychuk L.I., Prybyla A.V. (2017). The influence of quality of heat exchangers on the properties of thermoelectric liquid-liquid heat pumps. *J. Thermoelectricity,* 5, 59–64.
6. Havryliuk M.V., Konstantynovych I.A. (2013). Termoelektrychnyi prylad dlia elektroforezu [Thermoelectric device for electrophoresis]. *Naukovyi visnyk Chernivetskoho Universitetu. Fizyka. Elektronika – Scientific Bulletin of Chernivtsi University. Physics. Electronics,* 3(1), 33-42 [in Ukrainian].
7. Lee HoSung. (2016). *Thermoelectrics: design and materials*. Chichester, UK; Hoboken, NJ: John Wiley & Sons.
8. Alves-Filho O. (2015). *Heat pump dryers. Theory, design and industrial applications*. Boca Raton: CRC Press.
9. Akulich P.V. (2010). *Raschioty sushilnykh i teploobmennykh ustanovok [Calculations of drying and heat exchange installations]*. Minsk: Belarus navuka [in Russian].
10. Snezhkin Yu.F., Chalaiev D.M., Shapar R.A., Dabizha N.A. (2012). Osobennosti ispolzovaniia teplovykh nasosov v processakh sushki [Peculiarities of using heat pumps in drying processes]." *Materialy nauchno-tekhnicheskoi konferentsii "Teplonasosnyie tekhnologii v Ukraine. Sostoianiie i perspektivy vnedreniia" – Proc. of scientific and practical conference "Heat pump technologies in Ukraine. Current state and introduction prospects* (Ukraine, Kyiv, May 23–25, 2012). *Electronic journal ESCO, 6*. http://journal.esco.co.ua/2012_6/art365.pdf
11. Snezhkin Yu.F., Paziuk V.M., Petrova Zh.O., Chalaiev D.M. (2012). *Teplonasosna zernosusharka dlia nasinnevoho zerna [Heat pump grain dryer for seed grain]*. Kyiv: TOV Poligraph-Service [In Ukrainian].
12. *Patent* US 9700835 B2. Barnwell J.W. Thermoelectric compressed air and/or inert gas dryer.
13. *Patent* US 4065936 A. Fenton J.W., Lee J.S., Buist R.J. Counter flow thermoelectric heat pump with discrete sections.
14. Kshevetsky O.S. (2017). Otsinka energoefektyvnosti sposobu teplomasoobminu mizh rukhomoiu rechovynoiu i tepolvymy nasosamy [Estimation of energy efficiency of a method for heat and mass transfer between moving substance and heat pumps]. *Materialy Vseukrainskoi naukovo-praktychnoi konferentsii "Innovatsiini tekhnolohii v hotelno-restorannomu biznesi" – Proc. of All-Ukrainian scientific and practical conference "Innovation technologies in hotel and restaurant business"* (Ukraine, Kyiv, March 22–23). Kyiv: NUFT [in Ukrainian].
15. Kshevetsky O.S. (2017). Pro mozhlyvist pidvyshchennia enerhoefektyvnosti procesiv teplomasoobminu, yaki peredbachaiiut nahrivannia ta okholodzhennia rukhomoi rechovyny [On the possibility of increasing the energy efficiency of heat and mass transfer processes which involve heating and cooling of moving substance]. *Khimichna tekhnologiia ta inzheneriia: zbirnyk tez dopovidei Mizhnarodnoi naukovo-praktychnoi konferentsii - Chemical Technology and Engineering: collection of abstracts of International scientific and practical conference* (Ukraine, Lviv, June 26–30, 2017). Lviv: Lvivska Politekhnika [in Ukrainian].
16. Kshevetsky O.S., Shtangeieva N.I. (2017). Pro mozhlyvist vykorystannia dekilkokh teplovykh nasosiv dlia pidvyshchennia enerhoefektyvnosti deiakykh procesiv teplomasoobminu [On the possibility of using several heat pumps for increasing energy efficiency of some heat and mass transfer processes]. Tezy dopovidei X Mizhnarodnoi konferentsii "Problemy teplofizyky ta teploenerhetyky" – Abstracts of X International conference "Problems of thermophysics and heat power engineering" (Ukraine, Kyiv, May 23–26, 2017). *Promyshlennaia teploteknika – Industrial Heat Engineering,* 39(7), 79–80 [in Ukrainian].

Submitted 03.01.2018

Кшавецький О.С. *канд. фіз.-мат. наук, доцент*

Чернівецький торговельно-економічний інститут Київського національного торговельно-економічного університету,
Центральна площа, 7, м. Чернівці, 58002, Україна
e-mail: kshevos@gmail.com

ОЦІНКА ЕФЕКТИВНОСТІ ЧАСТИННОГО ВИПАДКУ ПРОЦЕСІВ ТЕПЛОМАСООБМІНУ МІЖ ТЕПЛОВИМИ НАСОСАМИ І РУХОМОЮ РЕЧОВИНОЮ, ЧАСТИНА 1

Отримані математичні вирази для оцінки ефективності роботи частинного випадку способу тепломасообміну між рухомою речовиною і тепловими насосами з їх теплообмінними частинами, при якому рухому речовину (або принаймні частину цієї рухомої речовини) приводять у тепловий контакт з теплопоглинаючою і тепловиділяючою теплообмінними частинами принаймні двох реальних теплових насосів. Бібл. 16, Рис. 3.
Ключові слова: тепловий насос, термоелектричний тепловий насос, рухома речовина, тепломасообмін, ефективність, енергоефективність.

Кшевецкий О.С. *канд. физ.-мат наук, доцент*

Черновицкий торгово-экономический институт
Киевского национального торгово-экономического университета,
Центральная площадь, 7, г. Чернівці, 58002, Украина
e-mail: kshevos@gmail.com

ОЦЕНКА ЭФФЕКТИВНОСТИ ЧАСТНОГО СЛУЧАЯ ПРОЦЕССОВ ТЕПЛОМАСООБМЕНА МЕЖДУ ТЕПЛОВЫМИ НАСОСАМИ И ПОДВИЖНЫМ ВЕЩЕСТВОМ, ЧАСТЬ 1

Получены математические выражения для оценки эффективности работы частного случая процесса тепломассообмена между подвижным веществом и тепловыми насосами с их теплообменными частями, при котором подвижное вещество (или по крайней мере часть этого подвижного вещества) приводят в тепловой контакт с теплопоглощающей и тепловыделяющей теплообменными частями по крайней мере двух реальных тепловых насосов. Библ. 16, Рис. 3.
Ключевые слова: тепловой насос, термоэлектрический тепловой насос, подвижное вещество, тепломассообмен, эффективность, энергоэффективность.

References

1. Anatychuk L.I., Prybyla A.V. (2016). Comparative analysis of thermoelectric and compression heat pumps for individual air-conditioners. *J. Thermoelectricity,* 2, 33–42.
2. Bonin J. (2015). *Heat pump planning handbook*. London and New York: Routledge.
3. Anatychuk L.I., Prybyla A.V., Rozver Yu.Yu. (2017). Experimental study of thermoelectric liquid-liquid heat pump. *J. Thermoelectricity,* 3, 47–53.
4. Anatychuk L.I., Prybyla A.V. (2017). Limiting possibilities of thermoelectric liquid-liquid heat pump. *J.Thermoelectricity,* 4, 49–54.
5. Anatychuk L.I., Prybyla A.V. (2017). The influence of quality of heat exchangers on the properties of thermoelectric liquid-liquid heat pumps. *J. Thermoelectricity,* 5, 59–64.
6. Havryliuk M.V., Konstantynovych I.A. (2013). Termoelektrychnyi prylad dlia elektroforezu [Thermoelectric device for electrophoresis]. *Naukovyi visnyk Chernivetskoho Universitetu. Fizyka. Elektronika – Scientific Bulletin of Chernivtsi University. Physics. Electronics,* 3(1), 33-42 [in Ukrainian].
7. Lee HoSung. (2016). *Thermoelectrics: design and materials.* Chichester, UK; Hoboken, NJ: John Wiley & Sons.
8. Alves-Filho O. (2015). *Heat pump dryers. Theory, design and industrial applications*. Boca Raton: CRC Press.
9. Akulich P.V. (2010). *Raschioty sushilnykh i teploobmennykh ustanovok [Calculations of drying and heat exchange installations]*. Minsk: Belarus navuka [in Russian].
10. Snezhkin Yu.F., Chalaiev D.M., Shapar R.A., Dabizha N.A. (2012). Osobennosti ispolzovaniia teplovykh nasosov v processakh sushki [Peculiarities of using heat pumps in drying processes]." *Materialy nauchno-tekhnicheskoi konferentsii "Teplonasosnyie tekhnologii v Ukraine. Sostoianiie i perspektivy vnedreniia" – Proc. of scientific and practical conference "Heat pump technologies in Ukraine. Current state and introduction prospects* (Ukraine, Kyiv, May 23–25, 2012). *Electronic journal ESCO, 6*. http://journal.esco.co.ua/2012_6/art365.pdf
11. Snezhkin Yu.F., Paziuk V.M., Petrova Zh.O., Chalaiev D.M. (2012). *Teplonasosna zernosusharka dlia nasinnevoho zerna [Heat pump grain dryer for seed grain]*. Kyiv: TOV Poligraph-Service [In Ukrainian].
12. *Patent* US 9700835 B2. Barnwell J.W. Thermoelectric compressed air and/or inert gas dryer.
13. *Patent* US 4065936 A. Fenton J.W., Lee J.S., Buist R.J. Counter flow thermoelectric heat pump with discrete sections.
14. Kshevetsky O.S. (2017). Otsinka energoefektyvnosti sposobu teplomasoobminu mizh rukhomoiu rechovynoiu i tepolvymy nasosamy [Estimation of energy efficiency of a method for heat and mass transfer between moving substance and heat pumps]. *Materialy Vseukrainskoi naukovo-praktychnoi konferentsii "Innovatsiini tekhnolohii v hotelno-restorannomu biznesi" – Proc. of All-Ukrainian scientific and practical conference "Innovation technologies in hotel and restaurant business"* (Ukraine, Kyiv, March 22–23). Kyiv: NUFT [in Ukrainian].
15. Kshevetsky O.S. (2017). Pro mozhlyvist pidvyshchennia enerhoefektyvnosti procesiv teplomasoobminu, yaki peredbachaiiut nahrivannia ta okholodzhennia rukhomoi rechovyny [On the possibility of increasing the energy efficiency of heat and mass transfer processes which involve heating and cooling of moving substance]. *Khimichna tekhnologiia ta inzheneriia: zbirnyk tez dopovidei Mizhnarodnoi naukovo-praktychnoi konferentsii - Chemical Technology and Engineering: collection of abstracts of International scientific and practical conference* (Ukraine, Lviv, June 26–30, 2017). Lviv: Lvivska Politekhnika [in Ukrainian].

16. Kshevetsky O.S., Shtangeieva N.I. (2017). Pro mozhlyvist vykorystannia dekilkokh teplovykh nasosiv dlia pidvyshchennia enerhoefektyvnosti deiakykh procesiv teplomasoobminu [On the possibility of using several heat pumps for increasing energy efficiency of some heat and mass transfer processes]. Tezy dopovidei X Mizhnarodnoi konferentsii "Problemy teplofizyky ta teploenerhetyky" – Abstracts of X International conference "Problems of thermophysics and heat power engineering" (Ukraine, Kyiv, May 23–26, 2017). *Promyshlennaia teploteknika – Industrial Heat Engineering,* 39(7), 79–80 [in Ukrainian].

Submitted 03.01.2018

V.P.Zaykov[1], *Candidate of Tech. science*,
V.I.Mescheryakov[2], *Doctor of Tech. science*,
Yu. I. Zhuravlov[3], *Candidate of Tech. science*

[1]SHTORM Research Institute, 27, Tereshkova str.,
Odesa, Ukraine; *e-mail: grand@i.ua;*
[2]Odesa State Ecological University, 15, Lvivska str,, Ukraine;
e-mail: grand@ua.fm;
[3]National University "Odesa Maritime Academy", 8,
Didrikhson str., Ukraine; *e-mail: zhuravlov.y@ya.ru.*

MODEL OF INTERRELATION BETWEEN RELIABILITY INDICATORS OF A SINGLE-STAGE COOLER AND THE GEOMETRY OF THERMOELEMENT LEGS

The paper deals with improving the reliability indicators of a single-stage thermoelectric cooler using a constructive method by developing and analyzing a reliability-oriented model relating reliability indicators to the geometry of thermoelements. The investigations were carried out for various temperature differences, a fixed thermal load for various operating modes. It is shown that with decreasing the ratio of thermoelement height to its cross section, the maximum cooling power is increased, the number of thermoelements is decreased and the probability of failure-free operation is increased. At the same time, the existing technology of manufacturing coolers does not change, the results of existing mechanical and climatic tests, the material of thermoelements, the cost of modules remain unvaried.. Bibl. 12, Fig. 11, Table. 3.

Key words: thermoelectric cooler, geometry of thermoelements, reliability indicators, cooling power, temperature difference.

Introduction

Reliability refers to the most important indicators of the means for ensuring the thermal modes of heat-loaded radioelectronic equipment [1]. In terms of mass dimensions, speed, climatic and mechanical operating conditions, thermoelectric devices (TEC) have an undeniable advantage over compression coolers [2]. Mathematical simulation of reliability indicators of TEC at all stages of the life cycle has become a prerequisite for creation of on-board equipment, the demands on which are constantly being toughened [3]. The development and analysis of the models makes it possible to take into account the influence of manufacturing technology [4], moisture [5], mechanical [6], climatic [7] factors, heat load [8], thermoelement materials [9] on reliability indicators, as long as potential for reducing the degree of their impact is built in exactly at simulation stage [10]. At the same time, in the literature, the issues of the influence of the structural component on the operational reliability of thermoelectric devices are insufficiently elucidated. There are several approaches to the design of thermoelectric cooling devices:

1. The geometry of thermoelement legs is set as l/s =const, where l is height, s is cross-section area of thermoelement leg. In this case, varying the value of operating current I, one can assure the work of TEC in different operating modes from $Q_{0\max}$ to $Q_0 = 0$ and thus to increase the reliability [11].

2. At the same time, in thermoelectric instruments making, various designs of unified modules are used with different geometry of thermoelement legs $l/s = \text{var}$, and the developer faces the question of choosing the

geometry of thermoelement legs in TEC for various operating conditions, which allows increasing the reliability indicators. Rational choice of the geometry of thermoelement legs with regard to all constraints is a rather relevant task.

The purpose of the work is development of a mathematical model of thermoelectric cooler relating reliability indicators to the geometry of thermoelement legs, the analysis of which allows optimization of reliability indicators at different temperature drops and operation modes.

Development and analysis of the model of interrelation between reliability indicators, structural and energy parameters in the modes $\lambda_{\min}$, $\Delta T_{\max}$ and heat pump ($\Delta T = 0$ K).

Let us consider the influence of the geometry of thermoelement legs on the main parameters and reliability indicators of a single-stage TEC for different temperature drops ΔT from 0 to 60 K.

As is known, cooling capacity of TEC Q_0 can be written as expression

$$Q_0 = nI^2{}_{\max}R(2B - B^2 - \Theta) = n\gamma(2B - B^2 - \Theta), \qquad (1)$$

where *n* is the number of thermoelements, pcs;

$I_{\max}$ is maximum operating current, $I_{\max} = \bar{e}T_0 \big/ R$, A;

R is electrical resistance of thermoelement leg, $R = I \big/ \bar{\sigma} s$, Ohm;

$\bar{e}$, $\bar{\sigma}$ are averaged Seebeck coefficient, V/K, and electrical conductivity of thermoelement leg, S/cm, respectively;

T_0 is temperature of heat-absorbing junction, K;

B is relative operating current $B = I/I_{\max}$, relative units;

I is the value of operating current, A;

Θ is relative temperature drop, $\Theta = \Delta T/\Delta T_{\max} = (T - T_0)/\Delta T_{\max}$, relative units;

T is temperature of heat-releasing junction, K;

$\Delta T_{\max}$ is maximum temperature drop, $\Delta T_{\max} = 0{,}5\bar{z}T_0^2$, K;

$\bar{z}$ is averaged thermoelectric figure of merit of thermoelement leg, 1/K;

γ is maximum thermoelectric cooling power, $\gamma = I_{\max}^2 R = \bar{e}^2 \bar{\sigma} T_0^2 \, s/l$, W.

Power consumption of TEC can be written as:

$$W = 2n\gamma B(B + (\Delta T_{\max}/T_0)\Theta \qquad (2)$$

Coefficient of performance *E* is determined by expression

$$E = Q_0/W = \left(2B - B^2 - \Theta\right) \Big/ 2B\left(B + (\Delta T_{\max}/T_0)\Theta\right) \qquad (3)$$

The relative value of failure rate λ / λ_0 [12] can be represented as:

$$\lambda/\lambda_0 = \frac{nB^2\left(\Theta + C\right)\left(B + (\Delta T_{\max}/T_0)\Theta\right)^2}{\left(1 + (\Delta T_{\max}/T_0)\Theta\right)^2} K_T \qquad (4)$$

where λ_0 is nominal failure rate, 1/h;

C is relative value of thermal load, $C = Q_0 \big/ \left(nI_{\max}^2 R \right) = Q_0 / n\gamma$;

K_T is temperature-dependent coefficient of significance.

The probability of failure-free operation of TEC can be determined by the known formula

$$P = \exp\left(-\lambda t\right) \qquad (5)$$

where t is assigned resource, hour.

Mode $\lambda_{\min}$.

Table 1 summarizes the results of calculating the main parameters and reliability indicators of a single-stage TEC for different ratios l/s in the mode $\lambda_{\min}$ $(B = \eta\Theta)$ with the following initial data:

– thermal load Q_0 = 2.0 W;

– temperature of heat-releasing junction T= 300 K;

– temperature drop ΔT = 0 K, 20 K, 40 K, 60 K;

– averaged thermoelectric figure of merit $\bar{z}_M = 2.4 \cdot 10^{-3}$ 1/K;

– $\lambda_0 = 3 \cdot 10^{-8}$ 1/h; $t = 10^4$ h.

With the same thermal load Q_0 and temperature drop ΔT for different geometry of thermoelement leg (l/s = var) the value $n\gamma$ = const.

Table 1

The results of calculating the main parameters and reliability indicators of a single-stage device for different temperature differences ΔT and geometry of thermoelement legs (l/S) at T = 300 K, Q_0 = 2.0 W, $\bar{z}$ = 2.4·10^{-3} 1/K; l = 4 mm in the mode λ_{min}

l/S, sm^{-1}	γ, W	n, pcs.	$R\cdot10^3$, Ohm	I_{max}, A	I, A	U, V	λ/λ$_0$	λ·10^8, 1/h	P	S=(a×b), mm
Δ*T*= 10 K										
Θ= 0.10; V = 0.071; ΔT_{max}= 100.9 K; $\Delta T_{max}/T_0$ = 0.35; W = 0.81 W; E = 2.46; K_T=1.007; z = 2.4·10^{-3} 1/K										
40.0	0.0762	709.4	44.4	1.31	0.093	8.83	0.0052	0.0155	0.99999845	1.0×1.0
20.0	0.162	335.5	22.2	2.70	0.192	4.23	0.00245	0.00735	0.99999926	1.5×1.5
10.0	0.324	167.0	11.1	5.40	0.383	2.12	0.00122	0.00366	0.99999963	2.1×2.1
4.5	0.720	75.1	5.0	12.0	0.852	0.953	0.00055	0.00164	0.99999984	3.1×3.1
3.25	0.997	54.3	3.61	16.6	1.18	0.69	0.00040	0.00119	0.99999988	3.6×3.6
2.0	1.62	33.4	2.22	27.0	1.92	0.423	0.000243	0.00073	0.99999993	4.6×4.6
1.0	3.24	16.7	1.11	54.0	5.0	0.212	0.000122	0.000365	0.999999964	6.5×6.5
Δ*T*= 20 K										
Θ= 0.214; V = 0.146; ΔT_{max}= 93.3 K; $\Delta T_{max}/T_0$ = 0.33; W = 2.23 W; E = 0.90; K_T=1.01; z = 2.38·10^{-3} 1/K										
40.0	0.071	499.4	42.6	1.29	0.19	11.7	0.1179	0.354	0.999965	1.0×1.0
20.0	0.143	246.7	21.3	2.60	0.38	5.90	0.059	0.177	0.999982	1.4×1.4
10.0	0.286	123.3	10.64	5.2	0.76	2.90	0.030	0.089	0.9999911	2.0×2.0
4.5	0.676	52.2	4.79	11.5	1.70	1.33	0.0125	0.038	0.9999963	3.1×3.1
3.25	0.880	40.0	3.46	15.9	2.30	0.96	0.0096	0.029	0.9999971	3.5×3.5
2.0	1.43	24.7	2.13	25.9	3.80	0.60	0.0059	0.018	0,9999982	4.5×4.5
1.0	2.86	12.3	1.06	52.0	9.9	0.30	0.0030	0.0089	0.99999911	6.3×6.3

Continuation of Table 1

ΔT= 40 K										
Θ= 0.5; V = 0.40; ΔT_{max}= 79.8 K; $\Delta T_{max}/T_0$ = 0,31; W = 6.34 W; E = 0,315;K_T=1.022; z = 2.37·10^{-3} 1/K										
40.0	0.0625	228.6	40.8	1.24	0.494	12.8	5.52	16.56	0.99835	1.0×1.0
20.0	0.125	114.3	20.4	2.47	1.0	6.40	2.76	8.30	0.99917	1.4×1.4
10.0	0.249	57.4	10.2	4.95	2.0	3.20	1.39	4.20	0.99958	2.0×2.0
4.5	0.554	25.8	4.59	11.0	4.4	1.44	0.625	1.87	0.99981	3.0×3.0
3.25	0.767	18.6	3.32	15.2	6.1	1.04	0.45	1.35	0.999865	3.5×3.5
2.0	1.246	11.5	2.04	2.47	10.0	0.64	0.28	0.84	0.999917	4.5×4.5
1.0	2.49	5.70	1.02	49.5	19.8	0.32	0.14	0.42	0.999958	6.3×6.3
ΔT= 60 K										
Θ= 0.9; V = 0.855; ΔT_{max}= 66.8 K; $\Delta T_{max}/T_0$ = 0.28; W = 47.9 W; E = 0.042; K_T=1.035; z = 2.32·10^{-3} 1/K										
40.0	0.053	477.8	38.8	1.17	1.0	47.9	276.6	830	0.9204	1.0×1.0
20.0	0.106	238.8	19.4	2.34	2.0	24.0	138.3	414.8	0.9594	1.4×1.4
10.0	0.212	119.4	9.71	4.67	4.0	12.0	69.15	207.5	0.9795	2.0×2.0
4.5	0.471	53.8	4.37	10.4	8.90	5.40	31.1	93.3	0.99071	3.0×3.0
3.25	0.625	38.8	3.16	14.3	12.3	3.90	22.4	67.3	0.9933	3.5×3.5
2.0	1.06	23.9	1.94	23.4	20.0	2.40	13.8	41.4	0.9959	4.5×4.5
1.0	2.12	11.9	0.97	46.8	40.0	1.20	6.9	20.6	0.9979	6.3×6.3

Analysis of calculated values of the main parameters and reliability indicators has shown that with decreasing the ratio l/s at given temperature drop ΔT and thermal load Q_0 in the mode λ_{min}:

– the value of operating current I is increased (Fig. 1, a);

– maximum cooling power γ is increased (Fig. 1, a);

– the drop of voltage U is decreased (Fig. 1, b);

– the failure rate λ is decreased, and the probability of failure-free operation P is increased (Fig. 2).

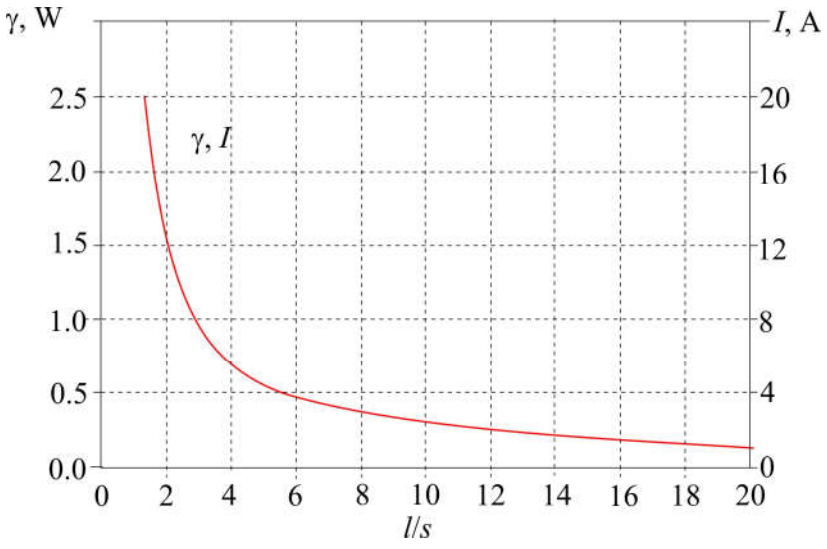

a)

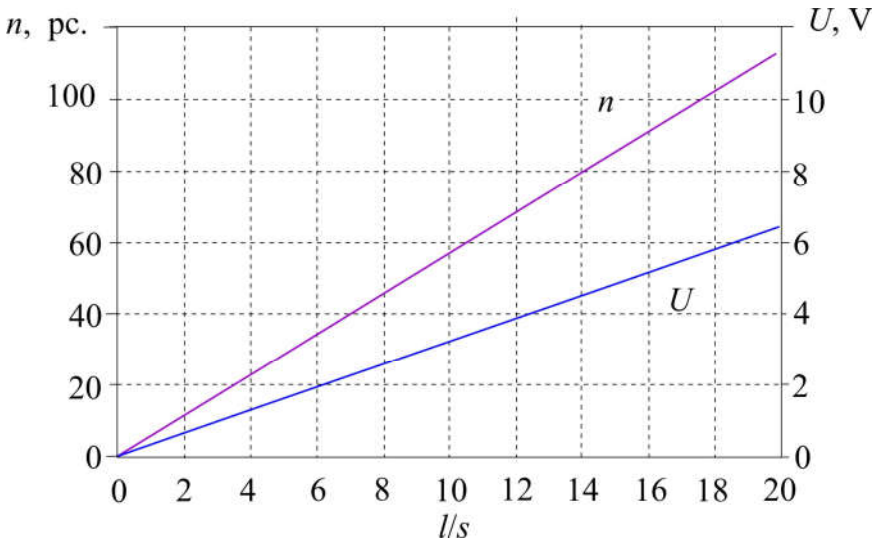

b)

Fig. 1. Dependence of parameters γ, I (a) and n, U (b) of a single-stage TEC on the value of ratio l/s at T = 300 K, ΔT = 40 K and Q_0 = 2.0 W in the mode λ_{min}

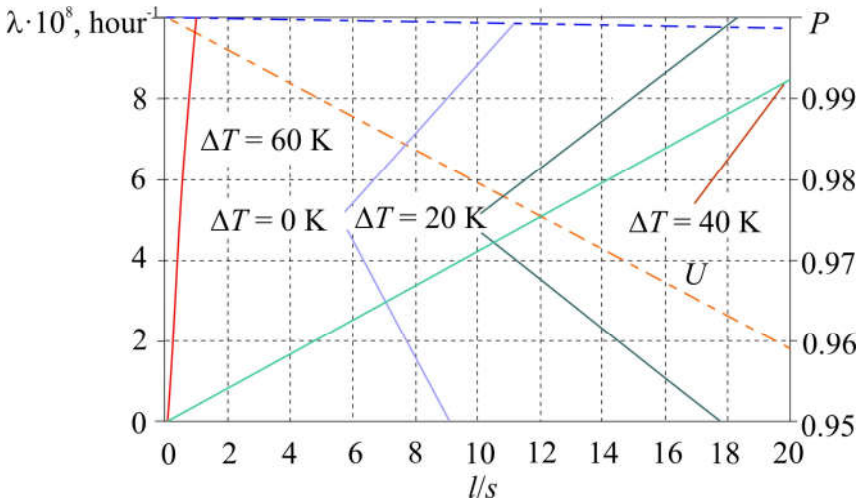

Fig. 2. Dependence of failure rate λ (solid lines) and probability of failure-free operation P (dashed lines) of a single-stage TEC on the value of ratio l/s at T = 300 K, Q_0 = 2.0 W, $\lambda_0 = 3 \cdot 10^{-8}$ 1/h, $t = 10^4$ h and different values of ΔT in the mode λ_{min}

With increase in temperature drop ΔT for different values of l/s in the mode $\lambda_{\min}$:

– maximum thermoelectric cooling power is decreased;

– the value of operating current *I* is increased (Fig. 3, a);

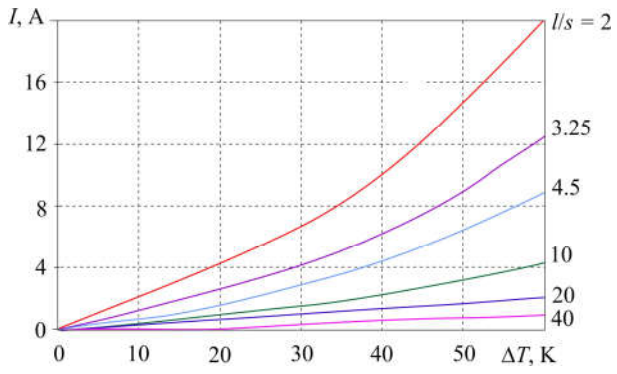

a)

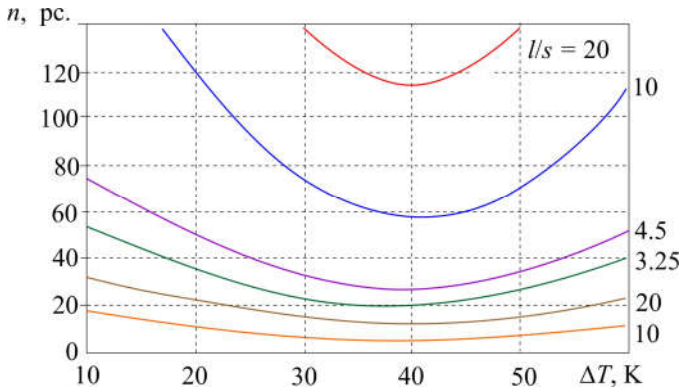

b)

Fig. 3. Dependence of operating current I (a) and the number of thermoelements n (b) of a single-stage TEC on temperature drop ΔT at T = 300 K, Q_0 = 2.0 W and different values of ratio l/s in the mode $\lambda_{min.}$

– functional dependence of the quantity of thermoelements in TEC on temperature drop. ΔT has a minimum for different values of ratio l/s (Fig. 3b), which can be explained by cooling capacity growth per one thermoelement Q_0/n at ΔT_{opt} at a point of minimum;

– failure rate λ/λ_0 is increased and the probability of failure-free operation *P* is reduced (Fig. 4).

It should be noted that with decreasing the ratio l/s the operating current I is increased (Fig. 5).

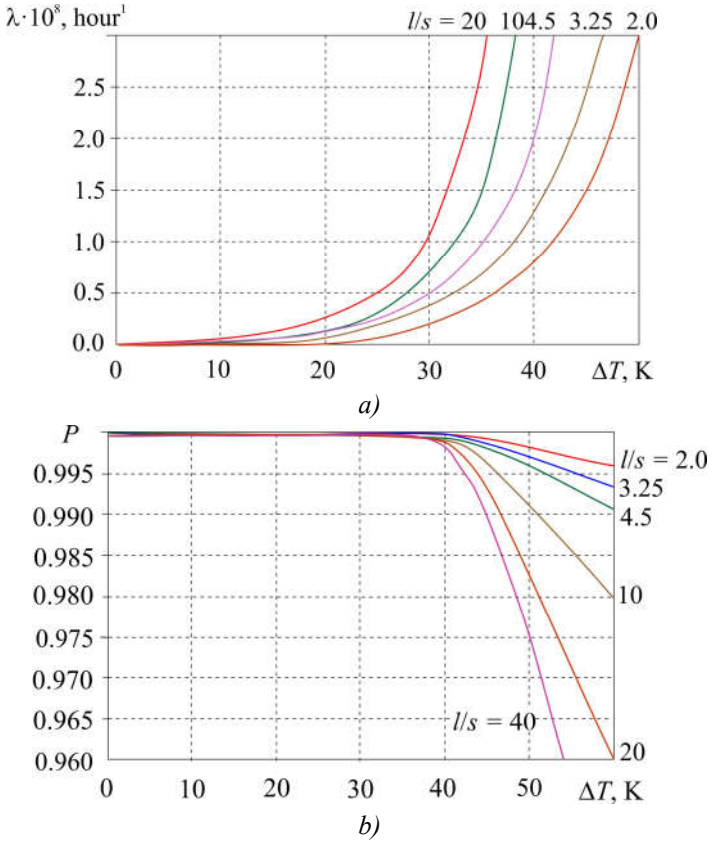

a)

b)

Fig. 4. Dependence of failure rate λ(a) and probability of failure-free operation P (b) of a single-stage TEC on temperature drop ΔT at T = 300 K, Q_0 = 2.0 W, $\lambda_0 = 3 \cdot 10^{-8}$ 1/h, t = 10^4 h and different values of ratio l/s in the mode λ_{min}

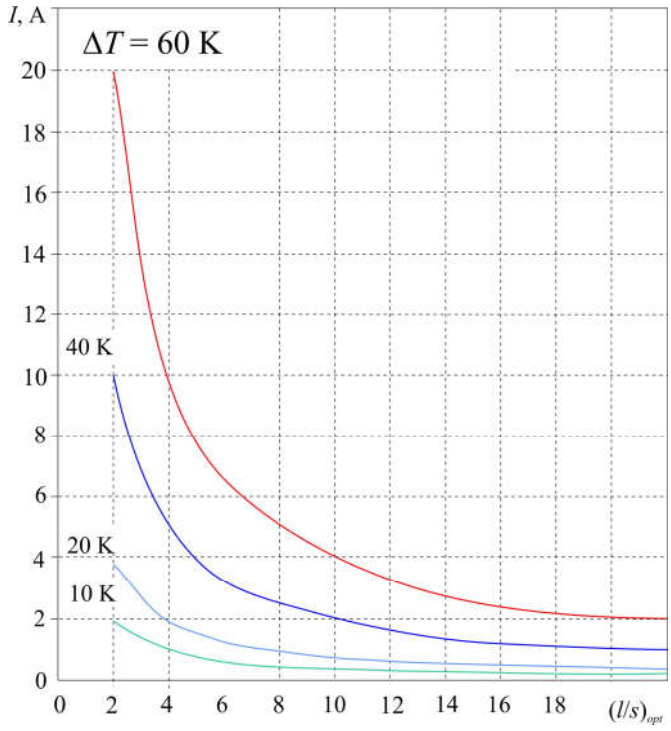

Fig. 5. Dependence of operating current I on the optimal ratio $(l/s)_{onm}$ of a single-stage TEC at T = 300 K, Q_0 = 2.0 W and different values of ΔT in the mode λ_{min}

For the mode $\lambda_{\min}$ at ΔT = 40 K and Q_0 = 2.0 W the decrease in the ratio l/s from 20 to 10 allows reducing failure rate by a factor of 2 (from $8.3\cdot10^{-8}$ to $4.2\cdot10^{-8}$ 1/h), hence, increasing the probability of failure-free operation *P*. In so doing, the quantity of thermoelements n is halved, the operating current *I* is increased from 1 to 2 A, and power consumption and coefficient of performance remain constant (*W* = 6.34 W, *E* = 0.315).

Mode $\Delta T_{\max}\left(Q_0 = 0\right)$**.** Let us consider a single-stage TEC and determine the optimal geometry of thermoelement legs providing for maximum temperature drop $\Delta T_{\max}$. For this purpose we will use known relations [12].

Cooling capacity Q_0 of cooling thermoelement can be written as

$$Q_0 = 2n\left[\bar{e}\,lT_0 - \tfrac{1}{2}I^2R - K(T - T_0)\right] \qquad (6)$$

or

$$Q_0 = 2n\left[\bar{e}\,lT_0 - \frac{1}{2}\frac{I^2(l/s)}{\bar{\sigma}} - \frac{\bar{\chi}}{(l/s)}(T - T_0)\right] \qquad (7)$$

where $\bar{e}, \bar{\sigma}, \bar{\chi}$ are averaged values of the Seebeck coefficient, V/K, electric conductivity, S/cm and thermal conductivity of thermoelement leg, W(smK), respectively.

Then the dependence of temperature of heat-absorbing junction T_0 on the geometry of thermoelement legs at given value of operating current *I* can be represented as:

$$T_0 = \frac{I^2\left(\frac{l}{s}\right)^2 + 2\bar{\chi}\bar{\sigma}T + \frac{Q_0\bar{\sigma}}{n}\frac{l}{s}}{2\bar{\sigma}\left(\chi^2 + \bar{e}I\frac{l}{s}\right)} \tag{8}$$

From condition $(dT_0/\mathrm{d}(l/s)) = 0$ one can determine optimal geometry of thermoelement legs $(l/s)_{opt}$, assuring maximum temperature difference ($\Delta T_{max} = T - T_{0min}$) at given operating current I:

$$\left(\frac{l}{s}\right)_{opt} = \frac{\bar{\chi}}{\bar{e}I}\left[\sqrt{1 + 2\bar{z}T\left(1 - \frac{Q_0}{2n\bar{e}IT}\right)} - 1\right] \tag{9}$$

From this expression it is seen that with increasing the thermal load Q_0, the value $(l/s)_{opt}$ is decreased, and at $Q_0 \to 0$, i.e. in the absence of thermal load, it will take on the form

$$\left(\frac{l}{s}\right)_{opt} = \frac{\bar{\chi}}{\bar{e}I}\left[\sqrt{1 + 2\bar{z}T} - 1\right] \tag{10}$$

It can be readily shown that the value $(l/s)_{opt}$, assuring maximum temperature drop ΔT_{max}, is practically the same as in the mode $Q_{0\max}\left(\Theta \to 1{,}0\right)$, which is equal to

$$\left(\frac{l}{s}\right)_{opt} = \frac{\bar{e}\bar{\sigma}T_0}{I} \tag{11}$$

As is seen in Fig. 6, in the mode ΔT_{max} with decrease in l/s, the operating current I is increased.

To calculate the main parameters and reliability indicators of a single-stage TEC, we will use the above relations. The results of calculations with the optimal geometry of thermoelement legs are given in Table 2.

Heat pump mode ($\Delta T = 0$). One of possible applications of thermoelectricity is the use of thermoelectric modules as a heat pump for thermal power output at $\Delta T = 0$ K.

The main characteristic of such a mode is the so-called thermal coefficient μ which is the ratio of the value of thermal power output Q_N to spent (consumed) W at $\Delta T = 0$ K:

$$\mu = \frac{Q_N = Q_0}{W} = \frac{2 - B}{2B} \tag{12}$$

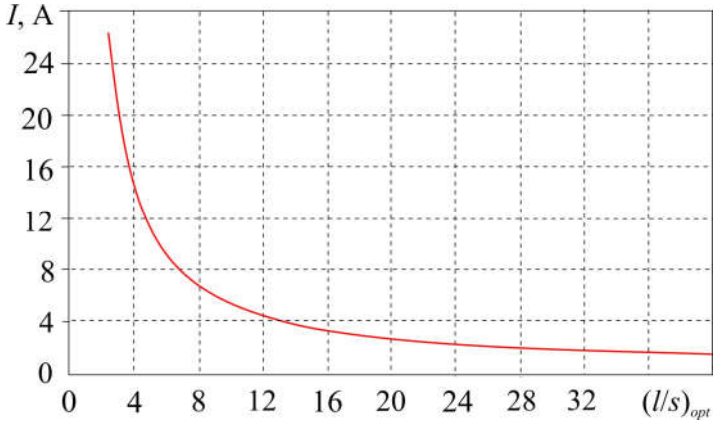

Fig. 6. Dependence of operating current I on the optimal ratio $(l/s)_{opt}$ of a single-stage TEC at $T = 300$ K, $Q_0 = 2.0$ W in the mode ΔT_{max}

Table 2

The results of calculating the main parameters and reliability indicators of a single-stage TEC with the optimal geometry of thermoelement legs at T = 300 K; T_{0min} = 235 K; Q_0 = 0 W; ΔT_{max} = 65 K; K_T = 1.04, $\bar{z}$ =2.4·10^{-3} 1/K; $\bar{e}$ = 2.0·10^{-3} V/K; σ = 900 S cm; $\bar{\chi}$ = 15·10^{-3} W/(S·K) in the mode ΔT_{max}

$(l/S)_{opt}$	$R\cdot10^{-3}$, Ohm	$I=I_{max}$, A	n, pcs.	λ/λ_0	$\lambda\cdot10^8$, 1/h	P	l, mm	$S=(a\times b)$, mm	γ, W
38.0	35.5	1.25	3	3.12	9.36	0.99906	4.0	1.0×1.0	0.055
			9	9.36	28.1	0.9972	3.0	0.8×0.8	
							2.0	0.7×0.7	
			27	28.1	84.2	0.99162	1.5	0.6×0.6	
							1.0	0.5×0.5	
19.0	17.7	2.25	3	3.12	9.36	0.99906	4.0	1.45×1.45	0.110
			9	9.36	28.1	0.9972	3.0	1.25×1.25	
							2.0	1.0×1.0	
			27	28.1	84.2	0.99162	1.5	0.9×0.9	
							1.0	0.7×0.7	
9.4	8.85	5.0	3	3.12	9.36	0.99906	4.0	2.0×2.0	0.220
			9	9.36	28.1	0.9972	3.0	1.7×1.7	
							2.0	1.4×1.4	
			27	28.1	84.2	0.99162	1.5	1.2×1.2	
							1.0	1.0×1.0	
4.3	4.0	11.0	3	3.12	9.36	0.99906	4.0	3.0×3.0	0.484
			9	9.36	28.1	0.9972	3.0	2.6×2.6	
							2.0	2.1×2.1	
			27	28.1	84.2	0.99162	1.5	1.8×1.8	
							1.0	1.5×1.5	
1.9	1.8	25.0	3	3.12	9.36	0.99906	4.0	4.5×4.5	1.089
			9	9.36	28.1	0.9972	3.0	3.9×3.9	
							2.0	3.2×3.2	
			27	28.1	84.2	0.99162	1.5	2.7×2.7	

Fig. 7a represents a dependence of thermal coefficient μ on the relative operating current B in the heat pump mode. With increasing the relative operating current B, coefficient μ decreases and at B = 1.0 it becomes equal to μ = 0.5, i.e. achieves its minimal value.

At a given value of thermal power output Q_N one can use modules or TEC with different number of thermoelements n at T = 300 K, ΔT = 0 K.

Fig. 7b represents a dependence of thermal coefficient μ on the number of thermoelements n for different value of thermal power output Q_N at T = 300 K, ΔT = 0 K. With increasing the number of thermoelements n, thermal coefficient μ is increased for different values of thermal power output Q_N. With increasing the value of thermal power output Q_N at given number of thermoelements n, thermal coefficient μ is decreased.

The value of relative operating current B for different values of Q_N and n can be determined from the expression

$$B = 1 - \sqrt{1 - C} \qquad (13)$$

where $C = \frac{Q_N}{nI_{\max}^2 R} = \frac{Q_N}{n\gamma}$;

$$\gamma = I_{\max}^2 R \tag{13}$$

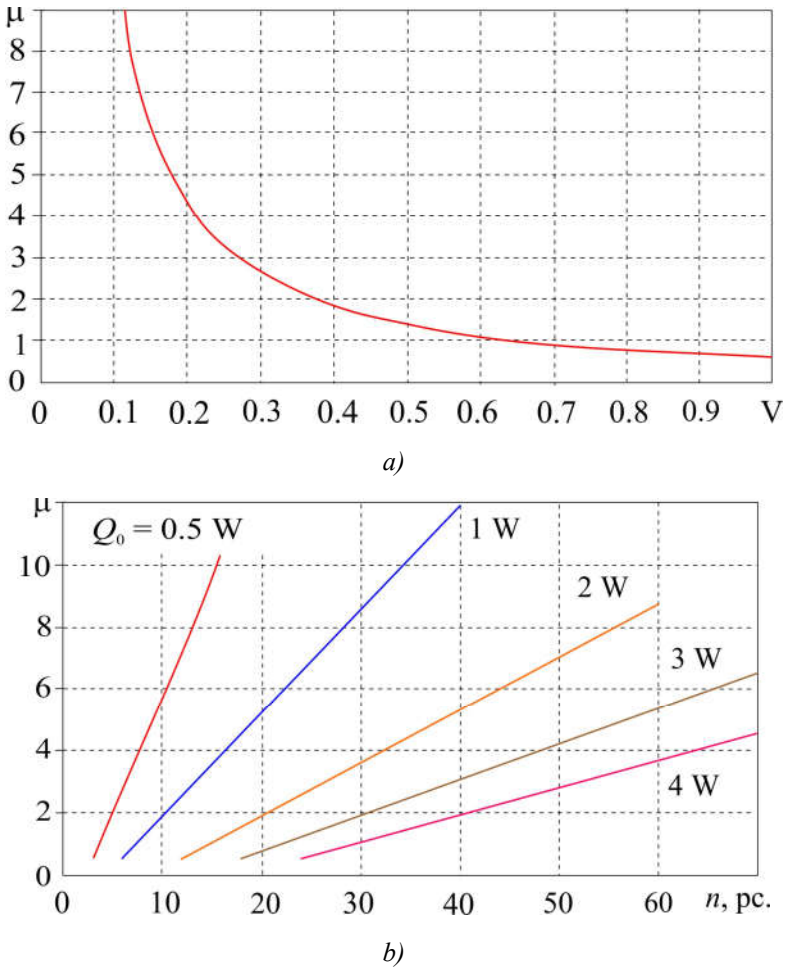

Fig. 7. Dependence of thermal coefficient μ of a single-stage TEC on relative operating current B (a) and the number of thermoelements n for different values of thermal power output (b) at T = 300 K, l/s = 20 in the heat pump mode (ΔT = 0 K)

Fig. 8 represents a dependence of relative operating current B on the number of thermoelements n for different thermal power output Q_N at $T = 300$ K, $\Delta T = 0$ K. With increasing the number of thermoelements n, the relative operating current B is decreased for different Q_N. At a given number of thermoelements n, with increasing the thermal power output Q_N, the relative operating current B is increased.

The relative value of failure rate λ/λ_0 of a single-stage TEC in the heat pump mode can be represented as [12]:

$$\lambda/\lambda_0 = nB^4C \tag{14}$$

in the heat pump mode ($\Delta T = 0$ K).

Fig. 9 represents dependences of relative value of failure rate λ/λ_0 and the probability of failure-free operation P of a single-stage TEC on the number of thermoelements n for different values of thermal power output Q_N in the heat pump mode.

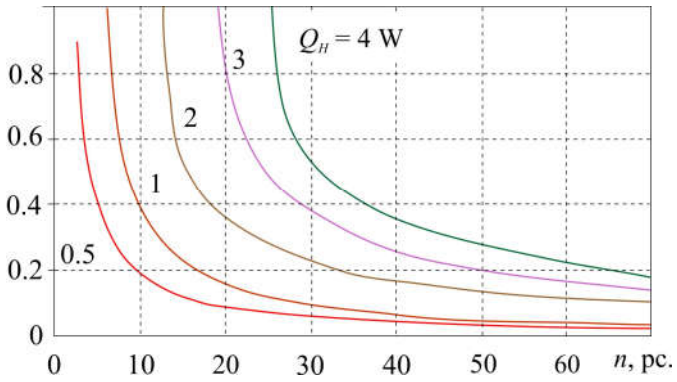

Fig. 8. Dependence of relative operating current B of a single-stage TEC on the number of thermoelements n at T = 300 K, l/s = 20 and different values of thermal power output Q_N

Let us consider the influence of the geometry of thermoelement legs of a single-stage heat pump on its main parameters and reliability indicators with a given number of thermoelements $n = 27$ in TEC and for different thermal power output $Q_N = 1.0; 2.2; 2.9; 4.0; 8.8$ W.

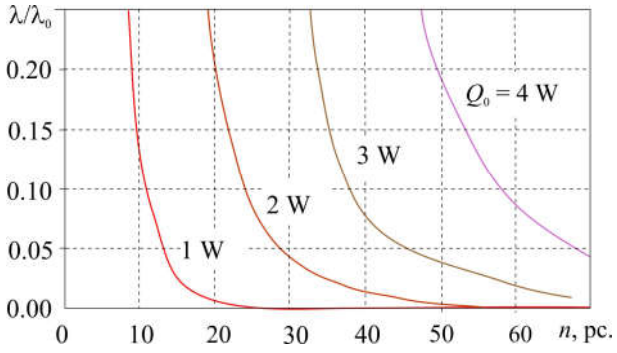

a)

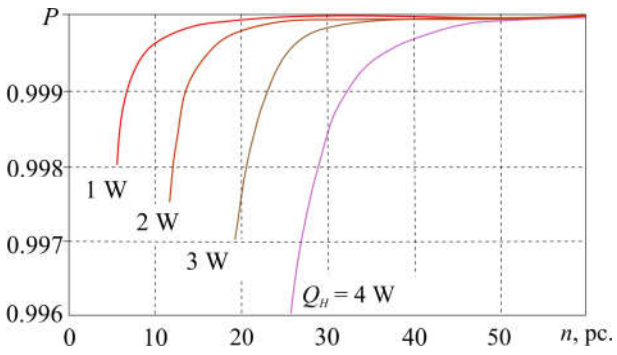

b)

Fig. 9. Dependence of relative failure rate λ/λ_0 (a) and the probability of failure -free operation P (b) of a single-stage TEC on the number of thermoelements n at T = 300 K, l/s = 20, $\lambda_0 = 3 \cdot 10^{-8}$ 1/h, t = 10^4 h and different values of thermal power output in the heat pump mode ($\Delta T = 0$ K).

The results of calculating the main parameters and reliability indicators of a single-stage TEC in the heat pump mode are given in Table 3.

With increasing the number of thermoelements *n,* the failure rate λ/λ_0 is decreased. With a given number of thermoelements *n*, the failure rate λ/λ_0 is increased with increase of Q_N from 1.0 to 4.0 W. As the number of thermoelements *n* in TEC is increased, the probability of failure-free operation *P* is increased for different values of Q_N.

With a given number of thermoelements *n,* the probability of failure-free operation *P* of a single-stage TEC is decreased with increasing the thermal power output Q_N.

Analysis of calculation results has shown that with decreasing the ratio *l*/*s* at given *n* for different power output Q_N in the heat pump mode:

– relative operating current *B* is decreased (Fig. 10);
– maximum operating current I_{max} is increased;
– operating current *I* is decreased;
– power consumption *W* is decreased;
– voltage drop *U* is decreased;
– thermal coefficient μ is increased;

failure rate λ/λ_0 is decreased and probability of failure-free operation *P* is increased (Fig. 11).

Table 3

The results of calculating the main parameters and reliability indicators of a single-stage TEC for different geometry of thermoelement legs at T= 300 K, n= 27, $Q_н$ = 2.2 W, $\overline{z}$ = 2.4·10^{-3} 1/K; $\overline{e}$ = 2,0·10^{-4} V/K; σ = 900 S/cm; $\overline{\chi}$ = 15·10^{-3} W/(S·K) and different thermal load in heat pump mode (ΔT = 0 K)

l/*S*	*R*·10^3, Ω	*B*	*I* max, A	*I*, A	*C*	*W*, W	*U*, V	μ	λ/λ0	λ·10^8, 1/h	*P*
$Q_н$ = 1.0 W											
40.0	44.4	0.26	1.35	0.36	0.458	0.30	0.84	3.3	0.06	0.18	0.99982
30.0	33.3	0.189	1.80	0.34	0.343	0.21	0.61	4.8	0.012	0.036	0.9999965
20.0	22.2	0.122	2.70	0.33	0.229	0.13	0.39	7.7	$1.37\cdot10^{-3}$	$4.1\cdot10^{-11}$	0.99999959
10.0	11.1	0.059	5.40	0.32	0.114	0.061	0.19	16.4	$3.73\cdot10^{-5}$	$11.2\cdot10^{-13}$	≈ 1.0
4.5	5.0	0.026	12.0	0.31	0.0514	0.026	0.085	38.0	$6.3\cdot10^{-7}$	$19.0\cdot10^{-15}$	≈ 1.0
2.0	2.22	0.0115	27.0	0.305	0.023	0.0116	0.037	86.2	$1.1\cdot10^{-8}$	$3.3\cdot10^{-16}$	≈ 1.0
$Q_н$ = 2.2 W											
40.0	44.4	1.0	1.35	1.35	1.0	4.37	3.2	0.50	27.0	81.0	0.9919
30.0	33.3	0.0	1.80	0.90	0.752	1.46	1.62	1.50	1.27	3.81	0.99962
20.0	22.2	0.29	2.70	0.79	0.50	0.735	0.33	3.0	0.0955	0.286	0.9999714
10.0	11.1	0.134	5.40	0.72	0.25	0.314	0.44	7.0	0.0022	0.0065	0.99999935
4.5	5.0	0.058	12.0	0.69	0.113	0.131	0.19	16.7	0.000034	0.0001	0.999999990
2.0	2.22	0.025	2.70	0.68	0.05	0.056	0.082	39.1	$5.53\cdot10^{-7}$	$1.65\cdot10^{-6}$	→1,0
$Q_н$ = 2.9 W											
30.0	33.3	0.93	1.80	1.67	0.996	5.0	3.0	0.58	19.8	59.3	0.9941
20.0	22.2	0.42	2.70	1.13	0.664	1.54	1.36	1.88	0.56	1.67	0.99983
10.0	11.1	0.182	5.40	0.98	0.332	0.58	0.59	5.0	0.01	0.030	0.9999970
4.5	5.0	0.078	12.0	0.94	0.149	0.237	0.25	12.8	$1.49\cdot10^{-4}$	0.00045	0.999999956
2.0	2.22	0.034	27.0	0.92	0.0664	0.101	0.11	28.7	$2.4\cdot10^{-6}$	$7.2\cdot10^{-14}$	→1.0

Continuation of Table 3

$Q_н$ = 4.0 W											
20.0	22.2	0.708	2.7	1.91	0.915	4.38	2.3	0.91	6.2	18.6	0.9981
10.0	11.1	0.263	5.4	1.42	0.458	1.21	0.85	3.3	0.06	0.18	0.999982
4.5	5.0	0.109	1.0	1.31	0.206	0.46	0.35	8.7	$7.85\cdot10^{-4}$	$2.36\cdot10^{-12}$	1.0
2.0	2.22	0.047	27.0	1.27	0.0915	0.193	0.152	20.7	$1.2\cdot10^{-5}$	$3.6\cdot10^{-13}$	1.0
$Q_н$ = 8.8 W											
10.0	11.1	1.0	5.4	5.4	1.0	17.5	3.24	0.50	27.0	81.0	0.9919
4.5	5.0	0.26	12.0	3.12	0.453	2.63	0.84	3.35	0.056	0.17	0.999983
2.0	2.22	1.106	27.0	2.86	0.89	2.21	0.77	4.0	$3\cdot10^{-4}$	$9\cdot10^{-12}$	→1.0

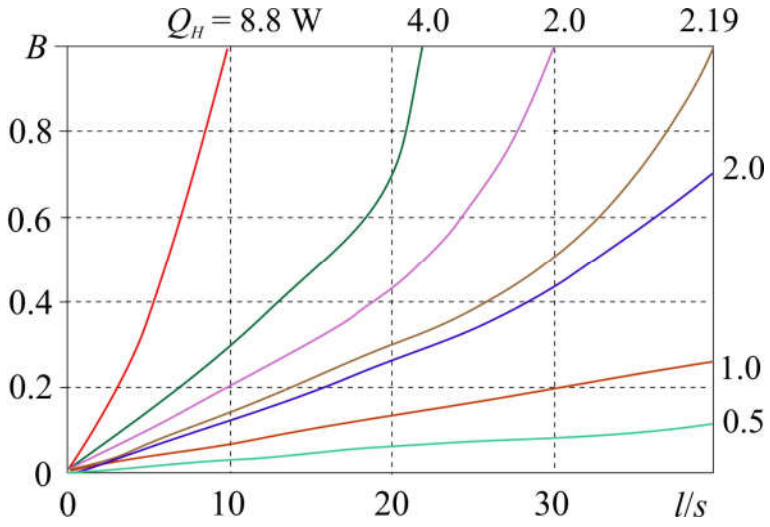

Fig. 10. Dependence of relative operating current B of a single-stage TEC on the ratio l/s at T = 300 K, n = 27 and different values of thermal power output in the heat pump mode (ΔT = 0 K).

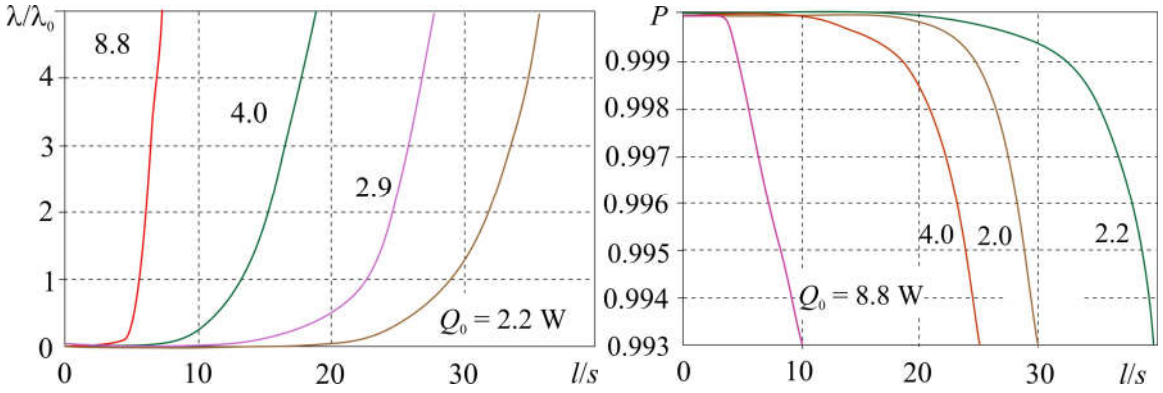

Fig. 11. Dependence of relative failure rate λ/λ_0 (a) and the probability of failure-free operation P (b) of a single-stage TEC on the ratio l/s at T = 300 K, $\lambda_0 = 3\cdot10^{-8}$ 1/h, $t = 10^4$ h, n = 27 and different values of thermal power output in the heat pump mode (ΔT = 0 K)

Thus, for instance, with the necessity of thermal power output Q_N = 2.2 W the use of module M40-27 instead of module M30-27 allows reducing failure rate λ by a factor of 21 and reducing power consumption by a factor of 3.

Discussion of analysis results

Analysis of calculated data has shown that:

1. With decreasing the ratio (λ/λ_0) of thermoelement leg of a single-stage TEC for different temperature drops ΔT and at given thermal load Q_0 in the mode λ_{min}:

– maximum cooling power γ is increased;

– the necessary number of thermoelements n is decreased

– the value of operating current I is increased;

– the value of voltage drop U is decreased;

– failure rate λ is decreased;

– the probability of failure-free operation P is increased.

With increasing temperature drop ΔT at given thermal load Q_0 for different values of the ratio l/s of thermoelement leg of a single-stage TED in the mode λ_{min}:

– maximum cooling power γ is decreased;

– the necessary number of thermoelements n (Q_{0max}) is increased; functional dependence $n = f(\Delta T)$ has a pronounced minimum, which is attributable to the presence of maximum cooling capacity at optimal ΔT.

– the value of operating current I is increased (except for the mode Q_{0max});

– the value of voltage drop U is increased;

– failure rate λ is increased;

– probability of failure-free operation P is decreased.

2. With decreasing the ratio l/s of thermoelement leg of a single-stage TEC at $Q_0 = 0$ W:

– electrical resistance R_B is decreased;

– maximum operating current I_{max} is increased;

– maximum temperature drop ΔT_{max} remains constant;

– failure rate λ remains constant value at given number of thermoelements n.

3. With decreasing the ratio l/s of thermoelement leg of a single-stage TEC at given n:

– relative operating current B and the value of operating current I are decreased;

– thermal coefficient μ is increased;

– failure rate λ is decreased, thus increasing the probability of failure-free operation P.

4. With increasing the number of thermoelements n in TEC at given ratio l/s and thermal load Q_N:

– thermal coefficient μ is increased;

– relative operating current B is decreased;

– the value of operating current I is decreased;

– failure rate λ is decreased;

– the probability of failure-free operation is increased P.

Conclusion

1. The model of interrelation between the reliability indicators and the main parameters of a single-stage TEC is proposed and justified for variations in the geometry of the thermoelement legss for different temperature drops ΔT at a fixed thermal load for the operation modes λ_{min}, ΔT_{max} ($Q_0 = 0$) and heat pump ($\Delta T = 0$).
2. The possibility of increasing the reliability indicators of a single-stage TEC like in the λ_{min} mode due to selection of the geometry of thermoelement legs with a smaller ratio l/S is determined.

3. The maximum temperature drop ΔT_{max} does not depend on the geometry of thermoelement legs *l*/*S* in TEC, but only on the thermoelectric figure of merit of the raw materials.
4. The failure rate λ of cooling thermoelement in the mode ΔT_{max} does not depend on the geometry of thermoelement legs *l/S* at their given number *n* in TEC, hence the probability of failure-free operation *P* remains constant.
5. To increase the reliability indicators of a single-stage heat pump, one should use thermoelectric modules with a greater number of thermoelements *n* and a small ratio *l/S*.

References

1. Moiseev V.F. (2003). Systems for providing of thermal modes for special-purpose radioelectronic equipment. *TRiO*, 1, 43–48 [in Russian].
2. Anatychuk L.I. (1979). Thermoelements and thermoelectric devices: Handbook. Kyiv: Naukova Dumka [in Russian]. .
3. Tsarev, A.V., Chugunkov, V.V.(2008). Investigation of thermoelectric devices characteristics for temperature control systems launch facilities. *Actual problems of Russian cosmonautics: Materials of XXXII Academic Conference on Astronautics.* Moscow: The Board of RAS [in Russian].
4. Rowe, D. M. (2012). *Thermoelectrics and its energy harvesting. Materials, preparation, and characterization in thermoelectrics.* Boca Raton: CRC Press.
5. Hyoung –Seuk Choi. (2011). Prediction of reliability on thermoelectric module through accelerated life test and physics –of –failure. *Electronic Materials Letter*, 7, 271.
6. Wereszczak A. A., Wang H. (2011). Thermoelectric mechanical reliability. *Vehicle Technologies Annual Merit Review and Peer Evaluation Meeting. Arlington*, 2011.
7. Melcor thermoelectric cooler reliability report. (2002). *Melcor Corporation*, April 9th., 36.
8. Singh, R. (2008). *Experimental characterization of thin film thermoelectric materials and film deposition VIA molecular beam epitaxial.* University of California, 54.
9. Jurgensmeyer, A. L. (2011). *High efficiency thermoelectric devices fabricated using quantum well confinement techniques.* Colorado State University, 2011.
10. Ping Yang. (2010). Approach on thermoelectricity reliability of board –level backplane based on the orthogonal experiment design. *International Journal of Materials and Structural Integrity*, 4(2–4), 170–185.
11. Zaikov V., Mescheryakov V., Zhuravlov Yu. (2017). Analysis of the model of interdependence of thermoelement branch geometry and reliability indicators of the single–stage cooler. *Eastern – European Journal of Enterprise Technologies*, 1/1 (85), 26–33 [in Russian].
12. Zaikov V.P., Kinshova L.A., Moiseev V.F. (2009). *Prediction of reliability figures of thermoelectric cooling devices. Vol.1. Single-state devices.* Odessa: Politekhperiodica [in Russian].

Submitted 19.01.2018

Зайков В.П. *канд. техн. наук.*[1]**,**
Мещеряков В.І. *доктор техн. наук.*[2]**,**
Журавльов Ю.І.[3] *канд. техн. наук.*

[1]Науково-дослідний інститут ШТОРМ,
вул. Терешкової, 27, Одеса, Україна;
e-mail: grand@i.ua;

[2]Одеський державний екологічний університет,
вул. Львівська, 15, Україна; *e-mail: grand@ua.fm;*
[3]Національний університет «Одеська морська академія»,
вул. Дідріхсона, 8, Україна; *e-mail: zhuravlov.y@ya.ru.*

МОДЕЛЬ ВЗАЄМОЗВ'ЯЗКУ ПОКАЗНИКІВ НАДІЙНОСТІ ОДНОКАСКАДНОГО ОХОЛОДЖУВАЧА З ГЕОМЕТРІЄЮ ГІЛОК ТЕРМОЕЛЕМЕНТІВ

Роботу присвячено підвищенню показників надійності однокаскадного термоелектричного охолоджувача конструктивним метоКм шляхом розробки та аналізу надійнісно-орієнтованої моделі, що зв'язує показники надійності з геометрією термоелементів. Ксліджження проведено для різних перепадів температури, фіксованого теплового навантаження для різних режимів роботи. Показано, що зі зменшенням відношення висоти термоелемента К перерізу збільшується максимальна потужність охолодження, зменшується кількість термоелементів і підвищується ймовірність безвідмовної роботи. При цьому не змінюється існуюча технологія виготовлення охолоджувачів, зберігаються результати існуючих механічних і кліматичних випробувань, матеріал термоелементів, вартість модулів. Бібл. 12, Рис. 11, Табл. 3.
Ключові слова: термоелектричний охолоджувач, геометрія термоелементів, показники надійності, потужність охолодження, перепад температур.

Зайков В.П. *канд. техн. наук.*[1]**,**
Мещеряков В.И. *доктор техн. наук.*[2]**,**
Журавлев Ю.И.[3] *канд. техн. наук*

[1]Научно-исследовательский институт ШТОРМ, ул. Терешковой, 27,
Одесса, Украина; *e-mail: grand@i.ua;*
[2]Одесский государственный экологический университет,
ул. Львовская, 15, Украина; *e-mail: grand@ua.fm;*
[3]Национальный университет «Одесская морская академия»,
ул. Дидрихсона, 8, Украина; *e-mail: zhuravlov.y@ya.ru.*

МОДЕЛЬ ВЗАИМОСВЯЗИ ПОКАЗАТЕЛЕЙ НАДЕЖНОСТИ ОДНОКАСКАДНОГО ОХЛАДИТЕЛЯ С ГЕОМЕТРИЕЙ ВЕТВЕЙ ТЕРМОЭЛЕМЕНТОВ

Работа посвящена повышению показателей надежности однокаскадного термоэлектрического охладителя конструктивным методом путем разработки и анализа надежностно-ориентированной модели, связывающей показатели надежности с геометрией термоэлементов. Исследования проведены для различных перепадов температуры, фиксированной тепловой нагрузки для различных режимов работы. Показано, что с уменьшением отношения высоты термоэлемента к сечению увеличивается максимальная мощность охлаждения, уменьшается количество термоэлементов и повышается вероятность безотказной работы. При этом не изменяется существующая технология изготовления

охладителей, сохраняются результаты существующих механических и климатических испытаний, материал термоэлементов, стоимость модулей. Библ. 12, Рис. 11, Табл. 3.
Ключевые слова: термоэлектрический охладитель, геометрия термоэлементов, показатели надежности, мощность охлаждения, перепад температур.

References

1. Moiseev V.F. (2003). Systems for providing of thermal modes for special-purpose radioelectronic equipment. *TRiO*, 1, 43–48 [in Russian].
2. Anatychuk L.I. (1979). Thermoelements and thermoelectric devices: Handbook. Kyiv: Naukova Dumka [in Russian]. .
3. Tsarev, A.V., Chugunkov, V.V.(2008). Investigation of thermoelectric devices characteristics for temperature control systems launch facilities. *Actual problems of Russian cosmonautics: Materials of XXXII Academic Conference on Astronautics.* Moscow: The Board of RAS [in Russian].
4. Rowe, D. M. (2012). *Thermoelectrics and its energy harvesting. Materials, preparation, and characterization in thermoelectrics.* Boca Raton: CRC Press.
5. Hyoung –Seuk Choi. (2011). Prediction of reliability on thermoelectric module through accelerated life test and physics –of –failure. *Electronic Materials Letter*, 7, 271.
6. Wereszczak A. A., Wang H. (2011). Thermoelectric mechanical reliability. *Vehicle Technologies Annual Merit Review and Peer Evaluation Meeting. Arlington*, 2011.
7. Melcor thermoelectric cooler reliability report. (2002). *Melcor Corporation*, April 9th., 36.
8. Singh, R. (2008). *Experimental characterization of thin film thermoelectric materials and film deposition VIA molecular beam epitaxial.* University of California, 54.
9. Jurgensmeyer, A. L. (2011). *High efficiency thermoelectric devices fabricated using quantum well confinement techniques.* Colorado State University, 2011.
10. Ping Yang. (2010). Approach on thermoelectricity reliability of board –level backplane based on the orthogonal experiment design. *International Journal of Materials and Structural Integrity*, 4(2–4), 170–185.
11. Zaikov V., Mescheryakov V., Zhuravlov Yu. (2017). Analysis of the model of interdependence of thermoelement branch geometry and reliability indicators of the single–stage cooler. *Eastern – European Journal of Enterprise Technologies*, 1/1 (85), 26–33 [in Russian].
12. Zaikov V.P., Kinshova L.A., Moiseev V.F. (2009). *Prediction of reliability figures of thermoelectric cooling devices. Vol.1. Single-state devices.* Odessa: Politekhperiodica [in Russian].

Submitted 19.01.2018

V.V. Lysko

V.V. Lysko, *Candidate Phys.-math. science*

Institute of Thermoelectricity of the NAS and MES of Ukraine,
1, Nauky str, Chernivtsi, 58029, Ukraine; *e-mail: anatych@gmail.com*

ON THE ERRORS IN MEASUREMENT OF ELECTRICAL CONDUCTIVITY OF THERMOELECTRIC MATERIAL SAMPLES BY TWO-PROBE METHOD

The results of computer studies of errors in measurement of electrical conductivity by two-probe method are presented. Conditions for minimization of the errors in measurement of electrical conductivity due to non-uniformity of current density in the sample are determined. The possibility of reducing the errors in measurement of electrical conductivity due to non-uniformity of current density in the sample by means of metal layers applied on sample end faces is investigated. The errors in measurement of electrical conductivity due to the influence of the Peltier effect are investigated, conditions for their minimization are determined.. Bibl. 7, Fig. 15.

Key words: electrical conductivity, Peltier effect, error, thermoelectric material.

Introduction

General characterization of the problem

An important role in the development and manufacture of thermoelectric power converters, as well as devices on their basis, is played by quality control of the original thermoelectric material. It is carried out by determining the thermoelectric parameters of material, namely electrical conductivity, thermal conductivity, thermoEMF and figure of merit. In so doing, the best in terms of measurement accuracy are comprehensive measurements of all these parameters on the same sample. Such measurements can be implemented using the absolute method [1]. The basis for determination of electrical conductivity is two-probe measurement method, whereby current is passed through sample end faces, and electrical potential on its surface is measured by two probes with a known distance between them [2, 3]. The electrical conductivity is calculated by the values of current and potential difference between the probes with regard to geometrical dimensions (sample cross-sectional area and the distance between the probes). This method is generally accepted for the research on semiconductor material (international standard SEMI MF397-02 “Test Method for Resistivity of Silicon Bars Using a Two-Point Probe”).

Analysis of the literature

Refs. [4, 5] are concerned with the main sources of errors of two-probe method for the case of long rods (ingots) of thermoelectric material:

- inhomogeneity of current density in the ingot due to current supply solely at points of contact with current conductors, rather than uniformly across its surface;

- nonisothermal conditions caused by the influence of the Peltier and Joule effects, and by the heat exchange with the environment.

This is dealt with by positioning the measuring probes as far as possible from current contacts, where the electric field is most one-dimensional. However, this reduces the distance between the probes, and, accordingly, decreases the potential difference, which reduces the accuracy of measurements. It becomes

more difficult to precisely define the distance between the probes, which also affects the measurement error.

It is even more difficult to satisfy the condition of sample isothermality. When current flows, its violation leads to the appearance on the probes, in addition to the potential difference, of thermoelectric power. Moreover, non-isothermality is primarily due to the action of the Peltier effect at points of electrical connections of the sample with the current contacts. In this case, the potential difference between the probes due to current flow and thermoelectric power due to nonisothermality of the sample may be values of one order, which leads to fairly gross errors. To reduce this error, it is advisable to pass through the sample an alternating current of sufficiently high frequency, which should prevent the influence of the Peltier effect. However, in this case there are difficulties in measuring potential difference on the alternating current due to the lack of precision of the measuring equipment and all sorts of crosstalk. Use is also made of measuring voltage drop at the moment of switching on the current, when the influence of the Peltier effect will be insignificant due to the heat capacity of the material.

The purpose of the work is to determine the values of errors in measurement of electrical conductivity of thermoelectric material samples by two-probe method due to non-uniformity of current density in the sample and the influence of the Peltier effect, as well as to find conditions for minimization of these errors.

Physical model of two-probe method for electrical conductivity measurement and its mathematical description

A physical model of two-probe method is shown in Fig.1. It comprises a sample of thermoelectric material through which by means of two current conductors an electric current of magnitude I is passed. Voltage drop U is measured between two probes arranged on the lateral surface of the sample.

The electrical conductivity of the sample material is determined by the formula

$$\sigma = \frac{I}{U}\frac{l}{S}, \qquad (1)$$

where S is cross-sectional area of the sample, l is the distance between measuring probes.

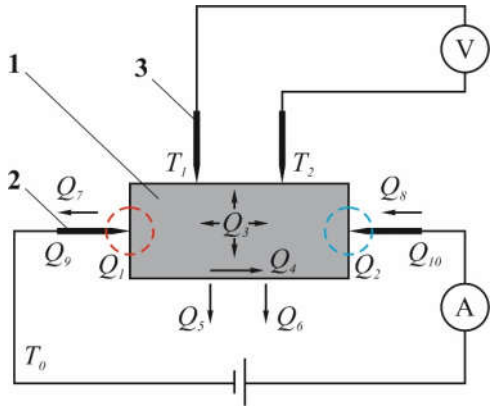

Fig. 1. Physical model of two-probe method for measuring the electrical conductivity of thermoelectric material.
1 – sample of thermoelectric material under study; 2 – current conductors; 3 – measuring probes.

The physical model takes into account heats Q_1-Q_{10} which occur in measuring. They include the Joule heat which is released in the sample and the conductors, the Peltier heat which is released and absorbed on the opposite sample ends, heat exchange between the sample and the environment.

To study the errors of measurement and the effect of various factors on them, it is necessary to find

the distributions of electrical potential and temperature in the sample. In so doing, as long as instantaneous measurements are used to eliminate the influence of the Peltier effect, the problem is a nonstationary one.

Equations for finding the electrical potential U and temperature T in this case will be given below

$$\begin{cases} \rho C \dfrac{\partial T}{\partial t} - \nabla\left(\left(\sigma\alpha^2 T + \kappa\right)\nabla T\right) - \nabla\left(\sigma\alpha T \nabla U\right) = \sigma\left(\left(\nabla U\right)^2 + \sigma\nabla T \nabla U\right) \\ \nabla\left(\sigma\alpha\nabla T\right) + \nabla\left(\sigma\nabla U\right) = -\nabla\left(\varepsilon\nabla\dfrac{\partial U}{\partial t}\right) \end{cases}, \qquad (2)$$

where ρ is density, C is heat capacity, σ is electrical conductivity, α is the Seebeck coefficient, κ is thermal conductivity, ε is dielectric permittivity.

Having solved system (2) with the corresponding boundary conditions, we obtain the distributions of the electrical potential and temperature in the sample. To calculate the temperature and electrical fields, as well as the influence on them of various factors, computer methods of object-oriented simulation were used, in particular, COMSOL Multiphysics software package [6].

Errors in measurement of electrical conductivity due to non-uniformity of current density in the sample

Computer simulation was used to obtain the dependences of the errors in measurement of electrical conductivity due to non-uniformity of current density on the geometry of sample under study. A sample of thermoelectric material based on *Bi-Te* (σ=1000 $cm^{-1}cm^{-1}$, α = 200 μV/K, κ = 1.4 W/(m*K), ρ= 7740 kg/m^3, C = 154 J/(kg*K) [7]) was considered.

The dependences of the error $\delta\sigma_1$ in the measurement of electric conductivity due to non-uniformity of current density on the sample length L, sample diameter d and the distance between the probes are presented in Fig. 2-4.

Fig. 5 shows a generalized dependence of error $\delta\sigma_1$ on the ratio between the sample length and the sample diameter at different values of distance between the probes. As is seen from the figure, for minimization of the errors the sample length must be at least 2-2.5 times larger than the sample diameter, and the distance between the probes must not exceed ¾ of the sample diameter.

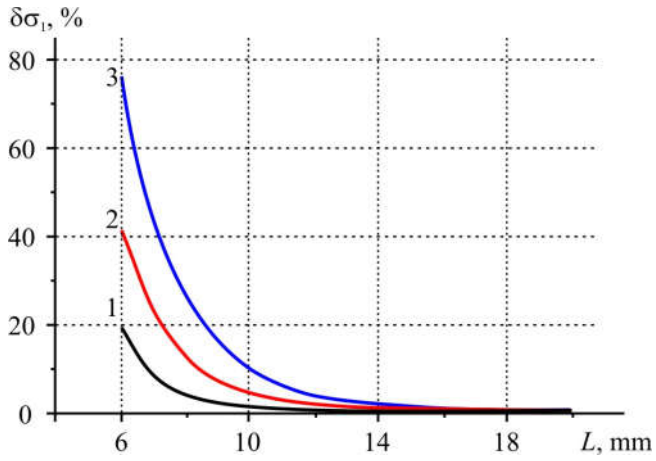

Fig. 2. Dependence of the error $\delta\sigma_1$ in measurement of electrical conductivity due to non-uniformity of current density on the sample length L for different values of sample diameter d(the distance between the probes a = 5 mm). 1 – d = 4mm; 2 – d = 6mm; 3 – d = 8mm.

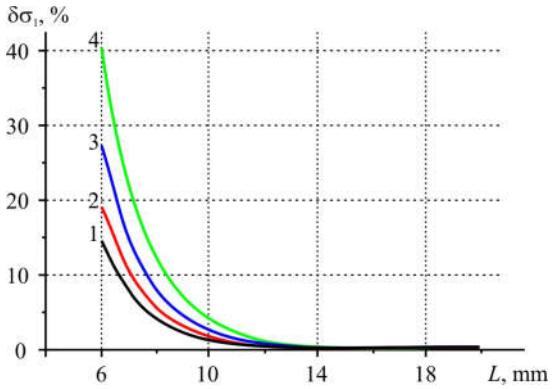

Fig. 3. Dependence of the error $\delta\sigma_{11}$ in measurement of electrical conductivity due to non-uniformity of current density on the sample length L for different values of distance between the probes (sample diameter d =6 mm). 1 – a = 2mm; 2 – a = 3mm; 3 – a = 4mm; 4 – a = 5мм.

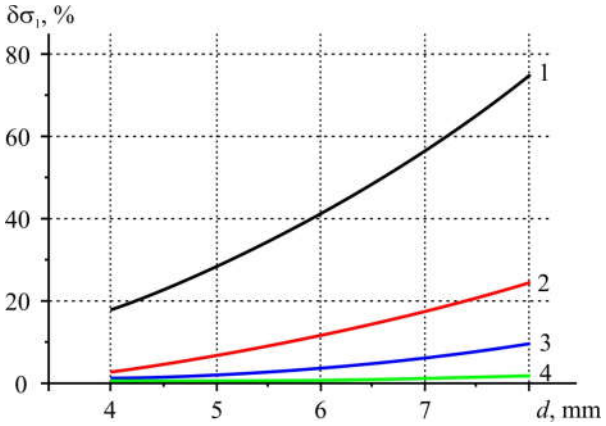

Fig. 4. Dependence of the error $\delta\sigma_1$ in measurement of the electrical conductivity related to non-uniformity of current density on the sample diameter d for different values of sample length L (the distance between the probes a = 5 mm). 1 – L = 6mm; 2 – L = 10mm; 3 – L = 15mm; 4 – L = 20mm.

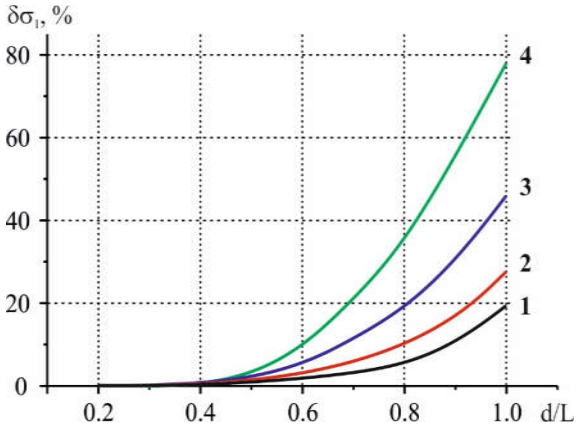

Fig. 5. Dependence of the error $\delta\sigma_1$ in measurement of electrical conductivity due to non-uniformity of current density on the ratio between sample diameter d and sample length L for different values of the distance between the probes. 1 – a = 2mm; 2 – a = 3mm; 3 – a = 4mm; 4 – a = 5mm.

The possibility of reducing the errors in measurement of electrical conductivity due to non-uniformity of current density in the sample, with the help of metal layers applied on the end faces of the sample (Fig. 6) was investigated. It is seen that to achieve the level of error not more than 0.2%, a layer of copper 50-60 μm thick would be sufficient. The use of copper layer 100 μm thick allows reducing the sample length by a factor of ~ 1.5 (from 15 to 9 mm) without sacrificing the accuracy of measurement.

Such a reduction is important for increasing the measurement speed with complex determination of the thermal conductivity and thermoEMF on the same sample, as the time required for installing steady-state conditions in the sample is proportional to the length of the sample.

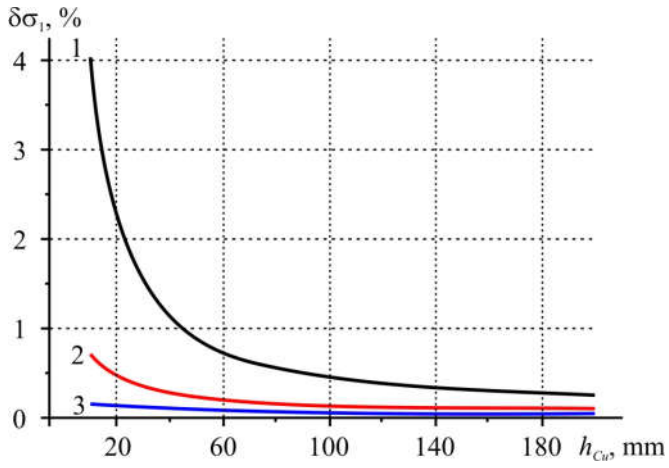

Fig. 6. Dependence of the error $\delta\sigma_1$ in measurement of electrical conductivity due to non-uniformity of current density on the thickness h_{Cu} of copper coating on the sample end faces for different values of sample length L (sample diameter d =6 mm, the distance between the probes a = 5 mm).1 – L = 6mm; 2 – L = 9mm; 3 – L = 12mm.

Errors in the measurement of electrical conductivity due to the influence of the Peltier effect

The type of temporal dependence of voltage drop on the sample with the use of instantaneous measurements is shown in Fig.7. It allows implementing two measurement variants, whereby the nonisothermality due to the Peltier effect can be eliminated – at the moment of current switch on and immediately after it is switched off.

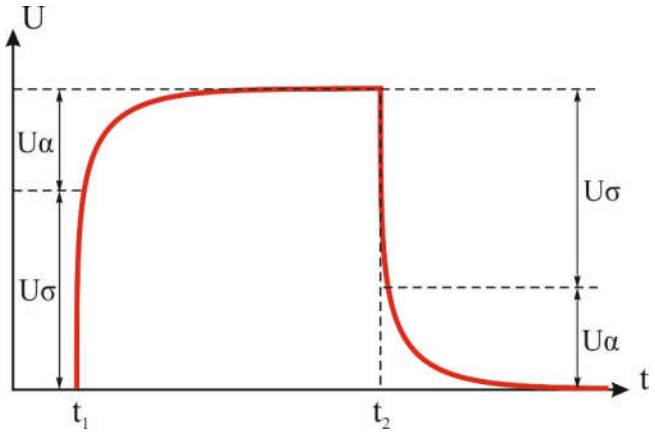

Fig. 7. The type of the temporal dependence of voltage drop between the probes in the measurement of electrical conductivity by two-probe method.

To determine the requirements to measurement speed, the temporal dependences of temperature distributions and electrical potential in the sample were investigated using computer simulation. Fig. 8 shows a temporal dependence of temperature drop between the probes due to the influence of the Peltier effect for a sample of diameter 6 mm and length 12 mm; the distance between the probes – 5 mm. As is seen from the figure, at such sample dimensions the influence of the Peltier effect very quickly extends to measuring probes, hence, leads to the origination of errors.

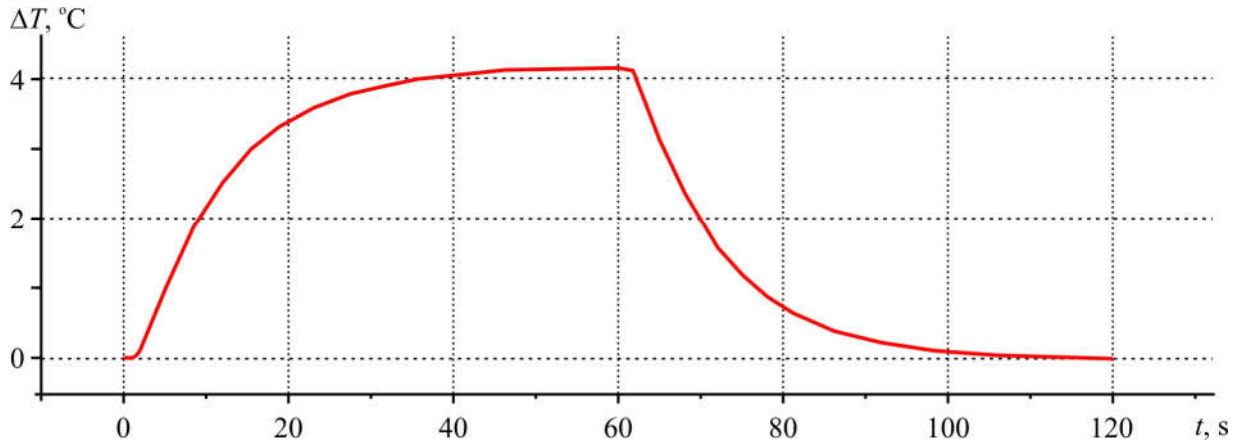

Fig. 8. Temporal dependence of temperature drop between the probes due to the influence of the Peltier effect.(sample diameter d =6 mm, sample length L =12 mm,the distance between the probes a = 5 mm)

Temporal dependence of the error $\delta\sigma_2$ in the measurement of electrical conductivity due to the influence of the Peltier effect is given in Fig. 9. To achieve an error level not higher than 0.2%, measurement must be made in less than 1 second after the current is switched on. This suggests the need for mandatory automation of the measurement process.

The influence on measurement accuracy of metal layers applied on the end faces to reduce the errors due to non-uniformity of current density in the sample was considered.

From Fig. 10 it is seen that the use of thin copper layers on the sample end faces (to 200 μm) by a factor of 1.2 – 1.5 increases the errors due to the influence of the Peltier effect as compared to the case of one central point contact on each of the end faces.

The use of thicker copper plates (Fig. 11) reduces the influence of the Peltier effect due to their high heat capacity – up to 10 times as compared to the case of one central point contact on each of the end faces (at plate thickness 5 mm). The dependnce of the error $\delta\sigma_2$ on plate thickness is given in Fig. 12.

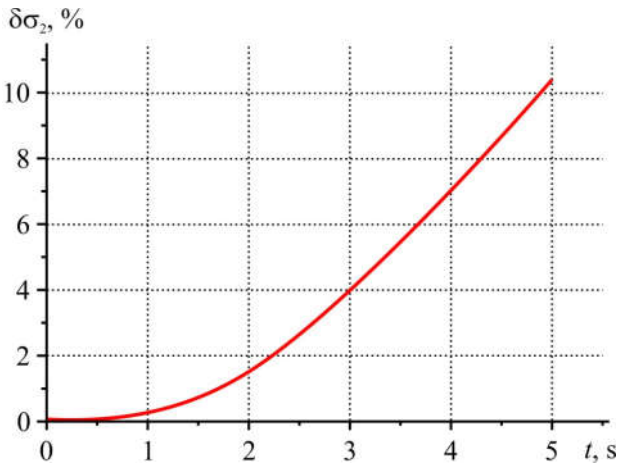

Fig. 9. Temporal dependence of the error $\delta\sigma_2$ in measurement of electrical conductivity due to the influence of the Peltier effect

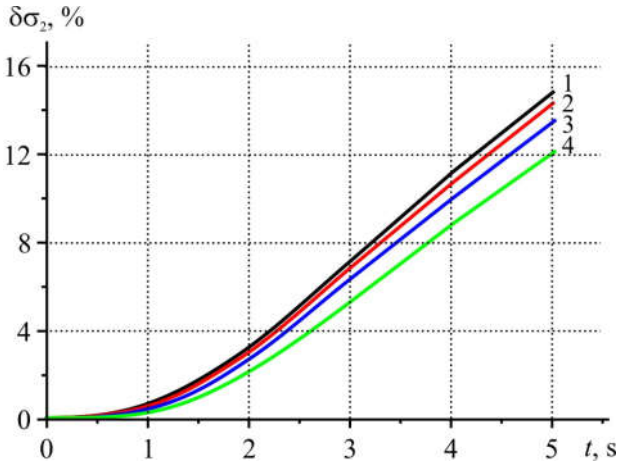

Fig. 10. Temporal dependence of the error $\delta\sigma_2$ in measurement of electrical conductivity due to the influence of the Peltier effect when using copper coating of thickness h_{Cu} on the end faces 1 – h_{Cu} = 10μm; 2 – h_{Cu} = 50 μm; 3 – h_{Cu} = 100μm; 4 – h_{Cu} = 200μm.

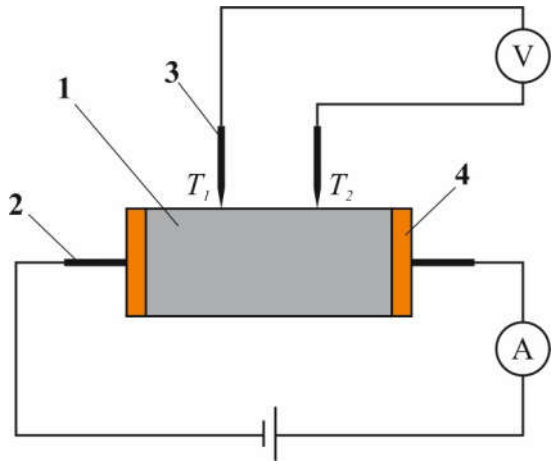

Fig. 11. The use of copper plates of thickness h on the end faces of the sample for reduction of the influence of the Peltier effect. 1 –thermoelectric material sample; 2 – current conductors; 3 – measuring probes; 4 – copper plates.

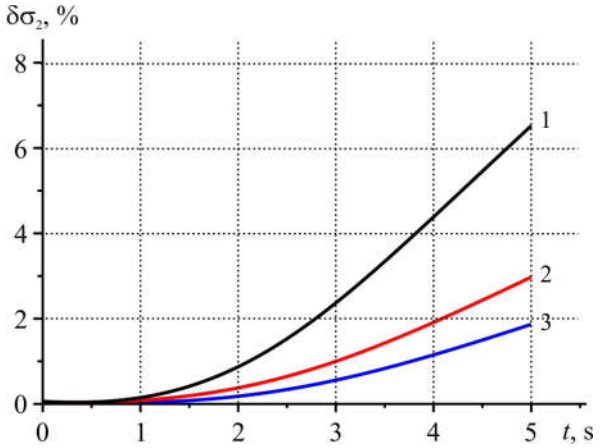

Fig. 12. Temporal dependence of the error $\delta\sigma_2$ in measurement of electrical conductivity due to the influence of the Peltier effect when using copper plates of thickness h on the end faces. 1 – h = 1mm; 2 – h = 3mm; 3 – h = 5mm.

For further reduction of the errors one can use thermostating of sample end faces with the aid of copper blocks (Fig. 13). Fig. 14 shows a dependence of the error in measurement of electrical conductivity due to the influence of the Peltier effect with the use of thermostating of sample end faces by means of copper blocks of diameter 12 mm and thickness 10 mm (for the sample of diameter 6 mm and length 12 mm; the distance between the probes – 5 mm).

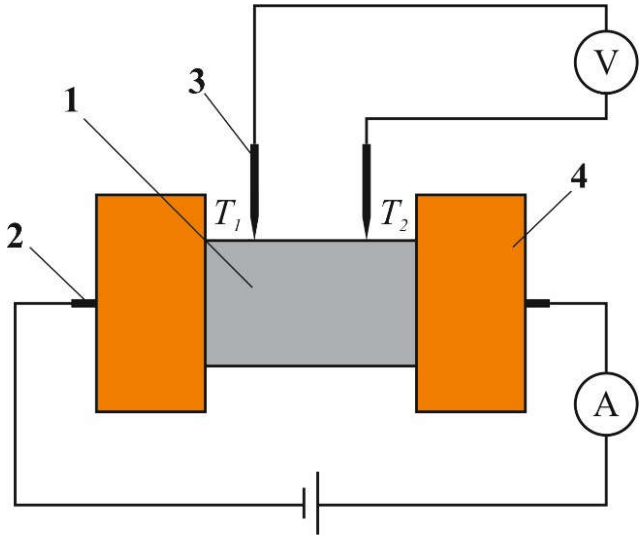

Fig. 13. Thermostating of sample end faces by means of copper blocks to eliminate the influence of the Peltier effect.1 –thermoelectric material sample; 2 – current conductors; 3 – measuring probes; 4 – thermostating copper blocks.

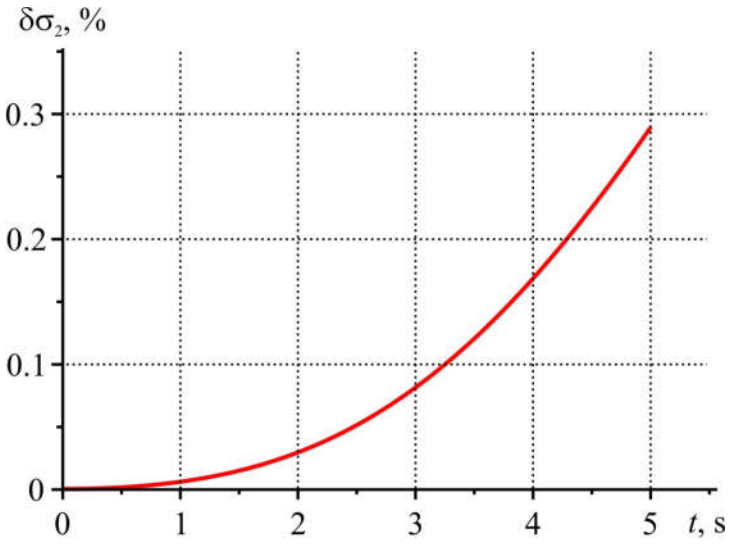

Fig. 14. Temporal dependence of the error $\delta\sigma_2$ in measurement of electrical conductivity due to the influence of the Peltier effect at thermostating of sample end faces by means of copper blocks.

Thus, thermostating of sample end faces by means of massive copper blocks practically eliminates the influence of the Peltier effect when measuring the electrical conductivity by two-probe method.

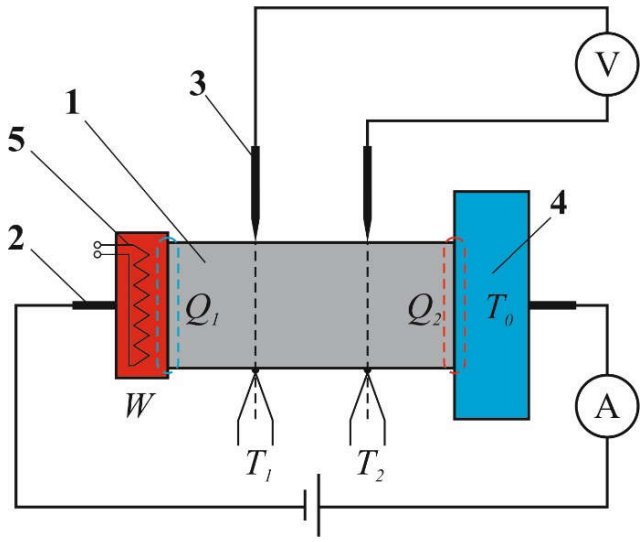

Fig. 15. Compensation of the influence of the Peltier effect by means of the heater at integrated measurement of parameters of thermoelectric materials by the absolute method. 1 –thermoelectric material sample; 2 – current conductors; 3 – measuring probes; 4 – thermostat; 5 – reference heater.

In the case of integrated determination of the sample parameters by the absolute method, when one of the end faces is thermostated, and the other accommodates a reference heater (Fig. 15), to eliminate the influence of the Peltier effect, one can use compensation of cooling action of the Peltier effect by the heat of the reference heater. Isothermality control can be carried out by means of thermocouples. Computer simulation confirmed the efficiency of such method for minimization of the influence of the Peltier effect.

Conclusion

1. Computer simulation was used to determine conditions for minimization of the errors in measurement of electrical conductivity by two-probe method due to non-uniformity of current density in the sample. It was established that for minimization of the errors the length of the sample must be at least a factor of 2-2.5 larger than the sample diameter, and the distance between the probes must not exceed ¾ of the sample diameter.
2. The possibility of reducing the errors in measurement of electrical conductivity due to non-uniformity of current density in the sample by means of metal layers applied on the end faces of the sample was investigated. It was established that to achieve the level of error not more than 0.2%, a layer of copper 50-60 μm thick is sufficient. The use of copper layer 100 μm thick allows reducing sample length by a factor of ~ 1.5 without essential loss in measurement accuracy.
3. The errors in measurement of electrical conductivity due to the influence of the Peltier effect were investigated. It was established that to achieve an error level not higher than 0.2%, measurement must be made in less than 1 second after the current is switched on.
4. It was established that the use of thin copper layers on the sample end faces (up to 200 μm) by a factor of 1.2 – 1.5 increases the errors due to the influence of the Peltier effect as compared to the case of one central point contact on each of the end faces. The use of thicker copper plates reduces the influence of the Peltier effect due to their high heat capacity – up to 10 times as compared to the case of one central point current conductor on each of the end faces (at plate thickness 5 mm).

5. Thermostating of sample end faces by means of massive copper blocks practically eliminates the influence of the Peltier effect when measuring electrical conductivity by two-probe method. For the case of thermal asymmetry of sample end faces (as in the case of integrated measurement of sample parameters by the absolute method, when one of the end faces is thermostated, and the other accommodates a reference heater), an effective method for elimination of the influence of the Peltier effect is compensation of cooling action of the Peltier effect by the heat of the reference heater.

References

1. Anatychuk L.I., Havryliuk M.V., Lysko V.V. (2015). Absolute method for measuring of thermoelectric properties of materials. *Materials Today: Proceedings*, 2, 737 – 743.
2. Anatychuk L.I. (1978). *Termoelementy i termoelektricheskiye ustroistva [Thermoelements and thermoelectric devices]*. Kyiv: Naukova dumka [in Russian].
3. Okhotin A.S., Pushkarskii A.S., Borovikova R.P., Simonov V.A. (1974). *Metody izmereniia kharakteristik termoelektricheskikh materialov i preobrazovatelei* [*Methods for measuring characteristics of thermoelectric materials and converters]*. Moscow: Nauka [in Russian].
4. Anatychuk L.I., Lysko V.V. (2008). High-precision method for measuring electric conductivity of thermoelectric material rods. *J.Thermoelectricity*, 1, 70-75.
5. Anatychuk L.I., Lysko V.V., Havryliuk M.V., Tiumentsev V.A. (2015). Automated equipment for measurement of properties of thermoelectric material rods. *J.Thermoelectricity*, 5, стр.?
6. Jaegle Martin. (2008). Multiphysics simulation of thermoelectric systems. *Proceedings of the COMSOL Conference* (Hannover, 2008). .
7. Goltsman B.M., Kudinov V.A., Smirnov I.A. (1972). Poluprovodnikovyie termoelektricheskiie materialy na osnove Bi_2Te_3 [Semiconductor thermoelectric materials based on Bi_2Te_3. Moscow: Nauka [in Russian].

Submitted 03.10.2017

Лисько В.В. *канд. фіз.-мат. наук* [1,2]

[1]Інститут термоелектрики НАН і МОН України, вул. Науки, 1,
Чернівці, 58029, Україна, *e-mail: anatych@gmail.com*;
[2]Чернівецький національний університет імені Юрія Федьковича,
вул. Коцюбинського 2, Чернівці, 58012, Україна
e-mail: anatych@gmail.com

ПРО ПОХИБКИ ВИМІРЮВАННЯ ЕЛЕКТРОПРОВІДНОСТІ ЗРАЗКІВ ТЕРМОЕЛЕКТРИЧНИХ МАТЕРІАЛІВ ДВОЗОНДОВИМ МЕТОДОМ

Представлено результати комп'ютерниходосліджень похибок, які виникають при вимірюванні електропровідності за допомогою двозондового методу. Визначено умови мінімізації похибок вимірювання електропровідності, пов'язаних з неоднорідністю густини струму у зразку. Досліджено можливість зменшення похибок вимірювання електропровідності, пов'язаних з неоднорідністю густини струму у зразку, за допомогою металевих шарів, нанесених на торці зразка. Досліджено похибки вимірювання електропровідності, викликані впливом ефекту Пельтьє,визначено умови їх мінімізації. Бібл. 7, Рис. 15.

Ключові слова: електропровідність, ефект Пельтьє, похибка, термоелектричний матеріал.

Лысько В.В. *канд. физ.-мат. наук* [1,2]

[1]Институт термоэлектричества, ул. Науки, 1,
Черновцы, 58029, Украина *e-mail: anatych@gmail.com*;
[2]Черновицкий национальный университет имени Юрия Федьковича,
ул. Коцюбинского 2, Черновцы, 58012, Украина
e-mail: anatych@gmail.com

О ПОГРЕШНОСТЯХ ИЗМЕРЕНИЯ ЭЛЕКТРОПРОВОДНОСТИ ОБРАЗЦОВ ТЕРМОЭЛЕКТРИЧЕСКИХ МАТЕРИАЛОВ ДВУХЗОНДОВЫМ МЕТОДОМ

Представлены результаты компьютерного моделирования погрешностей, возникающих при измерении электропроводности с помощью двухзондового метода. Определены условия минимизации погрешностей измерения электропроводности, связанных с неоднородностью плотности тока в образце. Исследована возможность уменьшения погрешностей измерения электропроводности, связанных с неоднородностью плотности тока в образце, с помощью металлических слоев, нанесенных на торец образца. Исследованы погрешности измерения электропроводности, вызванные влиянием эффекта Пельтье,определены условия их минимизации. Библ. 7, Рис. 15.

Ключевые слова: электропроводность, эффект Пельтье, погрешность, термоэлектрический материал.

References

1. Anatychuk L.I., Havryliuk M.V., Lysko V.V. (2015). Absolute method for measuring of thermoelectric properties of materials. *Materials Today: Proceedings*, 2, 737 – 743.
2. Anatychuk L.I. (1978). *Termoelementy i termoelektricheskiye ustroistva [Thermoelements and thermoelectric devices]*. Kyiv: Naukova dumka [in Russian].
3. Okhotin A.S., Pushkarskii A.S., Borovikova R.P., Simonov V.A. (1974). *Metody izmereniia kharakteristik termoelektricheskikh materialov i preobrazovatelei* [*Methods for measuring characteristics of thermoelectric materials and converters]*. Moscow: Nauka [in Russian].
4. Anatychuk L.I., Lysko V.V. (2008). High-precision method for measuring electric conductivity of thermoelectric material rods. *J.Thermoelectricity*, 1, 70-75.
5. Anatychuk L.I., Lysko V.V., Havryliuk M.V., Tiumentsev V.A. (2015). Automated equipment for measurement of properties of thermoelectric material rods. *J.Thermoelectricity*, 5.
6. Jaegle Martin. (2008). Multiphysics simulation of thermoelectric systems. *Proceedings of the COMSOL Conference* (Hannover, 2008). .
7. Goltsman B.M., Kudinov V.A., Smirnov I.A. (1972). Poluprovodnikovyie termoelektricheskiie materialy na osnove Bi_2Te_3 [Semiconductor thermoelectric materials based on Bi_2Te_3. Moscow: Nauka [in Russian].

Submitted 03.10.2017

S.O.Filin

S.O.Filin, *Doctor of tech. sciences*

West Pomeranian University of Technology, Szczecin
17, al.Piastow, Szczecin, 70-310, Poland
e-mail: Sergiy.Filin@zut.edu.pl

COMPARATIVE ANALYSIS OF ENERGY CHARACTERISTICS OF MODERN THERMOELECTRIC REFRIGERATORS

This article analyzes technical, primarily energy characteristics of modern thermoelectric refrigerators (TER), as well as the ways to increase their energy efficiency. The results of comparative tests of new TER models developed by the author are presented and their advantages over the world analogues are shown. Bibl. 7, Fig. 7, Table 3.

Key words: thermoelectric refrigerator, transport refrigerator, energy saving, temperature control.

Introduction

Enhancement of energy efficiency, without any doubt, is the main and global goal of technical progress in the early 21st century. The reduction in the energy consumption of thermoelectric refrigerators (hereinafter TER) is not only consistent with it, but is also a prerequisite for the competitiveness of thermoelectric products in the world market, and, first of all, in relation to compressor analogues. This problem remains unsolved from the very beginning of the era of thermoelectric cooling and is constantly in the focus of specialists' attention, especially in the context of constant enlargement of TER compartment capacity [1-4].

Hopes for a significant increase in the efficiency of thermoelectric materials, unfortunately, are not justified yet. Therefore, developers (designers) and manufacturers have to look for other ways to improve refrigerators that are not directly related to thermoelectric materials, based on serially produced thermoelectric cooled modules.

The new, more stringent requirements for the energy performance of household refrigerators introduced by EU directives have also affected thermoelectric refrigerators. From July 1, 2015, absorption and thermoelectric refrigerators of Class D and above can be sold at the European market. Before that, most TER models had the energy class **E** (Fig.1). Some manufacturers, such as Atlant or MPM, were forced to abandon the export of their TER to Europe. To meet these new requirements, some of the TER manufacturers took an approach of equipping them with an electronic temperature control system in the compartment, which reduces the supply voltage of module(s) in proportion to temperature decrease in the compartment, starting from some value. This led to a significant increase in the cost of refrigerators. Refrigerators by German-Italian firm *Indel-B* is a case in point [5]. In addition, this method of regulation has limited application, referring to the ambient temperature level. But, what is most important, it is practically not applicable in transport TERs, which are powered directly from the on-board DC mains 12V DC or 24V DC.

As it was shown in [6], the daily or annual energy consumption is not a suitable parameter for a correct comparison of different TERs. One of the main reasons is the lack of temperature regulation in the compartment. Different TERs operate in one of the modes (main or energy-saving) depending on the ambient temperature, on the degree of refrigerator loading and on the way it is used. The author has developed and proposed to use a more versatile parameter of comparison - the specific power consumption P_s. The physical meaning of this parameter is as follows: the electrical power P that must be fed to the

refrigerator in order to keep given temperature difference ΔT in the given capacity of its compartment. The P_s parameter is applicable, provided the heat insulation properties of the cabinet are equal, namely the thickness and the material of the thermal insulation. It should be calculated for each mode of operation separately.

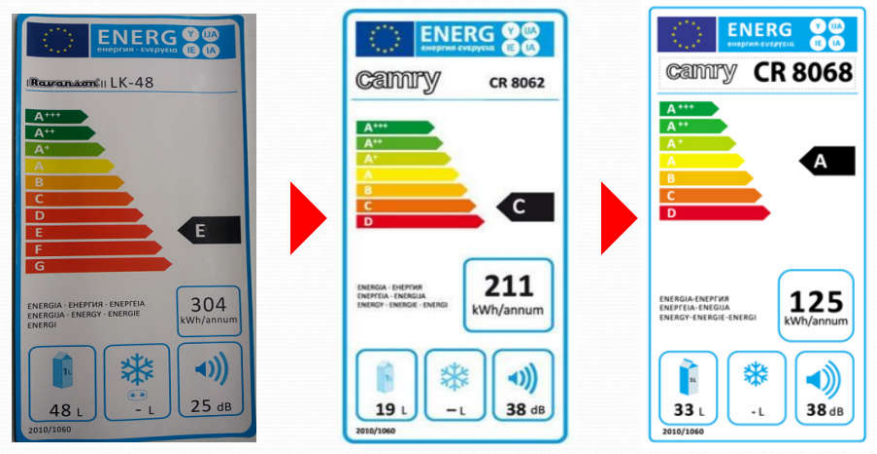

Fig. 1. Changes in the energy class of TER within recent five years

In practice, this means that, for example, at an ambient temperature of 22 ° C, the first refrigerator operating in the energy-saving mode may have the advantage. Its characteristic in Fig. 2 is shown in blue (dark) color. But at 25° C, this refrigerator no longer passes into this mode of operation. Consequently, the advantage then can go to the second refrigerator (grey color), which has a wider range of ambient temperatures, whereby it is possible to work in the energy-saving mode. This leads to a very important conclusion that when evaluating the energy efficiency of a TER, not only the absolute values of the P and P_s are important, but also the temperature range of the refrigerator in which they can be achieved.

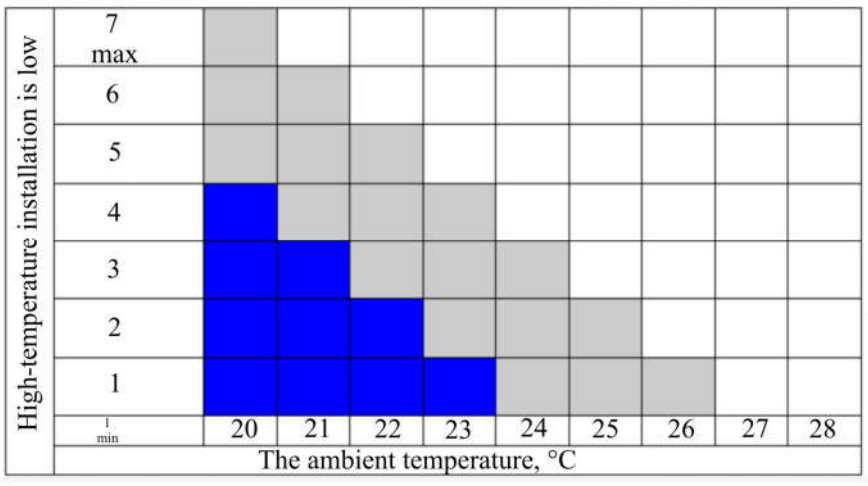

Fig. 2. The principle of comparing the width of the energy-saving mode zone of two TERs

Technical characteristics of modern TERs

Fig. 3 shows the dynamics of change in the specific power consumption P_s of TERs over the past 35 years: blue (darker) color shows refrigerators and mini-bars with a capacity of 40-60 liters, green (lighter) color - refrigerated showcases with a capacity of 70-110 liters. Refrigerators of the second generation (by convention we shall refer them to the period 1980-2000) were characterized by lower efficiency of

thermoelectric modules, absence of temperature control in the compartment, but greater created temperature difference. Their parameter P_s was from 0.10 to 0.12. The next (third) generation of TERs, which already employed various types of temperature control in the compartment, reached the value of P_s = 0.04-0.06. This decrease in P_s can be characterized as *artificial*, since the relative decrease in the power consumption exceeds the relative decrease in the temperature difference ΔT. The lower values of these P_s ranges are achieved in refrigerator bars and wine coolers, where the temperature in the compartment exceeds 10-12ºC. New author's developments, which can be attributed to the fourth generation, have P_s in the range of 0.02-0.04, which is almost twice lower than that of the previous generation.

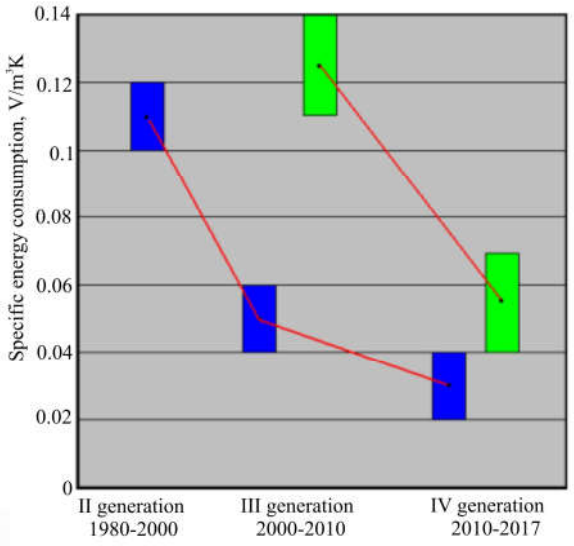

Fig. 3. Reduction of P_s of thermoelectric refrigerators within recent 35 years

A similar trend is observed in the category of thermoelectric refrigeration showcases. Glass doors of these products have a higher heat transfer coefficient, which, accordingly, is reflected on their P_s. With the exception of wine storage windows at a temperature of 14-18ºC, the universal show-cases have a P_s about 2 times worse than that of refrigerators.

Table 1 presents the present-day world level of household TER parameters. For the correctness of the comparison, refrigerators with an approximately equal compartment capacity were chosen, namely from 40 to 60 liters.

Table 1

Technical characteristics of the world's best energy consumption models of thermoelectric refrigerators

Technical data	Manufacturer, model						
	OmniTec (Spain)	*Electro-Line* (Canada)		*Indel B* (Italy-Germany)	*Grass Cavagna Group* (Poland-China)		*Space-Mate* (USA)
	Advance plus 42	BC42A	BC50A	DT40 plus	Ravanson		Igloo
					LK-40	LK-48	
Useful compartment capacity[l]	42	42	50	40	40	48	56,6
Temperature range in compartment [°C]	3...8	2…10	6,5…15	5…15	5…12	5…12	0…7
AC power supply voltage [V]	230	230	230	115/230	230	230	110/230

Continuation of Table 1

Installed power [W]	72	75	50	60	70	70	90
Power consumption in energy saving mode [W]	25	29	15	31	33	30	
Average daily power consumption [kWh /24h]	0.6	0.7	0.36	0.75	0.8	0.8	1.08
Annual power consumption [kWh/year]	219	255,5	132	274	292	292	394.2
Specific power consumption [W/(dm^{3}K)]	0.035	0.038	0.022	0.052	0.052	0.043	0.044
Overall dimensions							
width	450	500	500	399	510	510	399
depth	432	430	422	470	430	430	470
height [mm]	530	480	515	553	430	480	553
Weight [kg]	no data available	11.2	13.0	15.5	11.2	13.2	15.5

Among the models on the market, the BC50A refrigerator of the Canadian firm ElectroLine has the best parameters. Laboratory tests of this refrigerator conducted in 2018 at the West Pomeranian University of Technology, Szczecin, showed that this refrigerator cannot be used as a reference for two reasons. Firstly, the average thickness of the insulation of this refrigerator compartment is 40 mm, which is 5 mm larger than that of analogues. This fact alone gives the advantage in the energy characteristics of about 30%. Secondly, the energy characteristics of the BC50A model were measured when the thermostat was set for a relatively high temperature in the compartment, corresponding to the created temperature difference of 10-12 K, which is 2-3 degrees less compared to analogues. This adds another 15-20% of the advantages in power consumption. Therefore, the Ravanson LK-48 refrigerator was adopted as a comparison base for comparative tests of new and well-known TER models.

Objects and results of comparative tests

At the West Pomeranian University of Technology, Szczecin, prototypes were developed and models of new, fourth generation thermoelectric refrigerators HTT-48-1 and XTT-48-2 were tested. The models are based on the Ravanson LK-48 thermoelectric refrigerator cabinets and differed in the type of thermoelectric modules. The original unit of this refrigerator was demounted. In its place was installed the author's development unit.

Among the goals set before the beginning of the work were the following:

1. To increase the energy efficiency of transport and household TERs on the basis of serially produced thermoelectric cooling modules and to achieve the world's best (or, at least, comparable with the best world analogues) energy parameters of TERs with the use of innovative technical solutions.

2. Develop designs and manufacturing techniques for the above refrigerators. Perform tests of prototypes, including comparative tests with a basic refrigerator. In addition, it was necessary to confirm the efficiency of the use of manometric thermostats in power and temperature control circuits of TERs [7].

The specific and fundamentally important feature of comparative tests of these refrigerators was the fact that identical refrigerated cabinets with different refrigeration units were used (Fig. 4). This made it possible to exclude the impact of the insulating properties of the cabinet on the energy performance of the compared options.

Fig. 4. Compared objects during parallel tests:
on the left – the Ravanson LK-48 refrigerator, on the right - the XTT-48-1refrigerator

The HTT-48 refrigerators are designed for use on vehicles powered from on-board 12V DC mains, and the basic Ravanson LK-48 refrigerator is powered from AC 230V mains. Therefore, during the tests, we determined the electric efficiency η of the power supply unit of the Ravanson refrigerator and its dependence on the output voltage U_{dc} (Fig.5), which enabled us with sufficient accuracy to recalculate the power consumption of the refrigerator from 230V AC mains to 12V DC mains.

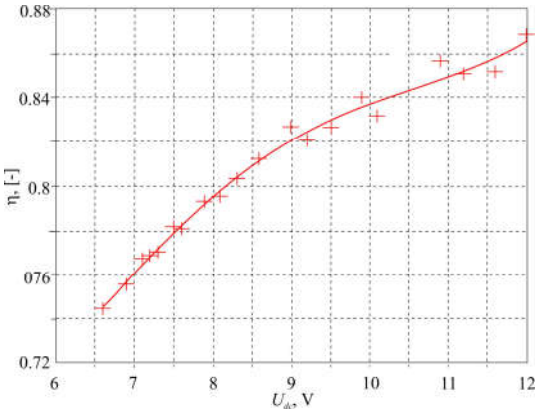

Fig. 5. Dependence of electrical efficiency $\boldsymbol{\eta}$ *of the Ravanson LK-48 refrigerator power unit on the output voltage* $\boldsymbol{U_{dc}}$

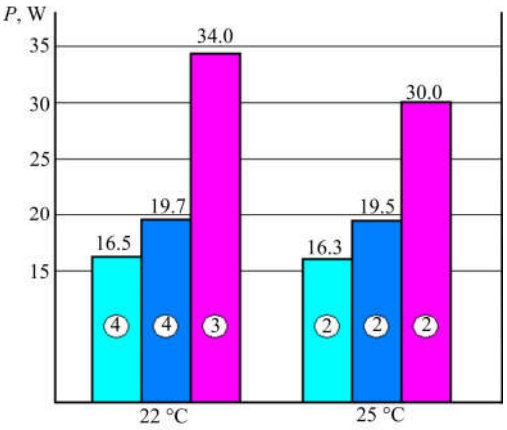

Fig.6. Average power consumption of refrigerators in energy-saving mode at two ambient temperatures T_{amb}*: - XTT-48-1, - XTT-48-2, - Ravanson LK-48; within the columns of the diagram, the thermostat is set in the range from 1 to 7*

The results of comparative tests of the refrigerators are presented in Figs. 6, 7 and in Tables 2, 3.

The tests were carried out at different ambient temperatures T_{amb}. Below are the results for temperatures 22ºC and 25ºC. At both temperatures, the HTT-48 coolers in energy-saving operation mode demonstrated a record-breaking low power consumption - less than 20 watts.

Table 2

Comparison of chosen technical characteristics of refrigerators at thermostat settings as in Fig. 6

Technical data	T_{amb},ºC	XTT-48-1	XTT-48-2	Ravanson LK-48
Time from switching on to power saving mode, min	22	68.5	60.0	132 (68 + 64)**
	25	56.0	41.5	160 (68 + 92)**
Created temperature difference $T_{amb} - T_{comp}$, K	22	16.8	15.3	12.6
	25	13.3	14.3	13.6
Indicator of specific power consumption, W/dm^{3}K	22	0.0205	0.0268	0.0562*
	25	0.0255	0.0284	0.0460*
Calculated daily energy consumption, W h	22	443.4		849.0*
	25	430.1		760.6*
Measured daily energy consumption, W h	25	435.8		762.1

* - values converted to power the cooler from the DC 12V DC.

** - In parentheses, the start-up time plus the transient time is given with a smooth decrease in the module supply voltage.

Taking power consumption from the AC network of the Ravanson refrigerator as 100%, it can be readily seen that power consumption of the HTT-48-1 refrigerator under the same operating conditions is 54.3%, i.e. almost half as much. At 22ºC, the advantage of the XTT-48 refrigerators is even greater.

The power consumption P_{a2} of the Ravanson LK-48 refrigerator was measured in the supply circuit of the thermoelectric module. Since the supply voltage of the external fan is synchronized with the power supply of the thermoelectric module, and the external fan in energy-saving mode remained at the same power supply of 12 V DC, the total power consumption, taking into account the fan consumption, was calculated according to formula (1):

$$P_{a2} = P_m + P_{ww} + P_{wz}\left(\frac{U_x}{U_n}\right)^2, \quad (1)$$

where: P_m is measured power consumption of the module, P_{ww} is rated power consumption of the internal fan, P_{wz} is rated power consumption of the external fan, U_x is fan voltage in energy-saving mode, U_n is rated supply voltage of the fan -12V.

The power consumption P_{a2} is influenced by the power consumption of the proportional temperature control unit, which, like in the domestic version, must be used in the transport version of the Ravanson refrigerator and which differs significantly from that used in the Ravanson LK-48 model. Therefore, according to experts on power circuits and converters, the voltage value should be increased by at least 15%. Nevertheless, the data presented in Table 2 does not take into account this increase, which creates a certain "margin of confidence" in the advantage of the new version.

The calculation of the daily energy consumption E of the refrigerators presented in Table 2 was carried out according to the following procedure:

- for the XTT-48 refrigerator:

$$E_1 = \frac{P_1 \cdot \tau_1 + P_3 \cdot \tau_3}{24 \cdot 3600}, \quad (2)$$

- for the Ravanson LK-48 refrigerator:

$$E_2 = \frac{P_1 \cdot \tau_1 + P_2 \cdot \tau_2 + P_3 \cdot \tau_3}{24 \cdot 3600}, \quad (3)$$

$$P_2 = \frac{1}{2 \cdot \sqrt{2}} (P_{2p} + P_{2k}), \quad (4)$$

where:
P_1 – average power consumption of the refrigerator in starting mode,
P_2 – average power consumption of the Ravanson refrigerator in transient mode,
P_{2p} – power consumption of the Ravanson refrigerator at the beginning of transient mode,
P_{2k} – power consumption of the Ravanson refrigerator at the end of transient mode,
P_3 – average power consumption of the refrigerator in energy-saving mode,
τ_1 – operating time of the refrigerator within 24 hours in starting mode,
τ_2 – operating time of the refrigerator within 24 hours in transient mode,
τ_3 – operating time of the refrigerator within 24 hours in energy-saving mode.

All power values are measured in watts, time- in seconds.

Minor differences in the calculated and measured values of E_1 and E_2 are due to the short (within one minute) period immediately after the refrigerator is turned on, when the power consumption is relatively high because of the slow increase in the temperature difference between the sides of the thermoelectric module. The second reason for the discrepancy between the calculated and measured values of E1 and E2 is the simplified averaging of P_2 value in the time interval $\tau 2$ in formula (4). Despite this, the correlation between calculated and measured values of E can be estimated as good.

Table 3

Comparison of chosen technical characteristics of refrigerators at ambient temperature T_{amb} = 25ºC

Technical data	Operating mode	XTT-48-1	Ravanson LK-48
Average temperature of hot radiator T_h, ºC	Starting	34.0	43.3
	Energy saving	30.7	39.0
Overheat of hot radiator $T_h - T_{amb}$, K	Starting	9.0	18.3
	Energy saving	5.7	14.0
Average temperature of cold radiator T_c, ºC	Starting	3.1	2.9
	Energy saving	8.5	3.5
Overcooling of cold radiator $T_{chamb} - T_c$, K	Starting	2.9	7.8
	Energy saving	3.2	7.6
Heat-exchange surface of hot radiator, m^2		0.257	0.159
Heat-exchange surface of cold radiator, m^2		0.092	0.053
Cooler weight, kg		10.64	10.56

* - constant operation of the unit without temperature control..

Table 3 shows other advantages of the XTT-48 refrigerator. These parameters demonstrate the rational arrangement of heat exchange on both sides of thermoelectric modules in operating and energy-

saving modes. Despite the increase in the heat exchange surfaces of the hot and cold radiator, the weight of the refrigerator has practically not changed.

As shown in Fig. 7, the HTT-48 refrigerator showed a significantly wider operating temperature range in energy-saving mode compared to its analogue. For example, with a standard thermostat setting in position 4, the difference is 2 degrees.

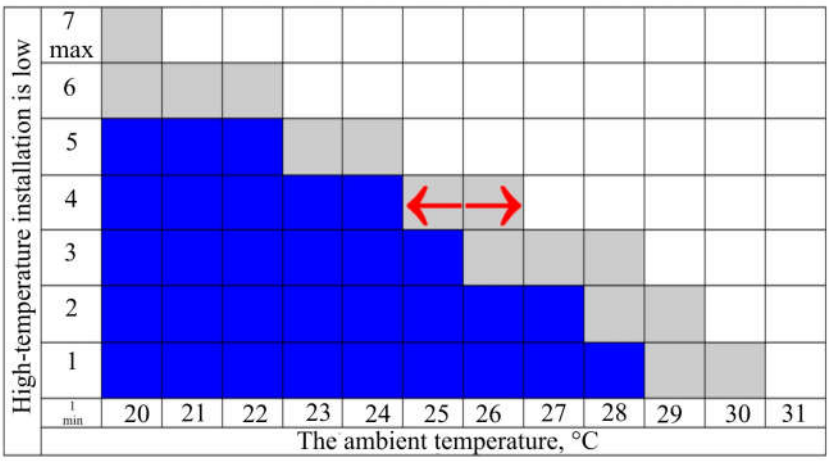

Fig. 7. Comparing the width of the energy-saving mode zone of tested refrigerators: dark colour – Ravanson LK-48, grey colour – XTT-48-1

Conclusion

Summarizing the results of this work and previous research and development work carried out under the supervision of the author at the West-Pomeranian University of Technology, Szczecin, it can be stated that the target goals were accomplished. For the selected product categories, the energy efficiency of transport and domestic TERs based on standard commercially available thermoelectric cooling modules was increased. The **world's best** parameters of specific power consumption were achieved.

Approaches and specific technical solutions that ensure the competitiveness of TERs with a compartment capacity from 30 to 100 liters, both in comparison with compressor analogues, and with the best world models of TERs, **have been developed, implemented, described and justified.**

The advantages of the developed refrigerators over the analogues were achieved due to:

1. Design optimization of the refrigeration unit, including the choice of the appropriate number of thermoelectric modules, the type and number of fans, the type of radiators and their surface, etc.
2. The choice of the best way to control the temperature in the compartment, namely a two-level control when using a manometric thermostat, which in particular for transport TER is provided by switching the power supply of the modules from parallel to series.
3. Stabilization of TER operation in energy-saving mode for an unlimited time.
4. Synchronization of switching the operating modes of fans and modules.

References

1. Vainer A.L., Moiseev V.F. (2002). Power consumption minimizing of the thermoelectric cooler at position control. J.Thermoelectricity. 2, 68-71.
2. Patent RP № 224189. S.Filin, B Jasińska, B.Zakrzewski, M.Chmielowski**.** Sposób redukcji zużycia energii przez chłodziarkę termoelektryczną i chłodziarka termoelektryczna. Publ. 06.12.2016.

3. Jasińska B., Filin S. (2015). Economical transport thermoelectric refrigerators with two-level temperature control: the experience of creation and test results. J. Thermoelectricity, 3, 38-44.
4. B. Zakrzewski (Ed.) (2015). Chłodnictwo i klimatyzacja. Podręcznik. Odessa: Astroprint.
5. Filin S., Jasińska B. (2013). Efektywność energetyczna transportowych chłodziarek termoelektrycznych. Energetycznie efektywne rozwiązania urządzeń chłodniczych, klimatyzacyjnych i pomp ciepła. XLV Dni Chłodnictwa. (Poznań, 13-14 11.2013). (s. 63-74).
6. Filin S.O., A.Owsicki, B.Zakrzewski. (2011). Experimental investigation of stationary thermoelectric coolers. Odessa: Astroprint [in Russian].
7. Filin S., Zakrzewski B. (2010). Zastosowanie dwupołożeniowego regulatora temperatury typu manometrycznego w chłodziarkach termoelektrycznych. Chłodnictwo, 1-2, 2010, 30-34.

Submitted 17.01.2018

Філін С.О., *доктор техн. наук*

Західнопоморський технологічний університет у Щецині
алея Піастів 17, Щецин, 70-310, Польща;
e-mail: Sergiy.Filin@zut.edu.pl

ПОРІВНЯЛЬНИЙ АНАЛІЗ ЕНЕРГЕТИЧНИХ ХАРАКТЕРИСТИК СУЧАСНИХ ТЕРМОЕЛЕКТРИЧНИХ ХОЛОДИЛЬНИКІВ

У статті проаналізовані технічні характеристики й у першу чергу енергетичні сучасних термоелектричних холодильників (ТЕХ), а також способи підвищення їх енергетичної ефективності. Представлено результати порівняльних випробувань нових, розроблених автором, моделей ТЕХ та показано їх переваги над світовими аналогами. Бібл. 7, Рис. 7, Табл. 3.
Ключові слова: термоелектричний холодильник, транспортний холодильник, енергозбереження, регулювання температури.

Філін С.О., *доктор техн. наук*

Западнопоморский технологический университет в Щецине
аллея Пиастов 17, Щецин, 70-310, Польша
e-mail: Sergiy.Filin@zut.edu.pl

СРАВНИТЕЛЬНЫЙ АНАЛИЗ ЭНЕРГЕТИЧЕСКИХ ХАРАКТЕРИСТИК СОВРЕМЕННЫХ ТЕРМОЭЛЕКТРИЧЕСКИХ ХОЛОДИЛЬНИКОВ

В статье проанализированы технические характеристики и в первую очередь энергетические современных термоэлектрических холодильников (ТЭХ), а также способы повышения их энергетической эффективности. Представлены результаты сравнительных испытаний новых, разработанных автором моделей ТЭХ и показаны их преимущества над мировыми аналогами. Библ. 7, Рис. 7, Табл.3.

Ключевые слова: термоэлектрический холодильник, транспортный холодильник, энергосбережение, регулирование температуры.

References

1. Vainer A.L., Moiseev V.F. (2002). Power consumption minimizing of the thermoelectric cooler at position control. J.Thermoelectricity. 2, 68-71.
2. Patent RP № 224189. S.Filin, B Jasińska, B.Zakrzewski, M.Chmielowski**.** Sposób redukcji zużycia energii przez chłodziarkę termoelektryczną i chłodziarka termoelektryczna. Publ. 06.12.2016.
3. Jasińska B., Filin S. (2015). Economical transport thermoelectric refrigerators with two-level temperature control: the experience of creation and test results. J. Thermoelectricity, 3, 38-44.
4. B. Zakrzewski (Ed.) (2015). Chłodnictwo i klimatyzacja. Podręcznik. Odessa: Astroprint.
5. Filin S., Jasińska B. (2013). Efektywność energetyczna transportowych chłodziarek termoelektrycznych. Energetycznie efektywne rozwiązania urządzeń chłodniczych, klimatyzacyjnych i pomp ciepła. XLV Dni Chłodnictwa. (Poznań, 13-14 11.2013). (s. 63-74).
6. Filin S.O., A.Owsicki, B.Zakrzewski. (2011). Experimental investigation of stationary thermoelectric coolers. Odessa: Astroprint [in Russian].
7. Filin S., Zakrzewski B. (2010). Zastosowanie dwupołożeniowego regulatora temperatury typu manometrycznego w chłodziarkach termoelektrycznych. Chłodnictwo, 1-2, 2010, 30-34.

Submitted 17.01.2018

NEWS
OF INTERNATIONAL THERMOELECTRIC ACADEMY

MURAD MAMEDOVICH MAMEDOV

(Dedicated to 80-th birthday)

In December this year Murad Mamedovich Mamedov, associate member of the International Thermoelectric Academy, Doctor of Science in Engineering, professor, chief research scientist of Photoelectricity and Thermoelectricity Laboratory at Physics and Mathematics Institute of the Academy of Sciences of Turkmenistan celebrated his 80-th birthday.

Murad Mamedovch Mamedov was born on December 12, 1937 in the village of Akdep, Ruhabat Etrap, Ahal Velayat, Turkmenistan. In 1956 he entered the correspondence department of Physics and Mathematics Faculty of A.M. Gorky Turkmen State University; in 1962 received a diploma of secondary school teacher of mathematics.

In 1972 M.Mamedov came to work at Physics and Technical Institute of the Academy of Sciences of Turkmenistan as engineer. In 1975 he maintained his Ph.D thesis, and in 1989 – DSc thesis. In 1976-1997 he worked in Heliotechnology Laboratory at Physics and Technical Institute of the Academy of Sciences of Turkmenistan, at the Institute of Solar Energy, at the "Sun" Scientific-Production Association of the Academy of Sciences of Turkmenistan, as well as at the Institute of Mechanics and Computer Technology of the Academy of Sciences of Turkmenistan as a junior, senior and chief research assistant. He also headed the Heat and Mass Transfer and Hydrodynamics Laboratory.

Since the early 1998 till August 2009 professor M.Mamedov worked in the Physics and Mathematics Research Centre at Magtymguly Turkmen State University as a chief research scientist. In September 2009 he was transferred to Physics and Mathematics Institute of the Academy of Sciences of Turkmenistan as a chief research scientist.

Since 2001 professor M. Mamedov has been actively engaged in the scientific problems of nonequilibrium thermodynamics. Murad Mamedov is a well-known scientist who developed new important scientific concepts in thermodynamics of nonequilibrium processes. Their application to thermoelectric power conversion opens up new lines in the theory of thermoelectricity, as well as in the possibilities of practical applications.

In 2010, taking into account his considerable contribution to progress in education, science and technology in Turkmenistan, as well as for the scientific success achieved in the field of nonequilibrium thermodynamics, professor M. Mamedov by special decree of Turkmenistan's president Gurbanguly Berdymukhamedov was awarded the honorary title of "Merited Worker of Science and Technology of Turkmenistan".

In 2017, M.Mamedov's work "Universal nonequilibrium thermodynamics and Thomson's hypothesis" was reported to International Forum on Thermoelectricity, in Belfast, in the homeland of Thomson.

The International Thermoelectric Academy, Institute of Thermoelectricity of the National Academy of Sciences and Ministry of Education and Science of Ukraine, "Journal of Thermoelectricity" Editorial Board congratulate the esteemed Murad Mamedovich Mamedov on his jubilee and wish him further creative success, good health and longevity.

ARTICLE SUBMISSION GUIDELINES

For publication in a specialized journal, scientific works are accepted that have never been printed before. The article should be written on an actual topic, contain the results of an in-depth scientific study, the novelty and justification of scientific conclusions for the purpose of the article (the task in view).

The materials published in the journal are subject to internal and external review which is carried out by members of the editorial board and international editorial board of the journal or experts of the relevant field. Reviewing is done on the basis of confidentiality. In the event of a negative review or substantial remarks, the article may be rejected or returned to the author(s) for revision. In the case when the author(s) disagrees with the opinion of the reviewer, an additional independent review may be done by the editorial board. After the author makes changes in accordance with the comments of the reviewer, the article is signed to print.

The editorial board has the right to refuse to publish manuscripts containing previously published data, as well as materials that do not fit the profile of the journal or materials of research pursued in violation of ethical norms (for instance, conflicts between authors or between authors and organization, plagiarism, etc.). The editorial board of the journal reserves the right to edit and reduce the manuscripts without violating the author's content. Rejected manuscripts are not returned to the authors.

Submission of manuscript to the journal

The manuscript is submitted to the editorial office of the journal in paper form in duplicate and in electronic form on an electronic medium (disc, memory stick). The electronic version of the article shall fully correspond to the paper version. The manuscript must be signed by all co-authors or a responsible representative.

In some cases it is allowed to send an article by e-mail instead of an electronic medium (disc, memory stick).

English-speaking authors submit their manuscripts in English. Russian-speaking and Ukrainian-speaking authors submit their manuscripts in English and in Russian or Ukrainian, respectively. Page format is A4. The number of pages shall not exceed 15 (together with References and extended abstracts). By agreement with the editorial board, the number of pages can be increased.

To the manuscript is added:

1. Official recommendation letter, signed by the head of the institution where the work was carried out.

2. License agreement on the transfer of copyright (the form of the agreement can be obtained from the editorial office of the journal or downloaded from the journal website – Dohovir.pdf). The license agreement comes into force after the acceptance of the article for publication. Signing of the license agreement by the author(s) means that they are acquainted and agree with the terms of the agreement.

3. Information about each of the authors – full name, position, place of work, academic title, academic degree, contact information (phone number, e-mail address), ORCID code (if available). Information about the authors is submitted as follows:

authors from Ukraine - in three languages, namely Ukrainian, Russian and English;

authors from the CIS countries - in two languages, namely Russian and English;

authors from foreign countries – in English.

4. Medium with the text of the article, figures, tables, information about the authors in electronic form.

5. Colored photo of the author(s). Black-and-white photos are not accepted by the editorial staff. With the number of authors more than two, their photos are not shown.

Requirements for article design

The article should be structured according to the following sections:

- *Introduction*. Contains the problem statement, relevance of the chosen topic, analysis of recent research and publications, purpose and objectives.
- *Presentation of the main research material* and the results obtained.
- *Conclusions* summing up the work and the prospects for further research in this direction.
- *References*.

The first page of the article contains information:

1) in the upper left corner – UDC identifier (for authors from Ukraine and the CIS countries);

2) surname(s) and initials, academic degree and scientific title of the author(s);

3) the name of the institution where the author(s) work, the postal address, telephone number, e-mail address of the author(s);

4) article title;

5) abstract to the article – not more than 1 800 characters. The abstract should reflect the consistent logic of describing the results and describe the main objectives of the study, summarize the most significant results;

6) key words – not more than 8 words.

The text of the article is printed in Times New Roman, font size 11 pt, line spacing 1.2 on A4 size paper, justified alignment. There should be no hyphenation in the article.

Page setup: "mirror margins" – top margin – 2.5 cm, bottom margin – 2.0 cm, inside – 2.0 cm, outside – 3.0 cm, from the edge to page header and page footer – 1.27 cm.

Graphic materials, pictures shall be submitted in color or, as an exception, black and white, in .opj or .cdr formats, .jpg or .tif formats being also permissible. According to author's choice, the tables and partially the text can be also in color.

Figures are printed on separate pages. The text in the figures must be in the font size 10 pt. On the charts, the units of measure are separated by commas. Figures are numbered in the order of their arrangement in the text, parts of the figures are numbered with letters – a, b, .. On the back of the figure, the title of the article, the author (authors) and the figure number are written in pencil. Scanned images and graphs are not allowed to be inserted.

Tables are provided on separate pages and must be executed using the MSWord table editor. Using pseudo-graph characters to design tables is inadmissible.

Formulae shall be typed in Equation or MatType formula editors. Articles with formulae written by hand are not accepted for printing. It is necessary to give definitions of quantities that are first used in the text, and then use the appropriate term.

Captions to figures and tables are printed in the manuscript after the references.

Reference list shall appear at the end of the article. References are numbered consecutively in the order in which they are quoted in the text of the article. References to unpublished and unfinished works are inadmissible.

Attention! In connection with the inclusion of the journal in the international bibliographic abstract database, the reference list should consist of two blocks: CITED LITERATURE and REFERENCES (this requirement also applies to English articles):

CITED LITERATURE – sources in the original language, executed in accordance with the Ukrainian standard of bibliographic description DSTU 8302:2015. With the aid of VAK.in.ua (http://vak.in.ua) you can automatically, quickly and easily execute your "Cited literature" list in conformity with the requirements of State Certification Commission of Ukraine and prepare references to scientific sources in Ukraine in understandable and unified manner. This portal facilitates the processing of scientific sources when writing your publications, dissertations and other scientific papers.

REFERENCES – the same cited literature list transliterated in Roman alphabet (recommendations according to international bibliographic standard APA-2010, guidelines for drawing up a transliterated reference list "References" are on the site http//www.dse.org.ua, section for authors).

To speed up the publication of the article, please adhere to the following rules:

- in the upper left corner of the first page of the article – the UDC identifier;
- family name and initials of the author(s);
- academic degree, scientific title;

begin a new line, Times New Roman font, size 12 pt, line spacing 1.2, center alignment;

- name of organization, address (street, city, zip code, country), e-mail of the author(s);

begin a new line 1 cm below the name and initials of the author(s), Times New Roman font, size 11 pt, line spacing 1.2, center alignment;

- the title of the article is arranged 1 cm below the name of organization, in capital letters, semi-bold, font Times New Roman, size 12 pt, line spacing 1.2, center alignment. The title of the article shall be concrete and possibly concise;
- the abstract is arranged 1 cm below the title of the article, font Times New Roman, size 10 pt, in italics, line spacing 1.2, justified alignment in Ukrainian or Russian (for Ukrainian-speaking and Russian-speaking authors, respectively);
- key words are arranged below the abstract, font Times New Roman, size 10 pt, line spacing 1.2, justified alignment. The language of the key words corresponds to that of the abstract. Heading "Key words" - font Times New Roman, size 10 pt, semi-bold;
- the main text of the article is arranged 1 cm below the abstract, indent 1 cm, font Times New Roman, size 11 pt, line space spacing 1.2, justified alignment;
- formulae are typed in formula editor, fonts Symbol, Times New Roman. Font size is "normal" – 12 pt, "large index" – 7 pt, "small index" – 5 pt, "large symbol" – 18 pt, "small symbol" – 12 pt. The formula is arranged in the text, center aligned and shall not occupy more than 5/6 of the line width, formulae are numbered in parentheses on the right;
- dimensions of all quantities used in the article are represented in the International System of Units (SI) with the explication of the symbols employed;
- figures are arranged in the text. The figures and pictures shall be clear and contrast; the plot axes – parallel to sheet edges, thus eliminating possible displacement of angles in scaling; figures are submitted in color, black-and-white figures are not accepted by the editorial staff of the journal;
- tables are arranged in the text. The width of the table shall be 1 cm less than the line width. Above the table its ordinary number is indicated, right alignment. Continuous table numbering

throughout the text. The title of the table is arranged below its number, center alignment;

• references should appear at the end of the article. References within the text should be enclosed in square brackets behind the text. References should be numbered in order of first appearance in the text. Examples of various reference types are given below.

Examples of LITERATURE CITED

Journal articles

Anatychuk L.I., Mykhailovsky V.Ya., Maksymuk M.V., Andrusiak I.S. Experimental research on thermoelectric automobile starting pre-heater operated with diesel fuel. *J.Thermoelectricity*. 2016. №4. P.84–94.

Books

Anatychuk L.I. *Thermoelements and thermoelectric devices. Handbook.* Kyiv, Naukova dumka, 1979. 768 p.

Patents

Patent of Ukraine № 85293. Anatychuk L.I., Luste O.J., Nitsovych O.V. Thermoelement.

Conference proceedings

Lysko V.V. *State of the art and expected progress in metrology of thermoelectric materials.* Proceedings of the XVII International Forum on Thermoelectricity (May 14-18, 2017, Belfast). Chernivtsi, 2017. 64 p.

Authors' abstracts

Kobylianskyi R.R. *Thermoelectric devices for treatment of skin diseases*: extended abstract of candidate's thesis. Chernivtsi, 2011. 20 p.

Examples of REFERENCES

Journal articles

Gorskiy P.V. (2015). Ob usloviakh vysokoi dobrotnosti i metodikakh poiska perspektivnykh sverhreshetochnykh termoelektricheskikh materialov [On the conditions of high figure of merit and methods of search for promising superlattice thermoelectric materials]. *Termoelektrichestvo - J.Thermoelectricity,* 3, 5 – 14 [in Russian].

Books

Anatychuk L.I. (2003). *Thermoelectricity. Vol.2. Thermoelectric power converters*. Kyiv, Chernivtsi: Institute of Thermoelectricity.

Patents

Patent of Ukraine № 85293. Anatychuk L. I., Luste O.Ya., Nitsovych O.V. Thermoelements [In Ukrainian].

Conference proceedings

Rifert V.G. Intensification of heat exchange at condensation and evaporation of liquid in 5 flowing-down films. In: *Proc. of the 9th International Conference Heat Transfer.* May 20-25, 1990, Israel.

Authors'abstracts

Mashukov A.O. *Efficiency hospital state of rehabilitation of patients with color carcer.* PhD (Med.) Odesa, 2011 [In Ukrainian].